II-2-2 Seismic Survey

1. Introduction

The seismic survey was carried out for the purpose to estimate underground structures, controling existence of geothermal fluids, represented by alteration zones and fracture zones, through the comprehension of geological structures which are displayed as bedding planes, faults and intrusive bodies, by the execusion of seismic reflection method.

The seismic survey is a method of exploration to estimate underground structures by means of elastic waves which are generated from the hypocenter of artificial earthquake in a shallow subsurface. The reflection method employs such waves as to reflect on the boundary surfaces of geological beddings whose elastic characters (reflection coefficient) are different one another in the underground.

Generally, in the area where geological structures are fairly complex as is seen in geothermal area, it is expected that the reflection waves are very delicate. For this problem, common reflection point and six fold stacking method were applied in the present survey.

Number of the survey lines is 5 (A, B, C, D and E line), total length of which is 14,225 meters, and number of the shot holes is 315 in this survey.

Process of the present seismic survey, from the field works to the compilation of the report, is shown in the following flow chart.

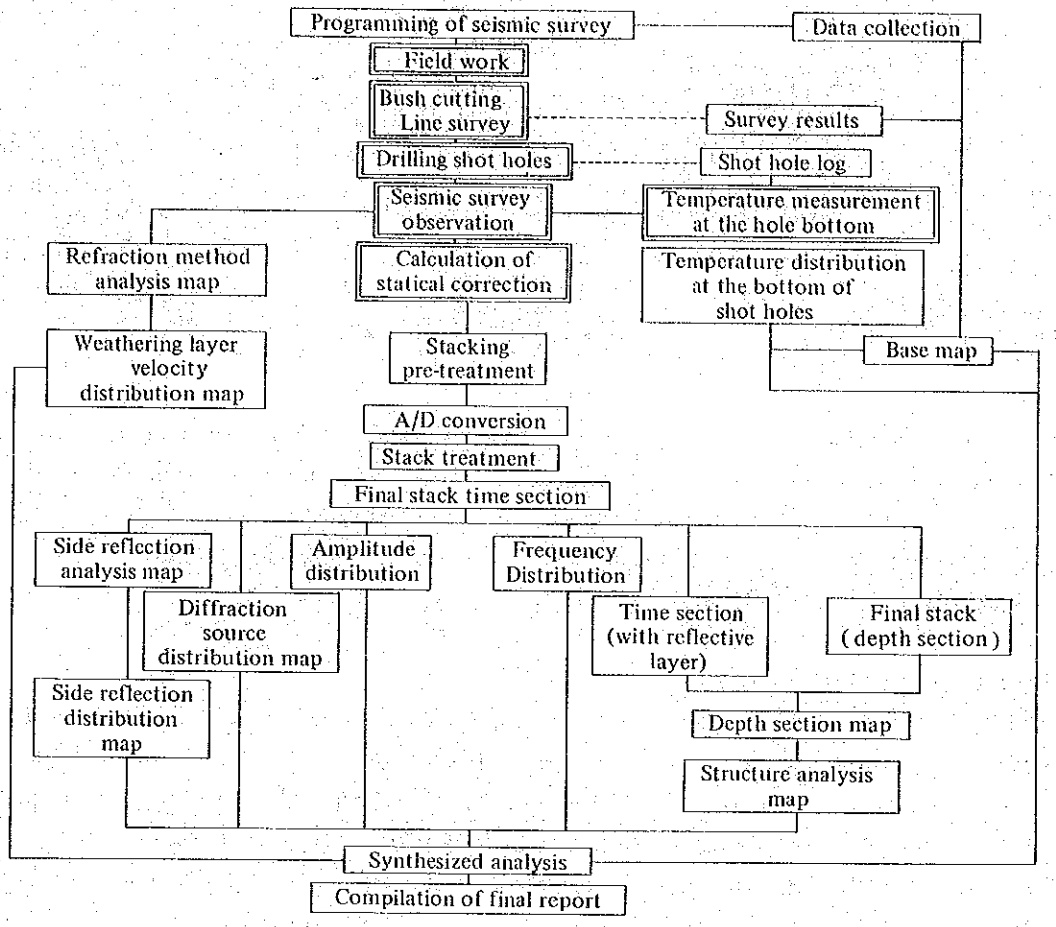

Fig. II.2.2-1 Flow chart of seismic survey

2. Field work

2-1 Establishment of the seismic survey lines

Five survey lines of A, B, C, D and E were established for this seismic survey by reflection method (PL. II.2.2-1). These survey lines were located in the favorable area for the geothermal development, which is the area along the Huai Pong fault. Details of the survey lines are shown in Table II.2.2-1.

As the ducts (hume concrete pipes) were laid close one another between the shot points of SP No. 65 and SP No. 70 along the survey line A, distribution of the spread was changed in that part, but the revised setting was done so that the programmed records could be obtained in full scale.

The survey line A is a line of approximate length of 5.5 km, running from the hilly land in the northwestern part of the surveyed area to Ban Mai village in the southwestern part, across the several estimated faults.

Table II.2.2-1 Survey lines

Line	Length (m)	Number of spread	Survey point		Shot point		Remarks
			Number	Interval (m)	Number	Interval (m)	
A	5,475	99	220	25	105	50	NW direction
B	2,025	30	82	25	36	50	NE direction
C	2,025	30	82	25	36	50	NE direction
D	2,025	30	82	25	36	50	NE direction
E	2,675	43	108	25	49	50	NE direction
Total	14,225	232	574	–	262	–	–

The survey lines of B to D are about 2 km in length and are established in the direction of NE-SW, almost in right angle to the survey line A. They are distributed from the foot of the hilly land in the western part of the surveyed area to the plain in the eastern part.

The survey line E is 2.7 km in length, established in the southernmost part of the surveyed area, where low and gentle hilly land is developed.

2-2 Drilling of shot holes

Drilling of the shot holes were completed by EGAT, whose engineers did whole of the field supervision and control of the works. By using 6 to 10 transportable rotary drill machines, every hole was drilled down to the depth of 10 meters, and vinyl chloride pipes 76 mm in diameter, were inserted in each of the shot holes to keep the wall of the holes out of collapse.

Geologically, it was turned out by the logging of the drill holes that chert and andesite are distributed along the A line, that chert, sandstone shale, limestone and sand ~ peblles are found along the survey lines of B to D, and that andesite is distributed along the survey line E.

2-3 Blasting and observation

Blasting was carried out by filling the shot holes with water, after the holes were charged with explosives of the weight of 10.0 ~ 12.5 kg at the bottom. At the time when the actual blastings were done, watchmen were distributed at every points which were thought to be dangerous spot such as roads and private houses, in order to prevent possible accidents. Transceivers were utilized effectively to have the communication as intimately as possible between observation crews and wiring crews, which brought high efficiency of the field works.

To obtain the data for the calculation of weathering layer correction, total 53 times of small blasting were carried out at every several spreads.

The small blasting was carried out by the explosives of the average weight of 500 g filled in the small holes, which had been digged at the programmed sites with iron bars of the diameter of 40 millimeters and of the length of 1.5 meters.

The observation was completed by measuring seismic waves with the apparatus of the 24 components seismic recording system of magnetic recording type, made by S.I.E. in U.S.A. (PT100 + MR20 + R-6B), and 36 groups of the geophones made by E.T.L. in U.S.A. (EV-15 type, proper frequency 20 cps). The geophone distribution is group-setting of 6 geophones (spacing 2 meters, linear distribution in the same direction as that of the survey line).

For the improvement of the S-N ratio (signal to noise ratio) of the reflection waves and for the increase of the structure resolving power, the 6 folds stack method was employed with the way of the terminal blasting.

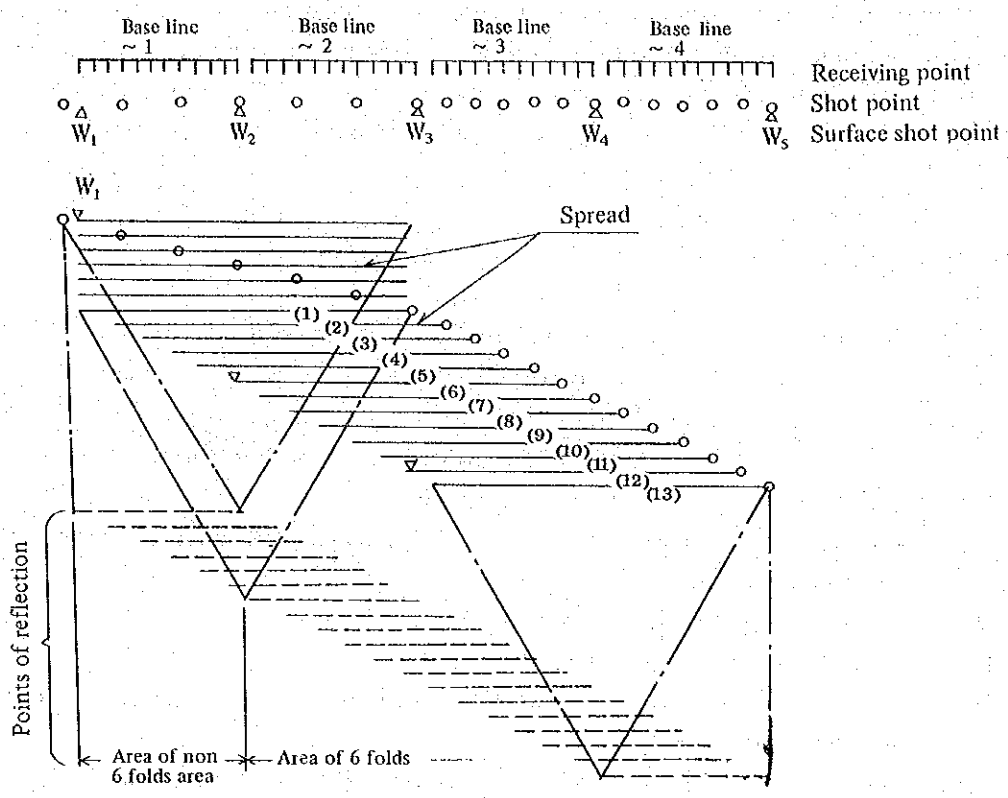

Fig. II.2.2-2 Process of measurement by common reflection point horizontal stack method (6 folds)

The process of measurement is as follows.

(1) To set base lines No. 1 to No. 3 and geophone No. 1 to No. 36.
(2) To connect base line cables (12 components and 3 cables, each) with switching device.
(3) To connect the input terminals of No. 1 to No. 24 of the seismic recording system with the output terminals of No. 1 to No. 24, through the switching device, of the geophone.
(4) To blast at the shot point SP 1 (SP = shot point) and to record on the magnetic recording tape.
(5) From the shot points of SP 1 to SP 7, to blast in the spread (1) and to record it.
(6) To connect the input terminals of No. 1 to No. 24 of the seismic recording system with the output terminals of No. 4 to No. 27, through the switching device, of the geophone.
(7) To blast at the shot point SP 8 and to record on the magnetic recording tape.
(8) To repeat the same operation as above.

Before the blasting and the observation, temperatures of every shot hole were measured at the bottom. The results of this temperature measurement were summarized in the Temperature distribution at the bottom of the shot holes (PL. II.2.2-15).

3. Method of analysis

3-1 Analysis of shallow structure by refrection method

3-1-1 Calculation for static correction

The calculation for static correction is required for the preparation of the stacking records by the refraction method. It is composed of the surface (weathering layer) correction and the datum correction to the datum elevation for the analysis (established at 300 meters above sea level in this survey). The amount of correction C is obtained as two-layered structure tentatively by the following formula.

$$C = \frac{1}{2}\{(T + U) + (T' + U') - E\} \sec i + \frac{H - hw - Hd}{Vd}$$

Here C : sum of surface correction time (first term of the right side) and datum correction time (second term of the right side)

(T + U) + (T' + U') : sum of the uphole time of the explosion and the initial motion travel time from two corresponding shot points

E : finishing time of the initial motion travel time

i : critical angle of seismic wave reflection between the surface layer and the first layer below the surface

H : elevation of the receiving point, above sea level (m)

hw : thickness of the surface layer

Hd : elevation of the datum surface (DL = Datum Line) above sea level (300 m above sea level in this survey

Vd : velocity in the first layer below surface (velocity of the second layer)

3-1-2 Depth calculation

In order to comprehend the distribution of shallow velocity layers in the surveyed area and to make use of it for the consideration of deep structure, calculation of the three-layered structure was executed employing initial motion travel time curves.

This calculation was based on the "Method of Selection of the Refractive Initial Motion Travel Time Curve and Analysis Method of the Refractive Motion Travel Time Curve by Zero Travel Time" (Shigetoshi KURIHARA).

The calculation for the analysis was done with the electronic computer of UNIVAC-1110 and the figuration was with the computer of CALCOMB 360.

The general calculation formula by this method are given below in case of No. n layer of velocity layer.

$$\alpha_1 = \frac{1}{2}\left(\sin^{-1}\frac{V_1}{V_{2^-}} - \sin^{-1}\frac{V_1}{V_{2^+}}\right)$$

$$i_1 = \frac{1}{2}\left(\sin^{-1}\frac{V_1}{V_{2^-}} + \sin^{-1}\frac{V_1}{V_{2^+}}\right)$$

$$V_2 = V_1 - i_1$$

$$\theta_1^{(n)} = \sin^{-1}\frac{V_1}{V_{n^-}} - \alpha_1$$

$$w_1^{(n)} = \sin^{-1}\frac{V_1}{V_{n^+}} + \alpha_1$$

$$\theta_m^{(n)} = \sin^{-1}\left(\frac{V_m}{V_{n-1}}\sin\theta_{n-1}^{(n)}\right) - \alpha_m - \alpha_{m-1}$$

$$w_m^{(n)} = \sin^{-1}\left(\frac{V_m}{V_{n-1}}\sin w_{m-1}^{(n)}\right) + \alpha_m - \alpha_{m-1}$$

$$V_n = V_{n-1}\ \mathrm{cosec}\ i_{n-1}$$

$$\alpha_{n-1} = \frac{1}{2}\sin^{-1}\left(\frac{V_{n-1}}{V_{n-2}}\sin\theta_{n-2}^{(n)}\right) - \frac{1}{2}\sin^{-1}\left(\frac{V_{n-1}}{V_{n-2}}\sin w_{n-2}^{(n)}\right)$$

$$i_{n-1} = \frac{1}{2}\sin^{-1}\left(\frac{V_{n-1}}{V_{n-2}}\sin\theta_{n-2}^{(n)}\right) + \frac{1}{2}\sin^{-1}\left(\frac{V_{n-1}}{V_{n-2}}\sin w_{n-2}^{(n)}\right)$$

$$\gamma_{n-1} = \frac{V_{n-1}}{2}\sec i_{n-1}\left[\mathrm{tngo} + \left(\sum_{2}^{n-1}\right)\frac{\gamma_{m-1}}{V_m}\cos(\theta_m^{(n)} + \alpha_m - \alpha_{m-1})\right.$$

$$\left. + \cos(w_m^{(n)} - \alpha_m + \alpha_{m-1}) - \left(\sum_{1}^{n-2}\right)\frac{\gamma_m}{V_m}(\cos\theta_m^{(n)} + \cos w_m^{(n)})\right]$$

Here symbols stand for

$\theta_m^{(n)}$, $w_m^{(n)}$: critical angle of the wave proceeding upward, after refraction on the surface of No. n layer

$$\theta_{n-1} = w_{n-1} = i_{n-1}$$
$$m = 2, 3, 4, \ldots\ldots n$$

tngo : zero travel time of No. n layer at the point G

$$\mathrm{tngo} = t_{n^+} - t_{n^-} - t_n$$

Z : angle of inclination of the boundary surface of velocity layers

r(n−1) : depth of No. (n−1) velocity layer

i(n−1) : critical angle of refraction wave on the boundary surface between No. (n) layer and No. (n−1) layer

The underground structure is obtained as an envelope of the circles with the radii of normal depth as calculated in the abovementioned way.

In order to express the results on the illustrated analysis map and to give some additional consideration on the velocity division, the Refraction method analysis map (PL. II.2.2-2) was drawn, on the assumption that their variation in the velocity layers against the depth is linear.

Although this analysis map could have been prepared by the two-layered structure profiles depending upon the results of calculation of the surface correction afore-mentioned, the results of the three-layered structure analysis by the refraction method were synthesized on this map in the present survey, utilizing the information of the first layer and the second layer of the travel time curves. In addition to the velocity distribution on this map, the distribution of the third layer velocity as well as the directions of the estimated faults are expressed in the Weathering layer velocity distribution map (PL. II.2.2-3).

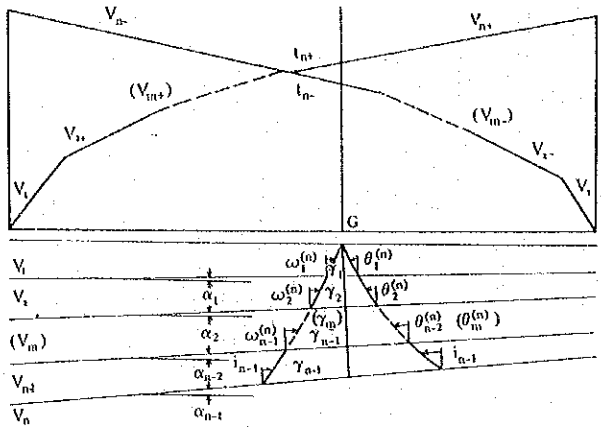

Fig. II.2.2-3 Dotted line in analysis of refractive method

3-1-3 Analysis of side-reflection wave

Generally, structural lines are estimated on the analysis profiles from velocity change of velocity layers, boundary steps of the velocity layers in the refraction method or from condition of discontinuity of reflection phases in the reflection method. Especially, direction and continuity of the estimated structure lines along each survey line on the plans are judged from the distribution and the conditions on the profiles. Therefore, it is desirable to establish sufficient number of survey lines in grid pattern, covering whole of the subject area.

However, in the present survey, there were 5 lines established; a line in the direction of NW-SE and 4 lines in the direction of NE-SW. It is thought that data would be somewhat short for the judgement of the continuity and the direction of extension of structure lines, if merely the materials of the refractive analysis were made use of. Accordingly, for the compensation of the above-stated shortage of data, a method was employed, in the following way, to utilize steeply inclined phases which were regarded as side-reflection travel time on the recorded profiles, as is mentioned in later paragraphs. Although some problems were thought to be there, because this method was based on the assumption that the continuation of steep inclination in the shallow part would represent side reflection on the structure line, the method was employed through the following treatment.

The seismic waves started from the shot point Gi on the survey line are thought to return to the receiving point (the point Gi in this case), after propagated near surface as well as to the depth and reflected at Ai or Bi (symmetrical point) on the structure line.

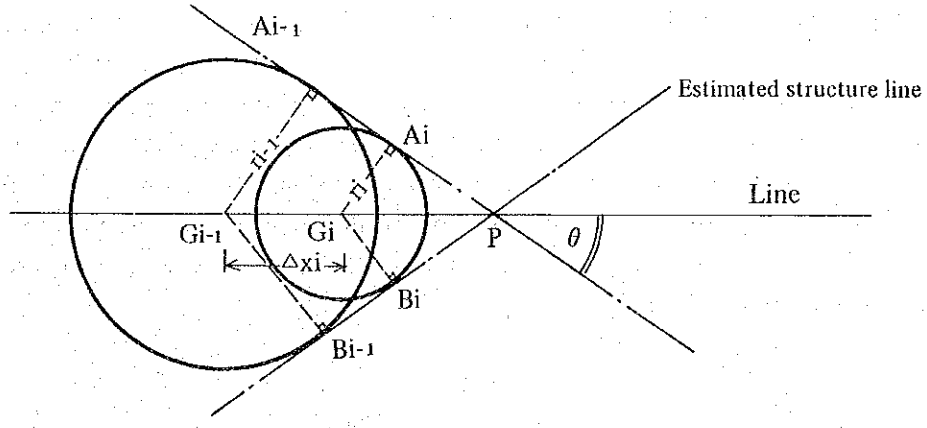

Fig. II.2.2-4 Side reflection

The distance ri between the shot point (or receiving point) Gi and the reflected point Ai on the structure line is determined by the propagated velocity Vw and the reflected travel time ti, and is expressed in the following formula.

$$ri = \frac{Vw}{2} \cdot ti$$

Also, the angle θ between the survey line and the structure line is determined by the following formula, from the difference of the travel times Δti and the distance Δxi of the neighbouring two shot points.

$$\theta = \sin^{-1}\left(\frac{Vw}{2} \cdot \frac{\Delta ti}{\Delta xi}\right)$$

As the values are in the range of $0 \leqq \sin \leqq 1.0$ in this calculation, it is necessary to select the reflection travel time of steeply inclined phase on the stacking records so that the upper limit should be $\Delta ti \leqq 2\Delta xi/Vw$. Accordingly, the detection was made with two values of the propagated velocity Vw of 1,500 m/s ~ 2,500 m/s and 3,000 m/s, using the Final stack (time section, PL. II.2.2-16 ~ 20). The results were as shown in the Side reflection analysis map (PL. II.2.2-4 ~ 8).

3-2 Analysis of deep structure by reflection method

3-2-1 Stack treatment

The horizontal stack treatment is to emphasize the reflected waves by stacking them in a record from several records of different distances of epi-centers at a reflection point, after the correction of the difference of reflection travel time caused by the difference of the distance.

By this method, S-N ratio of the reflected wave is improved as a result by the decrement of noises caused with mutual interference on the stacking, because the irregular noises have time lag, reverse to the signals.

For the preparation of the stacking record, first thing to do is to input into the computer, with other related data, the results of A-D conversion of the records which were obtained on the magnetic recording tapes in the field observation. Then they are synthesized as stacking record by integration of Wiggle and Variable area, after mechanical and electrical treatment such as correction, stacking, amplitude adjustment and filtering The stacking records are those treated with the datum level of analysis at the elevation of 300 meters above sea level. The following two figures were made.

(1) Final stack time section (PL. II.2.2-16 ~ 20)

This figure is the basic profile of final-stack time section, in which the corresponding 6 traces at every common reflection point in the records of the measurement are stacked (6 folds). In this figure, most of the informations are contained, though treated electrically and mechanically in afore-mentioned ways of amplitude adjustment and filtering etc. Many other indications than those on the horizontal reflection planes are recognized. They can be important informations for the detection of alteration zones and fault and fracture zones which are thought to be related to geothermal sources and to passages of geothermal solutions. Therefore, this figure was employed

for the side-reflection analysis, diffraction sources analysis and frequency-amplitude distribution analysis.

(2) Final stack (depth section) (PL. II.2.2-36 ~ 40)

This is the figure in which vertical records are exhibited by depth, after the depth conversion of the above-mentioned Final stack (Time selection). It was used as the base for the structure analysis, because various informations are contained in this figure in addition to the horizontal reflection planes.

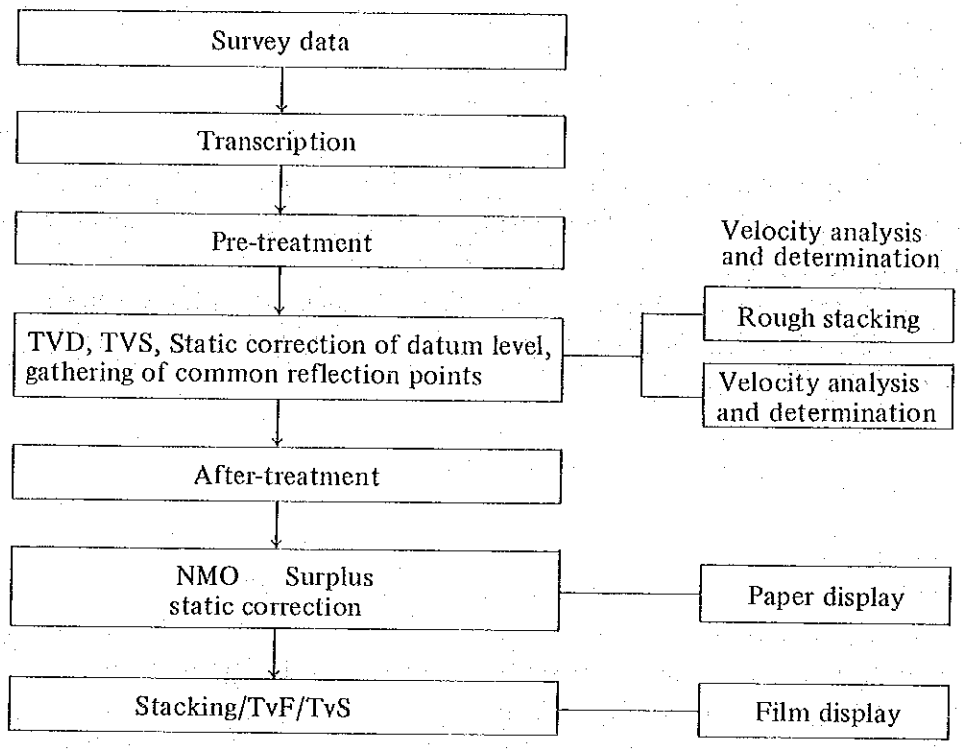

Fig. II.2.2-5 Process of stack treatment

3-2-2 Wave analysis on the stacking records

Of the waves on the stacking records, there are some waves which are obviously thought to be reflected from the boundary surfaces of the layers, viewing from the continuity of phases, while the other waves are also recognized.

There are the crossing waves by side reflection in the shallow part, as afore-stated in the paragraph 3-1-3, the diffracted waves in paraboloid-like form from the diffraction sources, and the anomalous waves whose frequency and amplitude are varied, compared to those in the peripheral zone.

If they are charged with some information from the underground, it is thought that they would compose a mean for the interpretation of the structure in the underground. From this point of view, the waves on the stacking records were employed as the data for the elucidation of geological structure, after the following treatment was applied.

(1) Frequency distribution

Concerning the frequency components expressed on the stacking records, waves of 10 ~ 60 Hz are emphasized, and most of the other waves have been eliminated by filtering. Therefore, the frequency distribution was considered by the division as follows.

Table II.2.2-2 Division of frequency

Range of frequency	Division
under 20 Hz	low frequency domain
over 20 Hz	high frequency domain

(2) S-N ratio distribution

The half wave amplitudes of the Variable area expressed on the stacking records (value of half wave amplitude is bigger than actual amplitude, as the base is in some way to (−) side) are classified as follows.

Table II.2.2-3 Division of S-N ratio

Range of half wave frequency	Division
under 2.0 mm	low S-N ratio area
over 2.0 mm	high S-N ratio area

(3) Distribution of diffraction sources

The part where faults and cracks are concentrated in the underground is thought to be the changing point of geological structure, undulation of beddings and porosity of the beds.

At the changing point as this, properties of one side are different from those of the other side, and the diffraction sources accompanying waves along parabola-like line are recognized.

This distribution of diffraction sources is thought to have important informations to detect fault structures.

In the present analysis, near surface structures are pursued by side reflection and deep structures were considered by the distribution of diffraction sources.

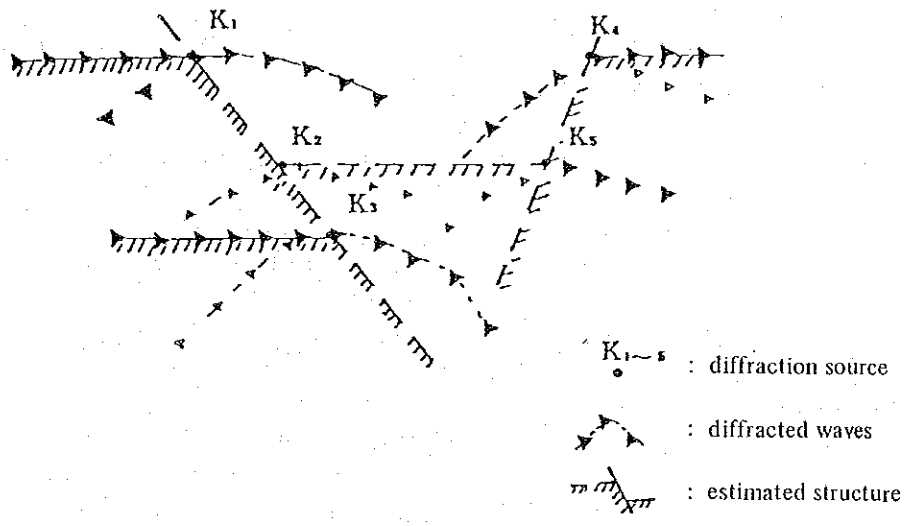

Fig. II.2.2-6 Diffraction sources

3-2-3 Depth section analysis

Depth section map was drawn up, by utilizing profiles of Final stack (Depth section) and Final stack time section, and by giving consideration to the continuity and intensity of the reflected wave phases.

On this treatment, making use of the above two profiles for deep structure and shallow structure analysis, horizons of L1 ~ L8 were assumed by connecting such reflecting layers as having comparatively remarkable continuation.

The fault structures cutting these assumed layers were estimated from the Side reflection distribution map expressing flat faces in the shallow part and from the Diffraction sources distribution map expressing the distribution along the section in the deep part. As the result, existence of total 11 fault structures marked by the symbols from (P) to (Z) has been estimated.

3-2-4 Structure analysis on plans

For the sake of the comprehension of the underground structure in the surveyed area as a whole, trend of the two assumed horizons of L4 and L8 in the Diffraction sources distribution map are expressed on plans of structure analysis.

On the Structure analysis map (PL. II.2.2-44, 45), are described the contour lines of every 500 meters above and below the datum level (DL = 300 meters above sea level) as well as faults, fractures, anticlines and synclines estimated in each of the above layers.

Another two plans of Deep structure analysis map (PL. II.2.2-46, 47) were drawn up, in which the assumed horizons at the levels of −1000 m and −2000 m below the datum level are expressed as well as the distribution of structure and the information of waves.

4. Results of the survey

4-1 Shallow structure by refraction method

Three-layered structure analysis with refraction method was executed by the initial motion travel time on the records of the field measurement. The principal characteristics obtained by the results of this analysis are as follows.

(1) Velocity distribution of every velocity layer along each survey line varies in comparatively wide range, which is shown in the following table.

Table II.2.2-4 Velocity distribution of subsurface velocity layers

Velocity layer	Velocity (m/s)	Remarks
No. 1 layer	400	Surface soil distributed in this layer, generally
No. 2 layer	2,050 ~ 2,800	Upper weathered zone, distributed in low velocity area around the crossing points of A and D survey lines
	2,300 ~ 3,700	Upper weathered zone, distributed in middle to high velocity area, generally
No. 3 layer	2,900 ~ 4,000	Mainly the basement underneath the low velocity area of No. 2 layer
	4,100 ~ 5,900	Basement underneath the middle to high velocity area of No. 2 layer.

(2) The depressed part of the equal velocity distribution curves is suggesting the area of lower velocity compared to the surrounding area, while the swelled part indicates the area of higher velocity. Especially it is noted that this area of low velocity is interpreted to correspond to alteration zone, fracture zone, fissilitic beds or lithological soft ground. It is not certain to which of the aboves it is actually corresponding.

(3) The near boundary between the low velocity area and the middle to high velocity area above-mentioned is comparatively well correspondent to parts of the side reflection analysis points stated in 4-2 paragraph.

(4) Subsurface velocity distribution

The subsurface velocity distribution was considered using the velocity of the No. 3 layer of the refraction analysis data. The velocities were divided into three groups as shown below and the Weathering layer velocity distribution map (PL. II.2.2-3) was drawn according to this division.

Table II.2.2-5 Division of velocity

Velocity division (km/s)	Velocity zone
under 4.0	low velocity zone
4.0 ~ 4.7	middle velocity zone
over 4.7	high velocity zone

The following items are clarified with the Weathering layer velocity distribution map.

1. Velocity zones are distributed in almost north-south direction. The eastern part of the surveyed area is high velocity zone, while the western part is low velocity zone.

2. The middle velocity zone, which is found in the central part of the surveyed area, is distributed between the high velocity zone in the eastern part and the low velocity zone in the western part. The area of the middle velocity zone narrows rapidly toward the south from the north. The width of the middle velocity zone is as much as 1,000 meters around the crossing point of A and C survey lines. In the high velocity zone in the eastern part, a middle velocity zone of the width of 300 to 400 meters and a low velocity zone as wide as 150 to 200 meters are recognized.

3. The direction of the boundaries of low middle and high velocity zones is almost correspondent to the direction of side reflection.

4. The surface trend of the No. 3 layer, expressed by contour lines in the Weathering layer velocity distribution map (PL. II.2.2-3), reveals repetition of depression and uplift. It seems that several inferred faults, estimated in the Time section map (PL. II.2.2-31 ~ 35), are located on the steep slope composed of such uplift and depression.
   The area where the geothermal indications are distributed in the surveyed area (the area surrounded by the survey lines of A, B and C) is also distributed on the steep slope.

4-2 Direction of shallow structure by side reflection

Assuming that the steeply inclined continuous phases on the stacking record would be side reflection, the direction was analysed. The characteristics obtained from the results of this analysis are given below.

(1) It was recognized that the included angle ($\theta°$) between each survey line and shallow structure lines which were estimated to be side reflection varies as widely as 20° ~ 80°.

(2) They are symmetrical in both sides of each survey line. Taking the one of the symmetric points a reflecting point (real image), the other is regarded to be a virtual image, but when the frequency distribution of the included angle $\theta°$ is expressed with the interval of 10°, it is as shown in the following figure (Fig. II.2.2-7).

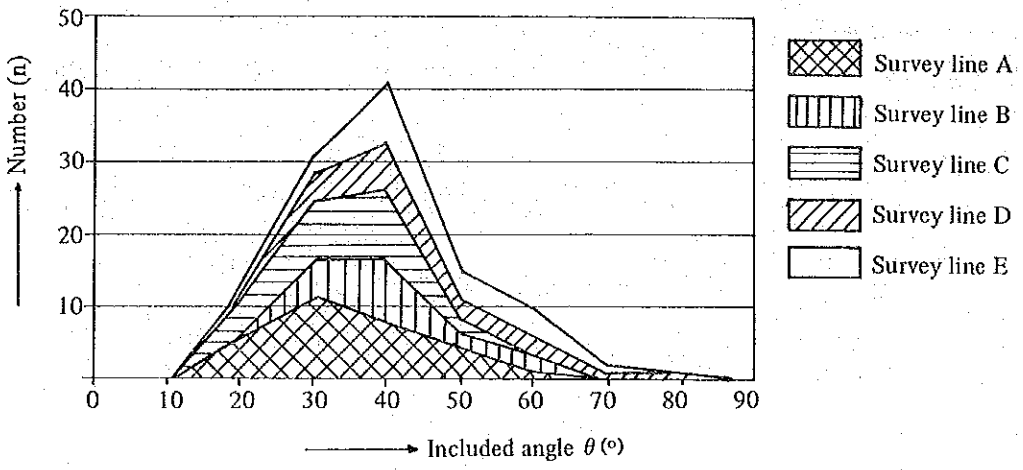

Fig. II.2.2-7 Frequency distribution of included angle $\theta^{(\circ)}$

From this Fig. II.2.2-7, predominant area of distribution of the included angles along each survey line is shown as follows.

Survey line A = 20° ~ 50°
Survey line B = 30° ~ 40°
Survey line C = 20° ~ 40°
Survey line D = 30° ~ 40°
Survey line E = 40° ~ 60°

(3) The angles of the principal side reflection to the true north are shown in the following figure (Fig. II.2.2-8).

By this figure the main directions of the structure lines represented by the side reflection are mostly N-S and NE-SW. It is thought that the side reflection would be caused either by fault structures or by beddings, viewing from their directions.

(4) It is thought that the crossing point of a survey line and the extension of a side reflection is correspondent to the point where a structure line crosses the survey line. Especially the point,

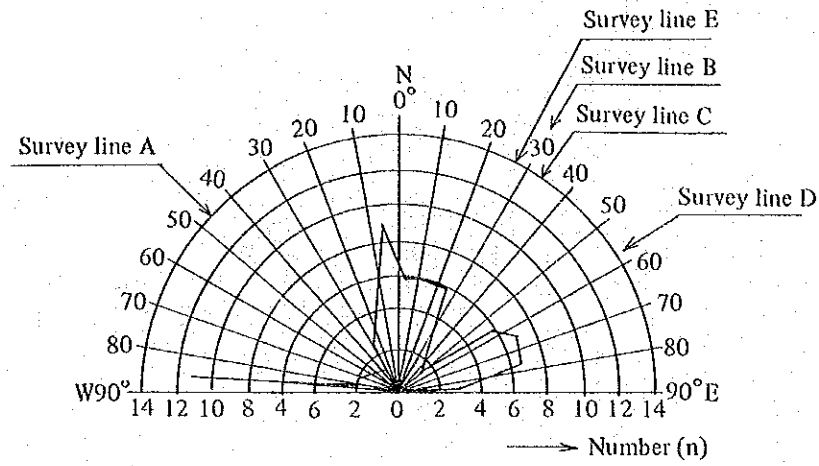

Fig. II.2.2-8 Frequency distribution of the direction of side reflection

around where several side reflections are entangled, has high probability to be. Viewing from the fact that most of the boundary surfaces of low, middle and high velocity zones are distributed around the above-stated points, the correlation is thought to be high.

(5) The included angles $\theta^{(o)}$ of the side reflections, though it is variable according to the difference of the values of the propagated velocity of reflected waves, are concentrated mostly in the range of 20° ~ 50°. On the stacking records, the detection of reflected waves with such included angles as in the range of 20° ~ 50° is possibly easier than those out of the range. Therefore, it is necessary for the interpretation of these matters, to give synthesized consideration by taking other data and information into account.
The table for the side reflection analysis is given as follows (Table II.2.2-6).

The velocity of the seismic wave for the analysis is Vw_1 = 1,500 ~ 2,500 m/s and Vw_2 = 3,000 m/s, which were obtained from the analysis results by the refraction method.

Table II.2.2-6 Side reflection analysis (1)

Survey line A

Symbol		Survey point	Difference of travel time Δt (sec)	Distance Δx (m)	Included angle between reflected surface and survey line	
					Vw_1=1,500 ~2,500(m/s)	Vw_2= 3,000(m/s)
A	1	18	0.07	95	33.5	–
	2	18	0.31	455	30.7	–
B	1	29	0.23	295	51.2	–
	2	29	0.30	460	40.7	78.0
C	1	46	0.21	360	35.7	61.0
	2	46	0.34	420	54.1	–
D	1	51	0.27	395	43.1	–
	2	51	0.33	472	44.4	–
E	1	63	0.37	374	81.6	–
	2	63	0.27	345	51.5	–
F	1	70	0.45	378	63.2	–
	2	70	0.33	442	48.3	–
G	1	85	0.44	445	47.9	–
	2	85	0.27	410	29.6	81.0
H	1	106	0.26	420	27.7	68.2
	2	106	0.29	450	28.9	75.2
I	1	115	0.34	364	44.5	–
	2	115	0.36	474	24.3	55.4
J	1	125	0.50	565	41.6	–
	2	125	0.20	400	22.0	48.6
K	1	142	0.36	470	35.1	–
	2	142	0.21	420	22.0	48.6
L	1	148	0.36	410	41.2	–
	2	148	0.21	462	19.9	43.0
N	1	162	0.43	560	73.7	–
	2	162	0.24	488	37.9	47.5
O	1	172	0.33	465	32.2	–
	2	172	0.24	443	24.0	54.4
P	1	202	0.33	472	31.6	–
	2	202	0.13	213	27.2	66.3
Q	1	215	0.40	543	33.5	–
	2					

Table II.2.2-6 Side reflection analysis (2)

Survey line B

Symbol		Survey point	Difference of travel time Δt (sec)	Distance Δx (m)	Included angle between reflected surface and survey line	
					Vw_1=1,500 ~2,500(m/s)	Vw_2= 3,000(m/s)
A	2	0	0.53	480	55.9	–
B	1	10	0.09	105	40.0	–
	2	10	0.33	550	26.7	64.2
C	1	23	0.23	330	31.5	–
	2	23	0.24	360	30.0	90.0
D	1	30	0.32	405	36.3	–
	2	30	0.33	385	40.0	–
E	1	35	0.34	372	43.3	–
	2	35	0.32	402	36.7	–
F	1	39	0.31	325	45.7	–
	2	39	0.26	343	34.6	–
G	1	48	0.41	496	38.3	–
	2	48	0.30	355	39.3	–
H	1	61	0.43	530	37.5	–
	2	61	0.26	318	37.8	–
I	1	77	0.35	470	34.0	–
	2	77	0.04	63	28.4	72.2
J	1	80	0.44	382	59.8	–
K	1	82	0.66	378	–	–

Survey line C

Symbol		Survey point	Difference of travel time Δt (sec)	Distance Δx (m)	Included angle between reflected surface and survey line	
					Vw_1=1,500 ~2,500(m/s)	Vw_2= 3,000(m/s)
A	1	9	0.11	132	38.7	–
	2	9	0.33	444	33.9	–
B	1	20	0.21	314	42.0	–
	2	20	0.30	386	51.0	–
C	1	26	0.30	520	35.2	59.9
	2	26	0.23	362	39.4	72.4
D	1	37	0.27	350	35.4	–
	2	37	0.19	320	26.4	63.0

Table II.2.2-6 Side reflection analysis (3)

E	1	42	0.30	378	36.5	–
	2	42	0.17	336	22.3	49.4
F	1	49	0.18	290	27.7	68.6
	2	49	0.30	488	27.5	67.2
G	1	53	0.23	353	29.3	77.8
	2	53	0.20	378	23.4	52.5
H	1	59	0.20	384	23.0	51.4
	2	59	0.12	245	21.6	47.3
I	1	65	0.23	500	20.2	43.6
	2	65	0.17	285	26.6	63.5
J	1	74	0.37	530	31.6	–
	2	74	0.05	80	28.0	69.6

Survey line D

Symbol		Survey point	Difference of travel time Δt (sec)	Distance Δx (m)	Included angle between reflected surface and survey line	
					Vw_1=1,500 ~2,500(m/s)	Vw_2= 3,000(m/s)
A	2	1	0.38	430	41.5	–
B	1	11	0.15	175	40.0	–
	2	11	0.36	422	39.8	–
C	1	20	0.25	336	33.9	–
	2	20	0.34	410	38.5	–
D	1	25	0.21	286	33.4	–
	2	25	0.32	453	32.0	–
E	1	32	0.27	408	29.8	83.1
	2	32	0.24	510	20.7	44.9
F	1	40	0.29	425	58.5	–
	2	40	0.26	372	60.9	–
G	1	46	0.30	316	71.7	–
	2	46	0.19	300	52.3	71.8
H	1	56	0.23	375	37.8	66.9
	2	56	0.17	283	36.9	64.3
I	1	65	0.38	423	63.9	–
	2	65	0.11	190	35.4	60.3
J	1	76	0.35	345	–	–

Fig. II.2.2-6 Side reflection analysis (4)

Survey line E

Symbol		Survey point	Difference of travel time Δt (sec)	Distance Δx (m)	Included angle between reflected surface and survey line	
					Vw_1=1,500 ~2,500(m/s)	Vw_2= 3,000(m/s)
A	2	1	0.36	490	47.3	–
B	1	6	0.08	91	61.5	–
	2	6	0.34	468	46.6	–
C	1	18	0.24	270	62.7	–
	2	18	0.28	460	37.5	65.9
D	1	31	0.26	324	37.0	–
	2	31	0.26	418	27.8	68.9
E	1	43	0.26	303	59.1	–
	2	43	0.29	442	41.0	79.3
F	1	56	0.36	415	40.6	–
	2	56	0.25	412	27.1	65.5
G	1	64	0.32	340	70.3	–
	2	64	0.21	335	38.8	70.1
H	1	75	0.33	424	51.1	–
	2	75	0.24	410	35.8	61.4
I	1	90	0.25	294	58.3	–
	2	90	0.17	228	48.2	–
J	1	99	0.24	308	35.8	–
K	1	108	0.29	350	38.4	–

4-3 Distribution of diffraction sources on the final stack (Time section)

Several diffracted waves are recognized in the final stack (Time section). Some of them are scattered very irregularly, while others are distributed in comparatively continuous forms in the perpendicular direction. The diffracted waves whose continuation is especially remarkable are estimated to represent planes of comparatively probable discontinuity, that is, fault structures. The peak of their frequency distribution in the perpendicular direction is at about 0.7 ~ 1.1 second (−1,500 ~ −2,500 meters below the datum level) and the frequency decreases gradually in the portion deeper than the peak. In this decreasing zone, the second and the third peaks are at 1.5 ~ 2.0 sec (−3,600 ~ −5,200 meters below the datum level) and at around 2.5 sec (−7,000 meters below the datum level).

The peaks as shown below are recognized along the respective survey lines.

A line RP, 13, 20, 39, 58, 93, 133, 187, 206,
B line RP, 10, 19, 23, 40, 75,
C line RP, 7, 21, 40, 61, 75,
D line RP, 9, 40, 50, 72,
E line RP, 10, 47, 73, 95,

RP: receiving point

There are several continuous distributions of the diffracted sources at around these peaks, some of which were marked by the symbols from (P) to (Z) and used for the deep structure analysis. Distribution of the low frequency domains (under 20 Hz) was also expressed in this figure.

Of the faults of (P) to (Z), those which were estimated by the seismic survey were 4 faults of (P), (R), (V) and (Y). Other faults were corresponding to the faults confirmed by the geological survey, in the points of their locations and directions.

Of the faults of (P) to (Z), those around which low frequency domains were recognized are as follows.

A line S, U, V, X,
B line S, T, U, V,
C line S, T, U, V,
D line Q,
E line –

4-4 Temperature distribution at the bottom of the holes

Temperature was measured at the bottom of the shot holes drilled in this survey. The measured temperature was generally 18° ~ 33°C. Using the result of this temperature measurement, the Temperature distribution map at the depth of 10 m (PL. II.2.2-15) was made, referring to the temperature distribution map in and around the area where the geothermal indications are distributed, prepared by the Thailand side. The followings are thought to be interpreted from this map.

(1) The values of the temperature were divided into following three groups, for consideration.

1) under 20°C

2) 20° ~ 30°C
3) over 30°C

(2) The high temperature values were found only between SP23 and SP28 of the survey line B and between SP1 and SP5 of the survey line E.

(3) Around the center of the high temperature zone, located near GTE-2 in the northwestern part of the surveyed area, concentric temperature structure is found, where the further the area is from the center, the lower the temperature goes down.

(4) The low temperature zone is found surrounding the above-stated high temperature zone, from the northeast to the southwest. In this low temperature zone, such areas of high and medium temperature are found distributed repeatedly in short range along the survey line A, whose trend of distribution is in N-S direction or in NW-SE direction. Their directions are similar to the direction of the main structure lines.

4-5 Wave analysis on the stacking records

It is an important mean, for the comprehension of the geological structure such as stratigraphy and faults, to detect continuity and phase variation of reflected waves from the reflection seismogram.

Meanwhile, it is effective for the estimation of geothermal indications or properties of geological layers to consider over frequency, amplitude and their variation of reflected waves.

The content and method of the present wave analysis using the stacking records are given in the following table (Table II.2.2-7).

Table II.2.2-7 Outline of wave analysis

Type of analysis	Result	Application	Method
Wave analysis trace type (LH group)	Frequency-Time curve Amplitude-Time curve Frequency-Fourier curve Amplitude-Frequency curve Amplitude-Fourier curve	comprehension of wave properties	Digital analysis by electronic computer
	Fourier analysis or Power analysis	as above	Digital analysis by electronic computer
Wave analysis profile type (each survey line)	Frequency distribution S-N ratio distribution	judgement of geothermal source and alteration zone	Digital analysis by electronic computer
Side reflection analysis (each survey line)	Side reflection analysis map Side reflection distribution map	judgement of boundaries of layers and formations and judgement of structure lines	Reading with eyes
Diffraction source analysis profile type (each survey line)	Diffraction source distribution map Diffraction compilation map	as above	as above

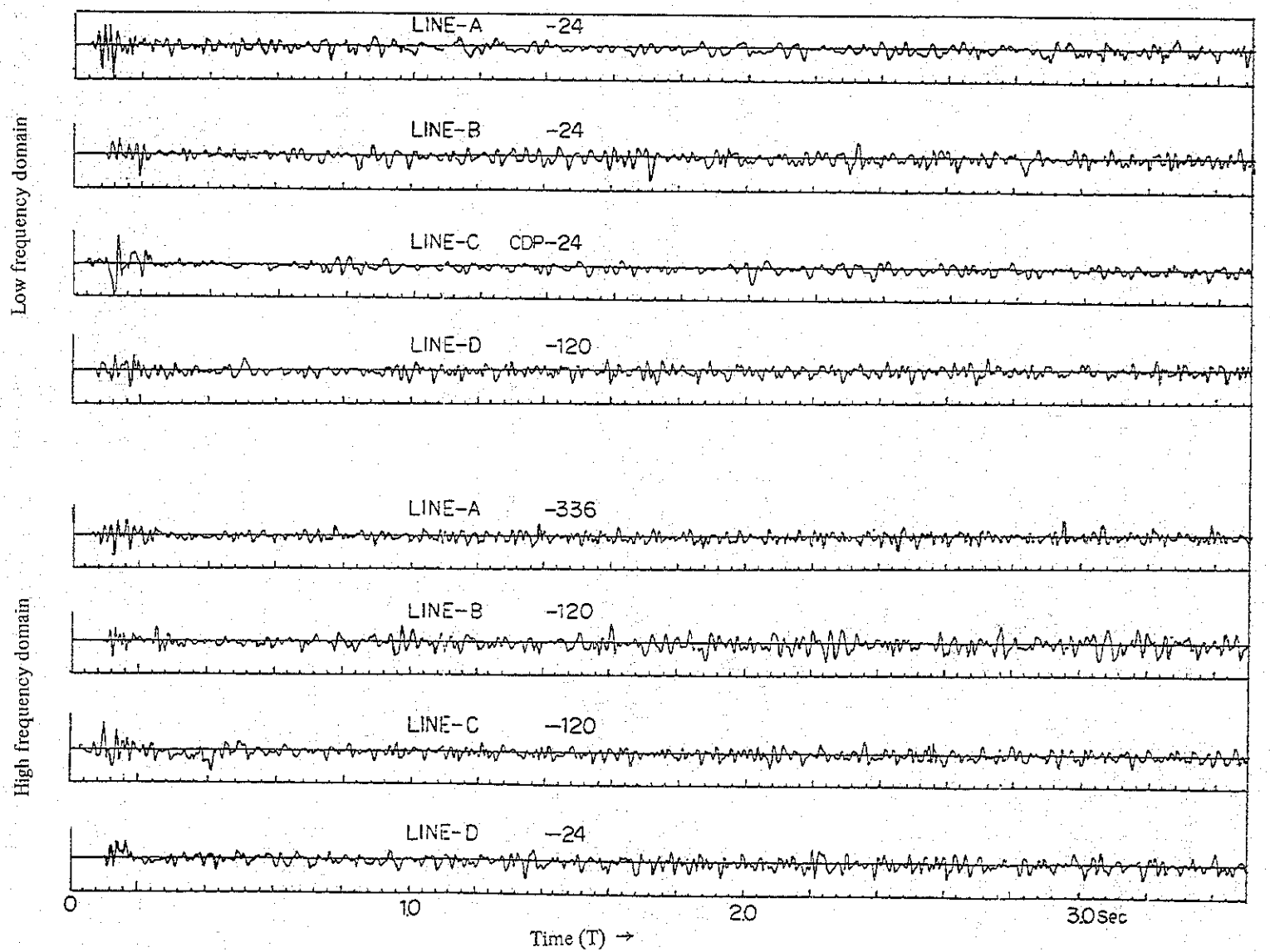

Fig. II.2.2-9 Wave curve on the stacking records

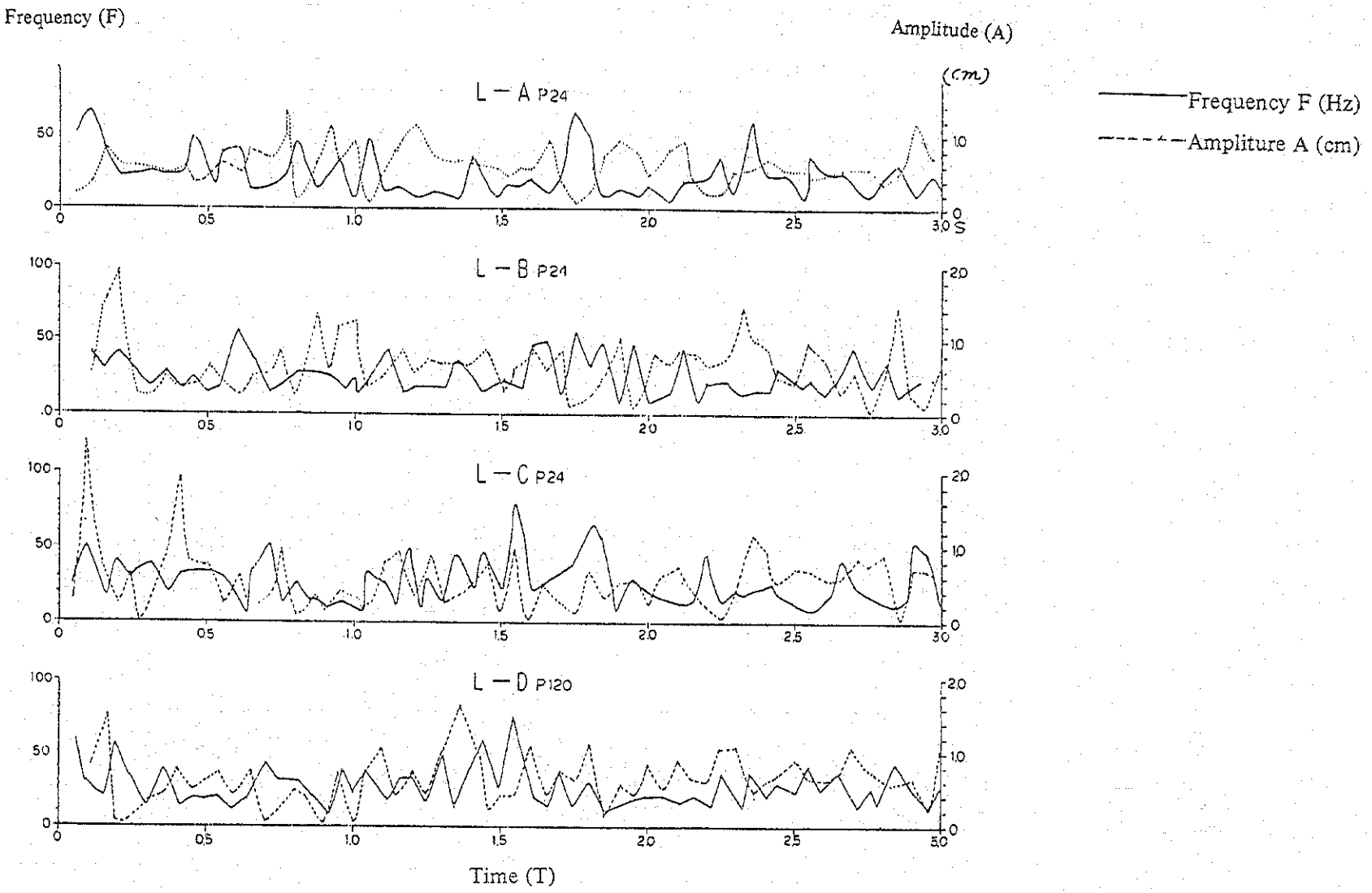

Fig. II.2.2-10 Time variation of amplitude and frequency on the stacking records (low frequency domain)

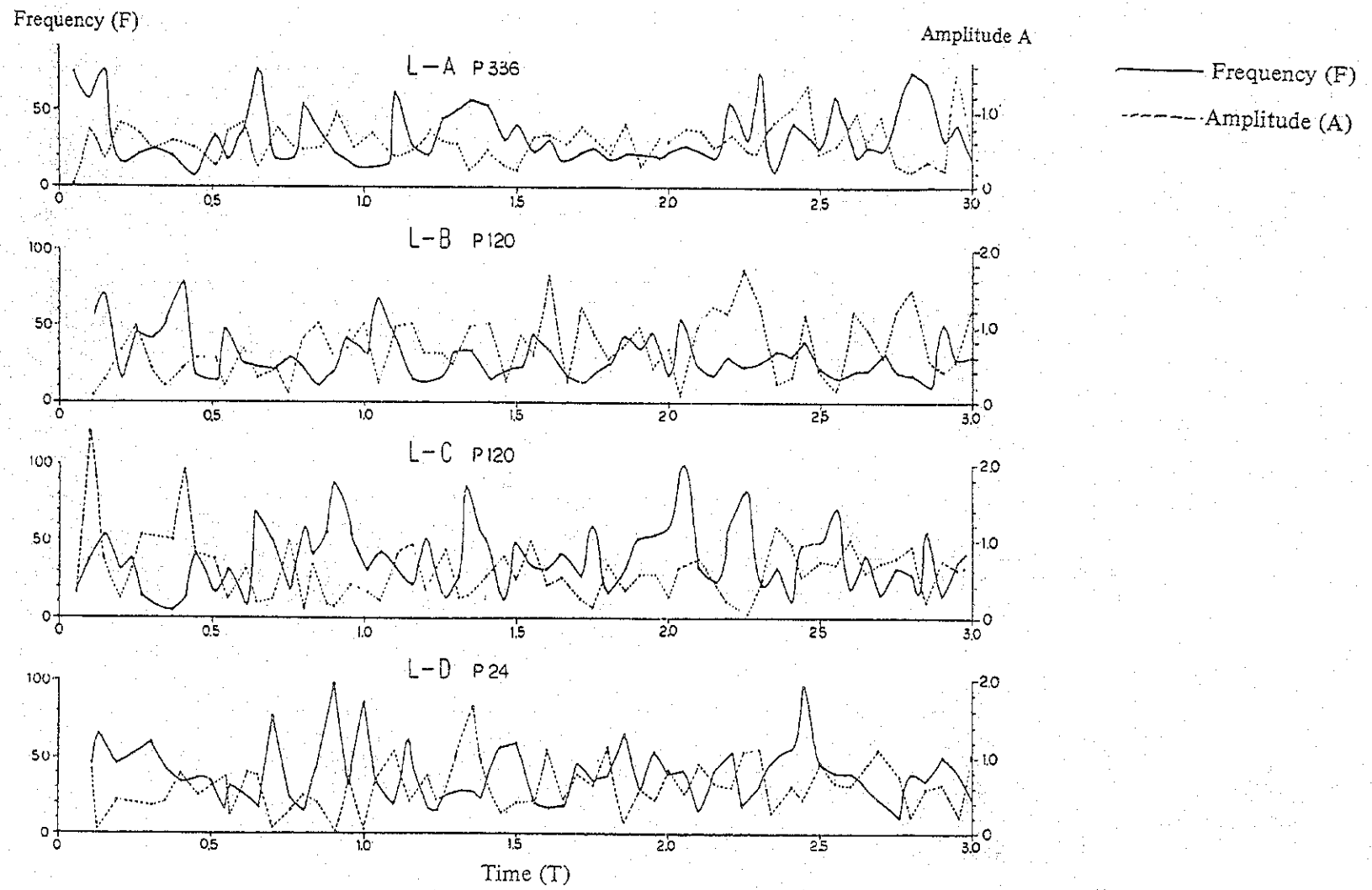

Fig. II.2.2-11 Time variation of amplitude and frequency on the stacking records (high frequency domain)

4-5-1 Wave analysis on the stacking records

Of the Frequency distribution map (Fig. II.2.2-14,15) by the stacking records of Table II.2.2-7, several traces of every low-high frequency domain (L ~ H) were selected and wave analysis on the traces was executed. In this analysis, properties of the waves were considered at every 0.1 sec in the time domain between 0.0 and 3.0 sec, and the wave power spectrum analysis was carried out in T = 0.0 ~ 3.0 on the trace.

(1) Variation of frequency and amplitude.

The frequency, amplitude–time curves of the waves are given as follows (Fig. II.2.2-12,13).

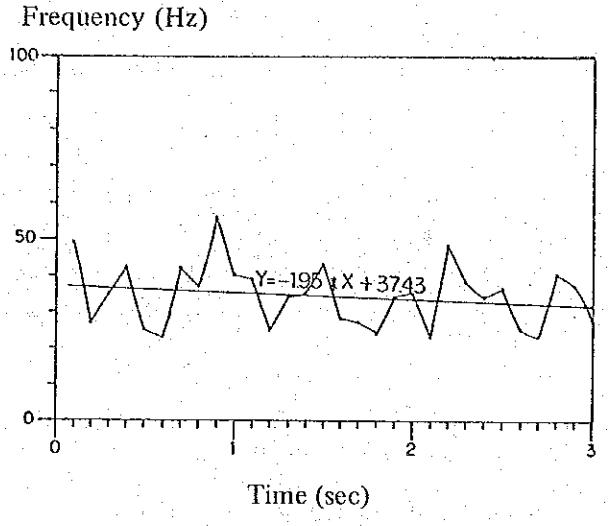

Fig. II.2.2-12 Frequency – Time curve

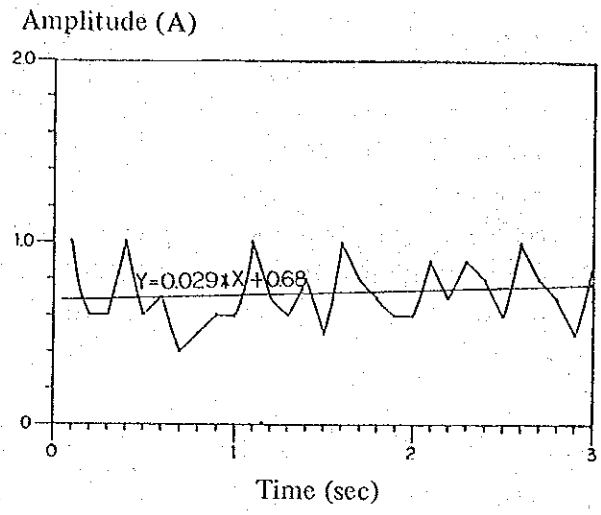

Fig. II.2.2-13 Amplitude – Time curve

In the Fig. II.2.2-11, the frequency decreases gradually or becomes flat with the passage of time, generally. But there are several varying points recognized in the trend of distribution. Low frequency waves are predominant in 0.4 ~ 0.6 sec and in 1.5 ~ 1.8 sec, while high frequency waves are in 2.2 ~ 2.4 sec. It is thought that the former low frequency domain is composed mostly of signal and its concerns while the latter is composed of noises rather than signals.

Amplitude, on the contrary, increases gradually or reveals almost flat distribution. However, as a whole, there is a tendency that low frequency domain is correlated to high amplitude domain. It is expected that remarkable layer of reflected waves exists around the above low frequency domains.

Generally, reflecting surface is a boundary plane where sonic impedance P varies, and reflection coefficent K is given by the following formula.

$$K = \frac{\rho_2 V_2 - \rho_1 V_1}{\rho_2 V_2 - \rho_1 V_1}$$

Here ρ_1, ρ_2 ; density of rock in both sides of the boundary

V_1, V_2 ; velocity of elastic wave (P wave) in both sides of the boundary

Intensity of reflecting energy and relation between reflected wave and incident wave are determined by the above reflection coefficient K, and reflection phenomena appears remarkably

in such area as the variation of ρV values is great. It is expected generally that the boundaries of reservoir, cap rock, basement etc. have wide variation of ρV values, in geothermal area.

(2) Summing up the appearance frequency of frequency in each class of every 2 Hz, the histogram is given in the following frequency fourier distribution (Fig. II.2.2-14,15).

According to the histogram, there are three or four peaks of frequency represented by P (18 ~ 23 Hz), P_2 (35 ~ 39 Hz), P_3 (~ 49 Hz) and P_4 (59 ~ 61 Hz) in the fourier distribution of frequency in both of the low and high frequency domains. In the low frequency domain, the peak of P_1 is the most distinguished, which is followed by the peaks of P_2 and P_3.The frequency of the peak of P_4 is fairly less than that of the above three peaks. It is notable that almost same number of the frequency is recognized with the peaks in the high frequency domain, generally.

The main frequency domain of the reflected waves is thought to be about 10 ~ 50 Hz, according to the tendency shown in this histogram. Taking the peaks of P_1 ~ P_3 as signals (S) and the peak of P_4 as noises (N), the S-N ratio of both of high and low frequency domain is estimated to be about 3.8 ~ 6.5, on the assumption that the S-N ratio of the reflected waves is correspondent to the formula of $(NP_1 + NP_2 + NP_3/NP_4$, which is calculated by the number of peaks NPi (Table II.2.2-8). Frequency of 50% F50 of the frequency accumulation curve and increasing rate $\Delta F = (F60 - F10)/50$ of frequency of the signals are also shown in the Table II.2.2-8.

Table II.2.2-8 S-N ratio in low and high frequency domains

Frequency domain	Frequency at peak (Hz)	S to be under 50 Hz, N to be over 50 Hz		
		S-N ratio estimated $(NP_1 + NP_2 + NP_3)/NP_4$	Frequency F50 of frequency commulative curve (Hz)	Increasing rate of frequency accumulation 10 ~ 60% ΔF
High frequency domain	$P_1 = 23$ $P_2 = 35$ $P_3 = 49$	(23 + 28 + 29)/20 = 3.85	37.3	0.52
Low frequency domain	$P_1 = 19$ $P_2 = 39$ $P_3 = 49$	(31 + 24 + 23)/12 = 6.50	32.7	0.50

(note) $\Delta F = (F60 - F10)/50$ (Hz/%)

By the table II.2.2-8, the average frequency F50 is about 33 ~ 37 Hz and as shown by the increasing rate of frequency ΔF, the frequency distributions of both of low and high frequency domains have similar pattern, with fair amount of scattering.

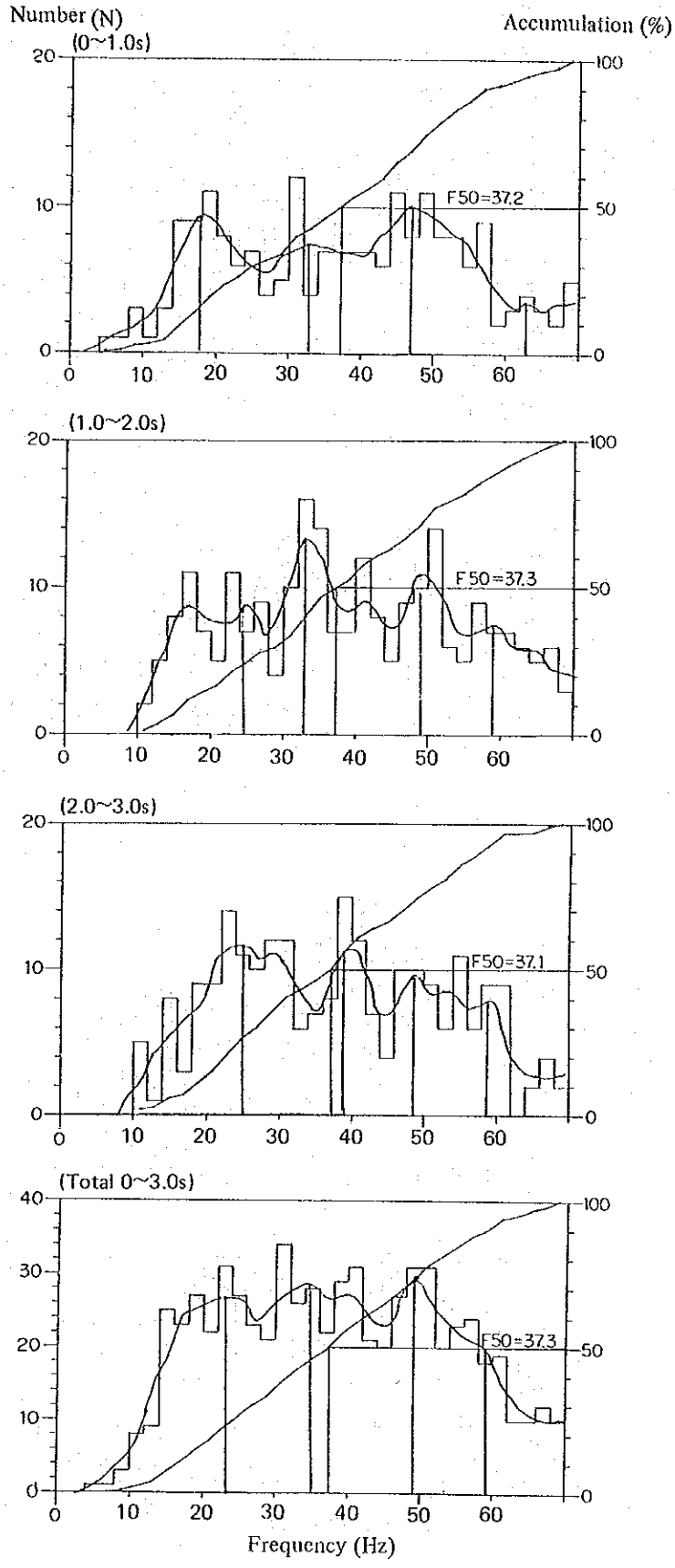

Fig. II.2.2-14 Histogram of frequency (high frequency domain)

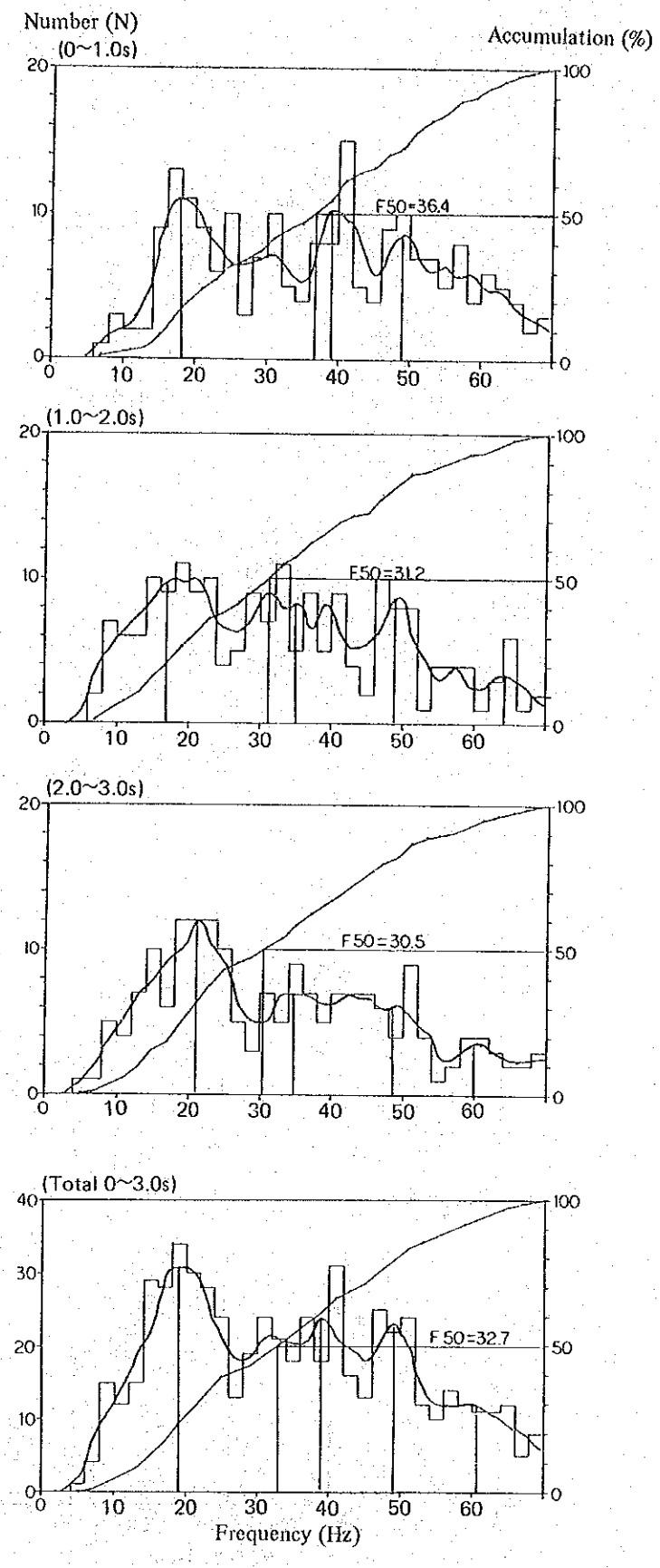

Fig. II.2.2-15 Histogram of frequency (low frequency domain)

(3) Relation between amplitude and frequency

The following figure was prepared for the relation between amplitude and frequency (Fig. II.2.2-16). By this figure, it is recognized that amplitude A decreases almost in the form of hyperbola with the increase of frequency.

$$A = 4.94\ F^{-0.665}$$

Here A : amplitude
F : frequency

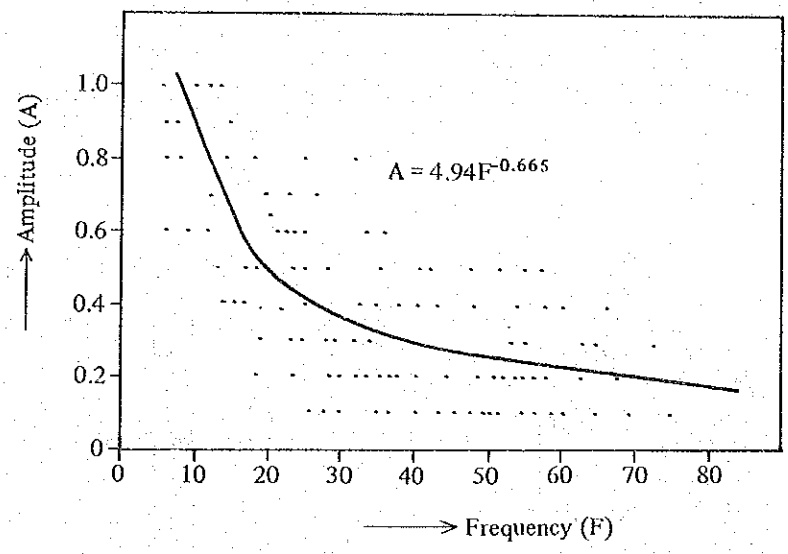

Fig. II.2.2-16 Relation between amplitude and frequency

4-5-2 Spectrum analysis of waves

Power spectrum analysis was carried out with the fundamental waves, composing part of waves on the stacking records, and their components. Four waves were selected from each of low and high frequency domains on the staking records for the analysis. They are all in 0.0 ~ 3.5 sec.

(1) Viewing tendency of the frequency distribution of the waves in the low frequency domain, the first peak is found around 7 ~ 15 Hz, the second peak is around 20 ~ 25 Hz and the third peak appears at around 35 Hz. Examining the spectrum in each trace, the first peak is hardly recognized in 24 ch of line B, but peaks are found in the area of the frequency of over 40 Hz. Other traces have similar tendency as this. That is, including line B-24 trace, the most remarkable peak is the second peak, followed by the peaks of the first and the third peaks.

(2) As for the waves in the high frequency domain, three peaks are recognized as is seen in the low frequency domain. The most remarkable peak is the second peak around 25 ~ 28 Hz, followed by the third and the first peaks. As a whole, they are distributed in higher frequency zone by about 10 Hz than those distributed in the low frequency domain.

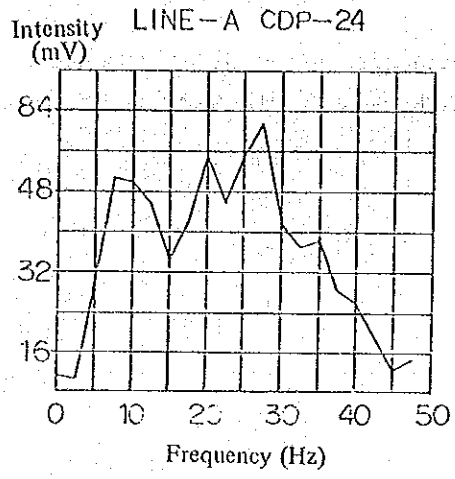

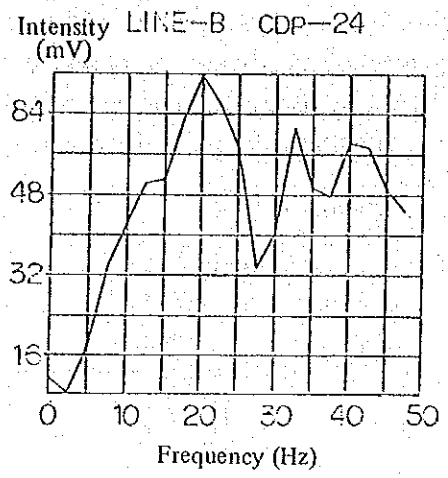

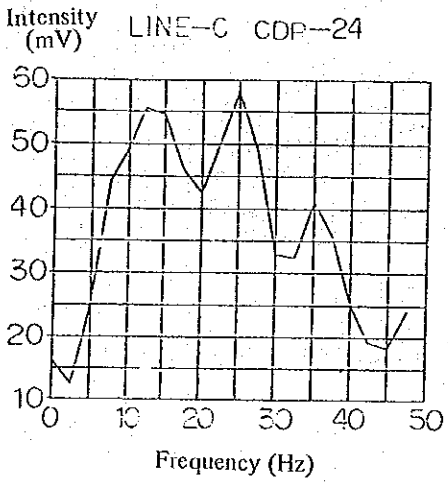

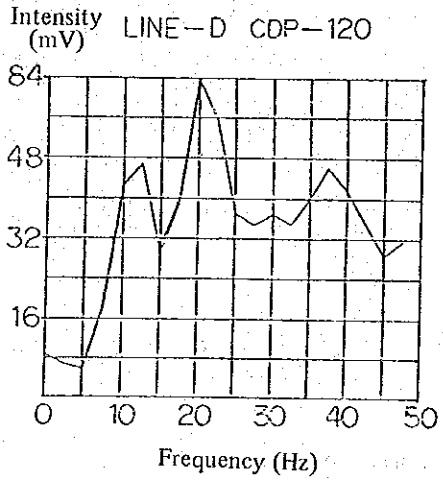

Fig. II.2.2-17 (a) Wave spectrum analysis (low frequency domain)

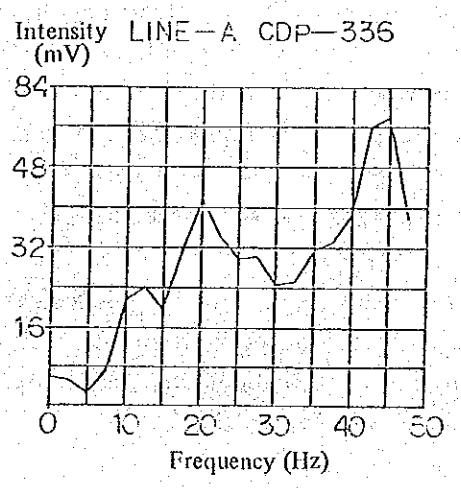

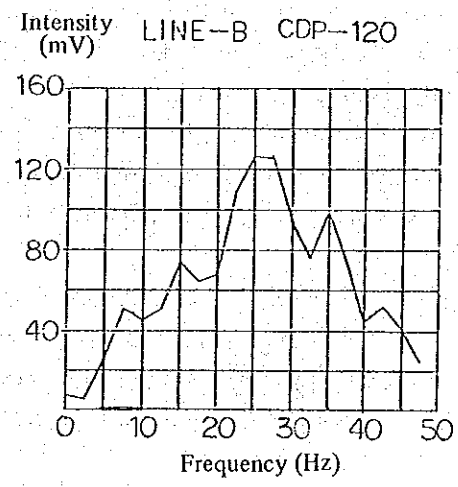

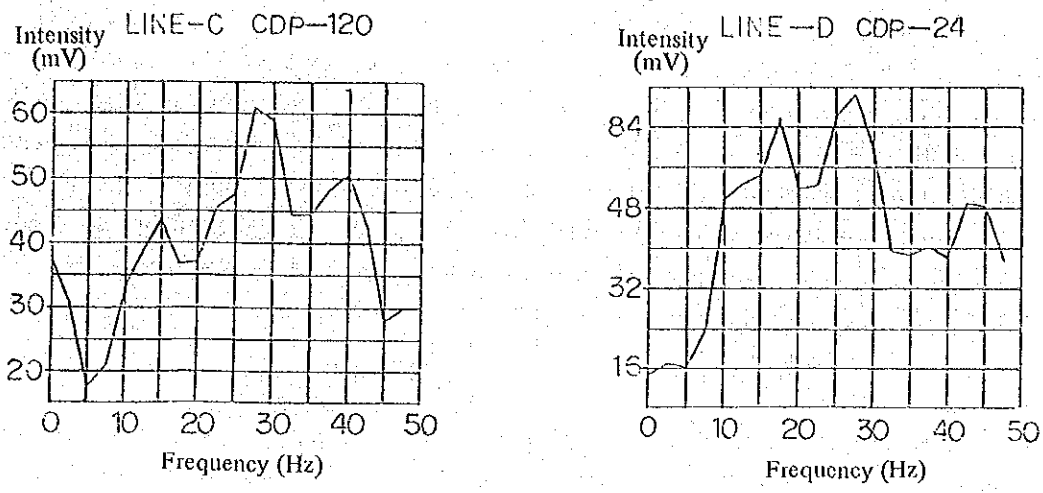

Fig. II.2.2-17 (b) Wave spectrum analysis (high frequency domain)

4-5-3 Characteristics and distribution of reflected waves

If the geological components are homogeneous physically, the reflection record would have a tendency that waves of high frequency are decreasing while those of low frequency would be left with the passage of time. However, the actual waves on the records have variations of frequency and S-N ratio in places. It is thought that some of these variations are corresponding to those related to the geology or the structure in the area the waves are propagated to.

Accordingly, it is required to consider the distribution forms of waves from the viewpoint of frequency and amplitude (S-N ratio).

(1) Frequency distribution

Frequency of the waves on the stacking records is divided into the following two groups (Table II.2.2-9). In the frequency distribution map (PL. II.2.2-26,30), the tendency of the frequency distribution is displayed. Generally, the tendency of the frequency distribution in each of the groups can be interpreted as follows, in correlation with geology and structure.

Table II.2.2-9 Outline of frequency distribution

Group	Frequency	Remarks
1	under 20 Hz	Predominantly distributed densely near intense alteration zone and fault structure mainly in perpendicular direction.
2	over 20 Hz	Mainly distributed in massive hard rocks with less amount of joint and cracks.

Tendency of the frequency distribution and its characteristics along each of the survey lines are given in the following.

1. Survey line A

Generally, low frequency domain of the frequency of under 20 Hz (the group 1) is distributed at the depth more than 0.5 sec, between RP 1 and RP 10, between RP 31 and RP 49 and between RP 60 and RP 70. The former two distributions have a tendency to extend in a columnar form in perpendicular direction and to be clustered along the faults of Ⓢ, Ⓤ and Ⓥ. The latter distribution between RP 60 and RP 70 has a tendency of scattering in vague columnar form. In most of the area south of RP 70, high frequency domain of the frequency of over 20 Hz (the group 2) is distributed, and the group 1 is found only sporadically.

2. Survey line B

The shallow part of 0.0 ~ 0.5 sec is occupied by the group 2 of the high frequency domain, as in seen in the survey line A. It is estimated that shallow part is composed of compact hard rock. Generally in the area of 0.5 ~ 1.5 sec, many of the crowded low frequency domain of the group 1 are found. Their distribution has a tendency to take flat and scattering form, poorly continuous to perpendicular direction. It is pointed out that the faults of Ⓡ, Ⓢ, Ⓤ and Ⓥ are along this group 1 of the low frequency.

In the part deeper than 1.5 sec, distribution of the group 2 is remarkable and the group 1 is found merely around RP 1 ~ RP 10 in the western part of the surveyed area. However they are not continuous upward.

3. Survey line C

In the area west of RP 15 in the central part of the survey line C, distribution of remarkable low frequency domain of the group 1 is recognized in columnar form, at the depth of more than 0.5 sec. Especially, around RP 1 ~ RP 6 in the western most part, the low frequency domain seems to be distributed continuously from the depth of more than 2.5 sec along the faults of Ⓢ, Ⓣ and Ⓥ. In the eastern part of the survey line, the group 1 is distributed flat in the shallow part of 0.3 ~ 0.5 sec, though the group 2 is distributed in most of this part.

4. Survey line D

Generally, the group 2 is distributed scatteringly at the depth of 0.2 ~ 0.6 sec in most part of this survey line. Around RP 1 ~ RP 5, a tendency of distribution in perpendicular direction at the depth of 0.1 ~ 0.6 sec, which is estimated to be caused by the Ⓠ fault, is recognized.

5. Survey line E

Along most of this survey line, the group 2 is distributed, though the group 1 is distributed in the shallower part than 0.4 sec in a narrow zone between the faults of Ⓠ and Ⓣ.

(2) Distribution of S-N ratio (amplitude)

Half wave amplitudes of the waves on the stacking records are divided into the following two groups, and the S-N ratio distribution maps (PL. II.2.2-21 ~ 25) have been drawn up to express the tendency.

Table II.2.2-10 S-N ratio

Group	Half wave amplitude	Remarks
1	over 20 Hz	related mainly with geological layer waves which are continuous laterally
2	under 20 Hz	correspond to the group 2 of the frequency distribution (high frequency domain) in many cases

Characteristics of the S-N ratio distribution are summarized in the following paragraphs.

1. Survey line A

High S-N ratio zones of the group 1 (half wave amplitude over 2 mm) are distributed densely in the part of 0.0 ~ 2.0 sec, generally. The distribution in almost flat and continuous forms are remarkable. In the areas between RP 1 and RP 10 and between RP 31 and RP 49, where low frequency domains are distributed, columnar forms of distribution continuous from the depth are recognized in many cases. At the depth deeper than 2.0 sec, low S-N ratio zones of the group 1 are distributed in flat form, amongst which the group 2 is scatteringly distributed.

2. Survey line B

Generally, the group 2 is distributed. Locally in the area west of RP 25, the group 1 is recognized to be distributed in the perpendicular direction at the depth of 0.0 ~ 1.0 sec. Relation between the S-N ratio and the frequency distribution is not recognized along the survey line.

3. Survey line C

The group 1 is distributed in the shallower part than 3.0 sec generally. This tendency is especially remarkable between L_3 horizon and L_5 horizon in the east of RP 15 (crossing point with A line). In the low frequency domain between RP 1 and RP 6, columnar distribution is dominant in perpendicular direction.

4. Survey line D

The group 2 is predominantly distributed in the shallower part than 0.5 sec, while in the part of 0.5 ~ 1.5 sec the group 1 is densely distributed. Flat continuity is recognized between L_3 horizon and L_5 horizon in the area west of the fault ⓧ.

5. Survey line E

The group 1 is distributed as a whole. This tendency is especially remarkable at the depth between L_1 horizon and L_2 horizon. In the deeper part that 1.5 sec, the group 2 is predominantly distributed in flat form. As above-mentioned, the forms of the low frequency domain and high S-N ratio zone, such as scattering type, flat type and columnar type, and the rate of their distribution seem to vary according to the area and to the depth. However, the differences of waves in the area where the above-noted signs are found are thought to be related to some geological and geothermal indications. Therefore, it is thought that they are notable informations for the elucidation of geological structure.

4-6 Deep structure by reflection method

Taking the remarkably continuous parts of the principal reflected waves on the Final stack time section (PL. II.2.2-16~20) and the Final stack (Depth section) to be reflection layer, several layers were assumed and deep structure analysis was executed upon this assumption.

4-6-1 Velocity distribution in perpendicular direction

Determination of the velocity distribution in perpendicular direction is the most important process of calculation for the deep structure analysis by reflection method. Although there are several methods to obtain average velocity in perpendicular direction, it is calculated generally on the basis of travel times and difference of travel times of the reflected waves, and data of well logging and result of velocity measurement of drilling cores are taken into the consideration, in many cases.

1. Average velocity in perpendicular direction

The average velocity was calculated from ΔT (Move out time) on the reflection records in this survey. The results of the velocity analysis at 2 to 4 places along each survey line are given in the following tables.

Table II.2.2-11 Result of velocity analysis

(A-line)

SP 7 – 8		SP 32 – 33		SP 57 – 58		SP 82 – 83	
(10^{-3} sec)	(m)	(10^{-3} sec)	(m)	(10^{-3} sec)	(m)	(10^{-3} sec)	(m)
0	4,000	0	4,000	0	4,000	0	4,000
700	4,500	770	4,440	850	4,250	950	4,500
1,450	4,760	1,430	4,750	1,500	4,700	1,700	4,850
2,620	5,580	2,530	5,500	2,500	5,400	2,500	5,200
4,000	6,200	4,000	6,200	4,000	6,200	4,000	6,150

(B-line)

SP 7 – 8		SP 27 – 28	
(10^{-3} sec)	(m)	(10^{-3} sec)	(m)
0	3,900	0	4,000
550	4,350	520	4,230
1,430	5,000	1,500	4,860
2,130	5,260	2,200	5,530
2,700	5,600	2,800	5,760
4,000	6,300	4,000	6,550

(C-line)

SP 7 – 8		SP 27 – 28	
(10^{-3} sec)	(m)	(10^{-3} sec)	(m)
0	4,000	0	4,000
900	4,750	1,000	4,820
1,570	5,080	1,600	5,100
2,200	5,400	2,200	5,480
4,000	6,000	4,000	6,300

(D-line)

SP 7 – B		SP 27 – 2B	
(10^{-3} sec)	(m)	(10^{-3} sec)	(m)
0	4,040	0	4,070
700	4,480	730	4,540
1,320	4,900	1,300	4,900
1,980	5,300	1,980	5,250
2,800	5,680	2,870	5,680
4,000	6,240	4,000	6,220

(E-line)

SP 7 – 8		SP 22 – 23		SP 37 – 38	
(10^{-3} sec)	(m)	(10^{-3} sec)	(m)	(10^{-3} sec)	(m)
0	3,940	0	4,000	0	3,980
250	4,010	200	4,130	300	4,130
900	4,420	800	4,450	830	4,400
1,530	4,660	2,000	4,950	1,680	4,860
2,500	5,050	2,900	5,600	2,680	5,340
4,000	6,100	4,000	6,150	4,000	6,100

Based on the results of the Table II.2.2-11, the relation between reflection travel time and average velocity is given in the following figure (Fig. II.2.2-18).

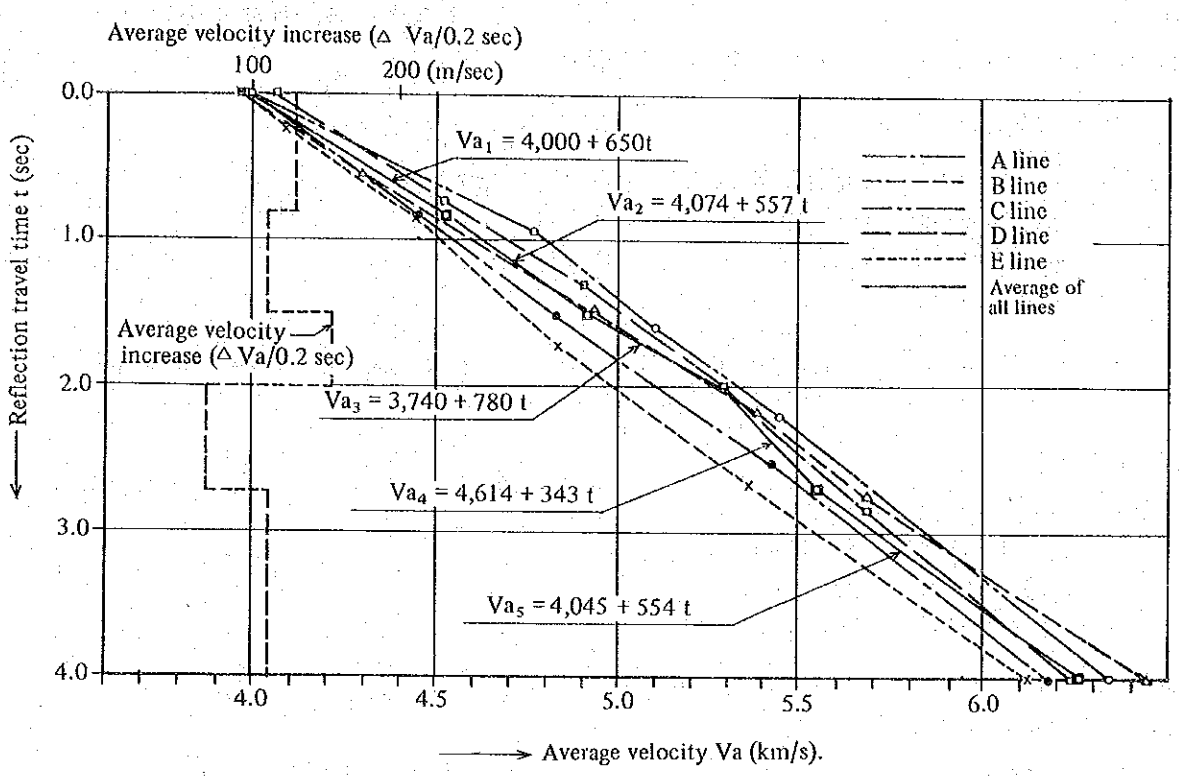

Fig. II.2.2-18 Relation between reflection travel time and average velocity

Mentioning about the general tendency of the relation between the reflection travel time (t) and the average velocity (Va) in this figure, though fair amount of difference is recognized according to the calculation points of each survey line, the initial velocity is Vo = 4,000 m/s near surface and is increasing toward the depth. The initial velocity reaches up to Va = 4.5 km/s at t = 0.8 sec of the reflection travel time, and Va = 6.3 km/s at t = 4.0 sec.

Table II.2.2-12 Reflection travel time, average velocity and average velocity increase

Average travel time t (10^{-3} sec)	Average velocity (m/sec)	Average velocity increase △Va (m/0.2 sec)
0	4,000	
		130
800	4,520	
		110
1,500	4,910	
		156
2,000	5,300	
		68
2,700	5,540	
		110
4,000	6,260	

The reflection travel time (t), the average velocity (Va) and the average velocity increase (Va/0.2 sec) are shown in Table II.2.2-12.

The relation between the average velocity (Va) and the reflection travel time (t) is given below in formulae with the relation of the average velocity to the travel time.

The relation between the average velocity Va and the reflection travel time t is given below in formulae with the relation of the average velocity to the travel time.

$$Va = Vo + (\alpha)t$$

Here Va : average velocity (m/s) at the reflection travel time t
Vo : average velocity (m/s) at the datum level
α : average velocity increase rate (m/s^2) below the datum level
t : reflection travel time (sec)

The relation of the average velocity to the reflection travel time is shown below in first degree formula.

$Va_1 = 4{,}000 + 650t$ (0 ~ 0.8 sec)
$Va_2 = 4{,}074 + 557t$ (0.8 ~ 1.5 sec)
$Va_3 = 3{,}740 + 780t$ (1.5 ~ 2.0 sec)
$Va_4 = 4{,}614 + 343t$ (2.0 ~ 2.7 sec)
$Va_5 = 4{,}045 + 554t$ (2.7 ~ 4.0 sec)

The characteristics of the distribution of the average velocity in these divisions are summarized as follows.

(a) The average velocity has bending points at the reflection travel time of t = 0.8, 1.5, 2.0 and 2.7 sec, by the change of increase rate of the average velocity, as shown by the above formulae of $Va_1 \sim Va_5$. The increase rate of the average velocity is highest between t = 1.5 and 2.0, while the lowest values are recognized in t = 2.0 ~ 2.7 sec.

(b) The average velocity increase ΔVa in each of 0.2 sec intervals of the reflection travel time is 110 ~ 130 m/0.2 sec between 0 and 1.5 sec and between 2.7 and 4.0 sec, as shown in Fig. II.2-2-12. Accordingly, it can be said to be the general tendency that the highest value is at about 1.7 sec, while the lowest value is at about 2.2 sec, with the repetition of gradual increase and gradual decrease around the highest and the lowest points.

(c) It is thought that the area around the changing points is correspondent to some geological borders or lithological boundaries.

(2) Layer velocity in perpendicular direction

The depth distribution in perpendicular direction, which is obtained from the average velocity stated in (1), is refered to in the following.

The layer velocity in perpendicular direction ($Vv = Vo + kZ$) is obtained from Z – t curve by the Milles's method (the formula given below).

$$Vo = kZ\frac{1}{e^{kT_1} - 1}$$

$$k = \frac{1}{T}\ln\left(\frac{Z_2 - Z_1}{Z_1}\right)$$

Here Z : arbitrary depth

Z_1 : depth for perpendicular travel time T_1

Z_2 : depth for perpendicular travel time T_2

T_1 : 1/2 of T_2 (1/2 of the reflection travel time)

k : increase rate of velocity

Here is shown, the results of the calculation of layer velocity in perpendicular direction from $T_2 = 0.2 \sim 2.4$ (sec), which are given in the relation formula of the depth and the reflection travel time subsequently stated (solid line of Z – T curve).

Table II.2.2-13 Calculation results of layer velocity in perpendicular direction

Perpendicular velocity (sec)		Depth (m)		Rate of increase K (1/sec)	Initial velocity Vo (m/sec)	Layer velocity Vv (m/sec)
T_1	T_2	Z_1	Z_2			
0.1	0.2	407	827	0.31	4,071	4,071 + 0.31Z
0.2	0.4	827	1,704	0.29	3,997	3,997 + 0.29Z
0.4	0.8	1,704	3,616	0.29	4,018	4,018 + 0.29Z
0.6	1.2	2,634	5,691	0.25	4,069	4,069 + 0.25Z
0.8	1.6	3,616	7,981	0.24	4,100	4,100 + 0.24Z
1.0	2.0	4,635	10,600	0.25	4,080	4,080 + 0.25Z
1.2	2.4	5,691	13,049	0.21	4,170	4,170 + 0.21Z
Average				0.26	4,072	4,072 + 0.26 Z

Vv(min) = 3,996 + 0.23Z
Vv(mean) = 4,072 + 0.26Z
Vv(max) = 4,193 + 0.27Z

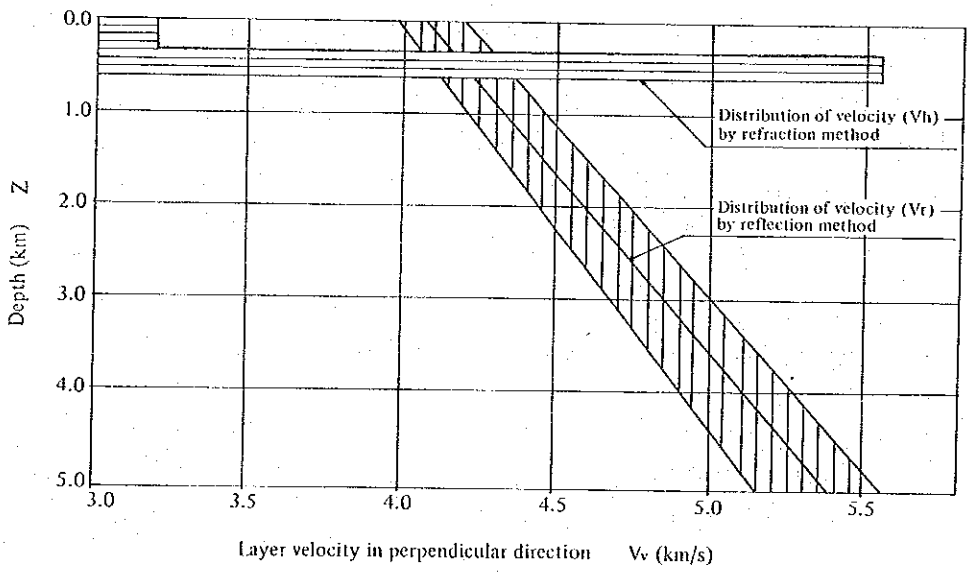

Fig. II.2.2-19 Rough distribution of layer velocity

The layer velocity in perpendicular direction Vv in this surveyed area is increasing linearly with the increase of the depth as shown in Fig. II.2.2-19, generally. The results of the above calculation are summarized below.

(a) The layer velocity Vv is distributed in the range similar to the distribution of the velocity obtained by the refration method Vh (mainly horizontal direction).

(b) Vv is included in the shadowed part in the Fig. II.2.2-19, although there is a tendency that the rate of increase of the velocity is rather high in the shallow part and low in the deep part.

(c) If the geological boundary between the granite and the Paleozoic formation is assumed at the level of −2,000 meters above sea level, the layered velocity is about 4.6 km/s, and if at the level of −3,000 meters, then it is about 4.8 km/sec.

4-6-2 Depth distribution in perpendicular distribution

In the following, is shown the relation between the reflection depth (Z) and the reflection travel time (t), which is obtained from the relation formula of the reflection travel time to the average velocity, mentioned in (1) (Fig. II.2.2-20).

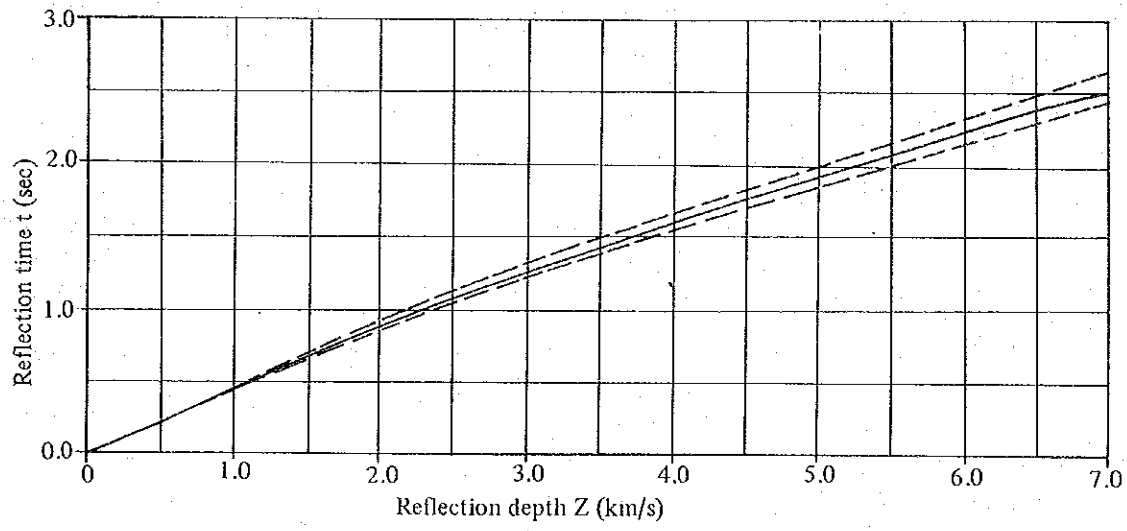

Fig. II.2.2-20 Relation between reflection travel time and reflection depth

According to the relation in this figure, the following items can be estimated.

(1) It is estimated that the continuous phases (reflection face) at around t = 0.9 sec and 1.8 sec of the reflection travel time on the Time section map (with reflective layer) (PL. II.2.2-31 ~ 35) along the survey line B are −2,000 meters and −4,500 meters above sea level, respectively.

(2) The horizons of L1 to L8 on the Depth section map (PL. II.2.2-41 ~ 43) are represented by continuous phases comparatively conspicuous in the range between t = 0.0 and 2.5 sec of the reflection travel time on the Time section map. They are distributed down to the depth of −7,000 meters above sea level.

(3) The levels of the bending points at t = 2.0 sec, shown by the relation formula of the reflection travel time (t) to the average velocity (Va) are hardly determined uniformly on each survey line. As a whole, continuous phases in a form of layer are recognized. The depth

is approximately −5,000 meters above sea level.

4-6-3 Depth section

Taking the remarkably continuous phases on the Final stack (Depth section) and on the Final stack time section to be planes of reflection waves, 8 horizons of L1 to L8 were assumed toward the depth, which were employed as the key beds for structure analysis underneath the survey lines.

The depth of the horizons and the characteristics as well as the results of the correlation to the geology (refer to the results of the present geological survey) are displayed in the following Table (Table II.2.2-14).

Table II.2.2-14 Outlines of assumed horizons

Assumed horizon	Area of existence		Thickness (m)	Remarks	Geological formation correlated
	Elevation (m)	Depth (m)			
Datum level	+300	0	0~1,900	High frequency domain, Density of reflection wave is low	Permain (andsite)
L 1	~ −1,800	0 ~ −1,800	0~1,500	Low S-N ratio zone. Phases are poorly continuous	Permian (shale, andsite, chert)
L 2	~ −3,200	0 ~ −3,200	300 ~ 800	High S-N ratio zone. Phases are remarkably continuous	Permian
L 3	300 ~ −4,100	− 600 ~ −4,400	500 ~1,200	High frequency domain. Density is rather low.	
L 4	− 800 ~ −5,000	−1,100 ~ −5,300	600 ~ 1,200	Phases are remarkably continuous. High S-N ratio zone. Low frequency domains are densely crowded.	
L 5	−1,600 ~ −5,800	−1,900 ~ −6,100	300 ~ 600	S-N ratio is rather low, compared to 0he upper layers (L_4~L_5 horizons)	
L 6	−1,900 ~ −6,100	−2,200 ~ −6,400	300 ~ 1,100	Density of reflection waves is high. High S-N ratio zone.	
L 7	(−2,800) ~ (−3,500)	(−3,100) ~ (−3,800)	0 ~ 3,000	Density of reflection waves is rather low, but S-N ratio is high.	Limestone (sandstone)
L 8	−2,900 ~ −6,700	−3,200 ~ −7,000		S-N ratio is rather low, compared to the upper layers.	Granites

As stated in the paragraphs of the frequency distribution and the diffraction source distribution, it is the horizon between L_2 and L_3 and between L_4 and L_5 that are recognized comparatively remarkably, concerning both the reflected waves and the refracted waves.

The characteristics along each of the survey lines on the Depth section map are described in the following.

(1) Survey line A

It is remarkable as to the underground structure along this survey line that there is a horst-like uplifted zone at around RP 70 ~ RP 90, in the general feature that dislocations in step-like form are developed due to the three faults of Ⓤ, Ⓥ and Ⓦ in the area between the Ⓢ fault near SP 6 and the Ⓧ fault around RP 150. The L_1 horizon is not recognized in this part between RP 6 and RP 150. Also, in this part, the horizon L_8 forms a plane elevated gently toward the north, which is different from the structure of the other upper horizons.

Dislocated by the Ⓢ fault, whole of this part forms a subsided zone. In the northernmost part, the horizons shallower than L_5 have been eroded out. In the area east of the Ⓦ fault, the structure is complicated, subsided or uplifted by Ⓨ and (Z) faults. As a whole an uplifted zone is formed in the area between the two faults of Ⓨ and Ⓩ. This zone has steeply subsiding structure toward outside of the survey line.

(2) Survey line B

Seven faults are estimated along this survey line. The central part of the line, between the Ⓡ fault and the Ⓤ fault, is the uplifted zone, from where the subsiding step fault structure is recognized toward outside of the survey line. At around the northeastern terminal point of this survey line, the L_5 horizon is not recognized, as is the case seen in northwestern end of the survey line A.

(3) Survey line C

The underground structure along this survey line has a general tendency that the central part of the survey line is uplifted zone to some extent, but the structure is rather complicated because the repetition of uplift and subsidence is recognized due to the movement of the several faults. The L_8 horizon, the deepest in the area, is distributed in almost flat form.

(4) Survey line D

Large scaled graben structure, dislocated vertically by 1200 to 1500 meters by the Ⓧ fault, the main tectonic line along this survey line is recognized. In the eastern part of the survey line, there is a tendency of the underground structure to form steep slope toward east. The western part reveals step-like structure with the faults of Ⓠ, Ⓣ and Ⓦ. The area around RP 26 between the Ⓣ fault and the Ⓦ fault, is an uplifted horst zone, from where subsiding step-fault structure is recognized.

(5) Survey line E

In the south of the Ⓩ fault, which is located in the northern part of the survey line E, subsidence by the step faults is recognized toward north generally, due to the faults of (Q), Ⓣ and Ⓨ, although the structure is flat in the area north of the Ⓩ fault. Accordingly, the graben

structure is remarkable in the area between the Ⓨ fault and the Ⓩ fault. The structure of the L_8 horizon is almost flat as a whole, though it composes slight anticline and syncline in the north of the Ⓨ fault. The depth of the L_8 horizon is about −6,500 meters above sea level, which is the deepest elevation of this horizon so far caught by the survey.

4-6-4 Deep structure analysis

Selecting L_4 and L_8 horizons in the Depth section map, for the comprehension of the general plane structure along and around the survey lines, the properties were displayed on the Structural planes (PL. II.2.2-44 ~ 45). The contour lines were drawn with 500 meter interval, taking the standard to be sea level, and the locations of faults and the axes of synclines and anticlines were entered in this map. Also for the analysis of the plane structures at the level of −1,000 meters and −2,000 meters, which were thought to be closely related to geothermal reservoirs, Depth structure analysis map (PL. II. 2.2-46 ~ 47) were prepared, on which the location of the faults, the distribution of the assumed horizons and the distribution of the low frequency domains were entered. The directions of the extension of the fault structures were determined, considering the direction of the shallow structure by the side reflection and the velocity distribution of the shallow structure analysis by the refraction method.

(1) Depth structure analysis map of L_4 horizon (PL. II.2.2-44)

This horizon is distributed in rather wide range of levels between −800 meters and −5,000 meters above sea level. That is, this horizon is situated at the elevation between −800 meters and −2,000 meters above sea level in the northern area, bounded by the Ⓧ fault of N-S trend, which is located latently in the southern half of the surveyed area. The distribution of this horizon in the southern side of the fault is between −2,500 meters and −5,000 meters above sea level. Therefore, there is a fair amount of difference of the elevations of the horizon in the east side and in the west side of the fault.

There is a remarkable uplifted zone around the area where the geothermal indications are distributed. This uplifted zone forms an anticline structure with the axis in the NW-SE direction. The surrounding area composes comparatively monotonous subsidence structure. It is recognized that the southeastern part of the Ⓧ fault would show a subsided zone in the SE direction, which forms a syncline structure. The axis is found at around the EGAT CAMP. It can be said that the surveyed area is divided into several blocks by such faults as represented by the faults of Ⓢ, Ⓣ and Ⓤ faults of NW-SE trend, by the Ⓨ and Ⓩ faults of N-S trend and by the Ⓡ fault of E-W trend.

(2) Depth structure analysis map of L_8 horizon (PL. II.2.2-45)

This L_8 horizon is the deepest horizon estimated in the present seismic survey and is distributed at the elevation between −2,100 meters and −6,500 meters above sea level. As a whole, the structures of E-W trend are remarkable on this horizon, which is almost in right angle to the structure of the upper L_4 horizon having N-S trend. This fact suggest that there is an incongruous relation between the upper L_4 horizon and this L_8 horizon, and it is thought that the portion below this L_8 horizon is correlated to granites intruding the Paleozoic formations. As a whole, the horizon is dipping toward east. In the area east of the Ⓢ fault, the part around the terminal points of the survey lines B, C and D is recognized to have been uplifted. Repetition of synclines and anticlines of E-W trend is recognized in the area north of the Ⓧ fault, while the

structures of N-S trend is found to be general in the south of the fault.

(3) Depth structure analysis map at the elevation at – 1,000 meters above the datum level (PL. II.2.2-46)

On the horizon at the elevation of –1,000 meters above the datum level, the geological layers found between the horizons of L_2 and L_4 are distributed mainly, in the area between the Ⓢ fault and the Ⓧ fault.

Between the survey line B and C, there is an anticlinal uplifted zone with the axis trending in NW-SE direction, around the area where the geothermal indications are distributed. Subsidence is recognized toward the wings. The structures along C and D lines are similar to the structure in the area between the survey lines B and D, but the axis of the anticline is in N-S direction.

In the area south of the survey line D, the lower horizons from L_3 to L_5 are distributed, according to the distance from the survey line. In the southern side of the Ⓧ fault, the shallower horizons than the L_1 horizon are mainly distributed.

Most of the low frequency domain are distributed around the Ⓦ fault between the survey line B and the survey line D. The extension of the distribution of the low frequency domains are in harmony with the axis of the anticline.

(4) Depth structure analysis map at the elevation of – 2,000 meters above the datum level (PL. II.2.2-47)

In this plan, are distributed the horizons of L_1 to L_6. As seen in the Depth structure map at the elevation of –1,000 meters above the datum level, the main structure is composed of the uplifted zone with the axis in NW-SE direction, passing through the area where the geothermal indications are distributed. Around the area where the well of GTE-2 is located, are distributed the horizons of $L_5 \sim L_6$, the deepest horizons between the subject levels.

It is remarkable that the low frequency domains are distributed along the Ⓢ fault as well as along the Ⓥ fault between the survey lines of B and C, with the width of 400 ~ 500 meters.

As to the distribution of the low frequency domains respectively at the horizon of –2,000 meters and at the horizon of –1,000 meters above the datum level, the tendency is recognized that the distribution of the former is concentrated along and around the Ⓢ fault or the Ⓦ fault in the western part, while the distribution of the latter is found along and around the Ⓦ fault in the eastern part of the surveyed area.

5. Summary

The results of the deep structure analysis, the wave analysis and the shallow structure analysis by the seismic reflection and refraction methods are summarized as follows.

5-1 Velocity distribution

5-1-1 Subsurface (Refraction method Vh)

Subsurface velocity layers are divided into three units, from the velocity distribution.

No. 1 layer	400 m/s	surface soil
No. 2 layer	2,050 ~ 2,080 m/s	weathered zone

	2,300 ~ 2,700 m/s	
No. 3 layer	2,900 ~ 4,000 m/s	
	4,100 ~ 5,700 m/s	hard rock

The velocity zone of the upper part of the No. 2 layer is distributed mainly in the low velocity area around the crossing point of A and D survey lines, and its velocity is lower by 10 ~ 20% compared to that in the other area. As for the velocity distribution on the surface of the No. 3 layer, the one in the eastern part of the surveyed area is different from that in the western part, and they are bounded by the existence of the central part. Values of the velocity in the eastern part compose high velocity zone, while those in the western part are forming middle to low velocity zone. The direction of the boundary dividing these velocity zones corresponds approximately to that of the side reflection.

5-1-2 Depth (Va, Vv by the reflection method)

According to the results of the velocity analysis by the reflection records, average velocity and layer velocity are shown by the following assumption formulae.

Average velocity (unit: km/s)

$Va_1 = 4{,}000 + 650t$ ..... $t = 0.0 \sim 0.8$ sec

$Va_2 = 4{,}074 + 557t$ ..... $t = 0.8 \sim 1.5$ sec

$Va_3 = 3{,}740 + 780t$ ..... $t = 1.5 \sim 2.0$ sec

$Va_4 = 4{,}614 + 343t$ ..... $t = 2.0 \sim 2.7$ sec

$Va_5 = 4{,}045 + 554t$ ..... $t = 2.7 \sim 4.0$ sec

Average of values of the layer velocity

$Vv = 4{,}072 + 0.26Z$ ..... average (m/s)

The average velocity reveals almost linear variation, but small change in the increasing amount is recognized around the 2.0 second (about 5,000 meters below the datum line). It is expected that certain geological boundary would be located there.

5-2 Subsurface analysis

5-2-1 Side reflection

Concerning the side reflection, N-S system and NE-SW system are remarkable. It is thought that some of them are caused by the fault structures while others are due to the strikes of the beddings. Continuous side reflection is in many cases corresponding to the velocity boundary caught by the three-layered analysis.

5-3 Analysis of wave form

5-3-1 Frequency distribution

(1) The low frequency domains (under 20 Hz) grouped as (1) are hardly recognized along the survey lines of D and E, while they are distributed at the levels of the depth more than 0.5 sec (approximately 1,000 meters below the datum line) along the survey lines of A, B and C. Espccially in parts along the survey lines of A and C, they are distributed continuously at the levels of the depth of more than 2.5 sec (approximately 7,000 meters below the datum line).

It is thought that they would have certain relation to the geothermal passages.

(2) Many of the low frequency domains are recognized to be along the fault structures in the deep, generally. It is especially noted that such indications are found along and around the faults of Ⓢ, Ⓤ and Ⓥ remarkably.

5-3-2 S-N ratio distribution

(1) It is notable that the high S-N ratio zones of (1) group have a pattern of horizontal distribution generally between 0.0 and 1.5 seconds. This tendency is especially remarkable in the No. 3 to No. 5 layers.

(2) Columnar distribution in perpendicular directin is seen remarkably in the area where low frequency domains are well developed along the survey lines of A and C. However, no such relation has been recognized along the survey line of B.

5-3-3 Distribution of diffraction sources

(1) Of the diffracted waves, remarkably continuous ones are thought to be representing fault structure. The peak of their frequency distribution in the perpendicular direction is at about 0.7 ~ 1.1 sec (−1500 ~ −2500 meters below the datum line) and the frequency decreases gradually in the portion deeper than the peak. The following peaks are recognized along the survey lines.

A line ; RP, 13, 20, 39, 58, 93, 133, 187, 206
B line ; RP, 10, 19, 23, 40, 75
C line ; RP, 7, 21, 40, 61, 75
D line ; RP, 9, 40, 50, 72
E line ; RP, 10, 47, 73, 95

RP: receiving point

(2) Diffraction sources are densely distributed mainly around the above peaks, composing continuous distribution. From the tendency of such distribution, existence of fault structures marked by the symbols from Ⓟ to Ⓩ have been estimated.

5-4 Deep structure analysis

Horizons remarkable on the stacking records of the seismic reflection survey have been selected assumingly as L_1 to L_8. Of these horizons, the general tendency of the horizons of L_4 and L_8 has been summarized on the Structure analysis map (PL. II.2.2-44, 45). Also, for the comprehension of the structures at the levels of −1,000 meters and −2,000 meters above the datum line, another structural maps have been prepared for each of these levels. The summary is given as follows.

(1) On the L_4 horizon, there is an anticlinal structure from the central part of the survey area to the northern part of it. The folding axis passes the area where the geothermal indications are distributed (around GTE-2). In its vicinity, subsidence is recognized toward the faults of Ⓢ and Ⓧ. Especially in the area south of the fault Ⓧ, the subsidence is quite violent.

(2) The portion deeper than the horizon L_8 is inferred to be composed of intrusive body such as granite. The structural trend of this part is mainly E-W and is almost rectangular to that of the upper horizons (L_1 ~ L_7 horizons), which reveal the structure of N-S trending.

(3) The horizons of L_4 and L_8 are distributed at the depth as shown below.

L_4 horizon	S.L. −800 ~ −5,000 m
L_8 horizon	S.L. −2,900 ~ −6,700 m

The low frequency domains at the level of −2,000 meters below the datum line are found to be concentrated around the faults of Ⓢ and Ⓥ, and those at the level of −1,000 meters below that are concentrated around the Ⓦ fault.

5-4-2 Fault structure

Mainly from the tendency of the distribution of the diffraction sources, total 11 faults have been estimated to exist; 6 faults of NW-SE trending, 4 faults of N-S trending and a fault of E-W trending.

(1) As for NW-SE trending faults, 6 faults of Ⓠ, Ⓢ, Ⓣ, Ⓤ, Ⓥ and Ⓦ, are estimated to be running toward the southeast from the starting point of the survey line A. It is thought that the dipping of the fault Ⓤ is to the southwest while the other faults are dipping to the northeast. The faults of Ⓣ, Ⓤ and Ⓥ are thought to be thrust fault.

(2) As the N-S trending faults, the fault Ⓟ in the northern part of the survey area and the faults Ⓧ, Ⓨ and Ⓩ in the southeastern part can be mentioned. All these faults are thought to be dipping toward the east, except for the fault Ⓩ, which has the dip to the west. The fault Ⓟ is thought to be thrust fault.

Along the northern side of the area where the geothermal indications are distributed, the fault Ⓡ is estimated to run in E-W direction.

(3) The order of the periods of the formation of these faults are estimated to be as follows.

older	Ⓢ, Ⓣ	NW-SE trend
↓	Ⓧ, Ⓨ, Ⓩ	N-S trend
↓	Ⓤ, Ⓠ	NW-SE trend
↓	Ⓥ, Ⓦ	NW-SE trend
younger	Ⓟ, Ⓡ	N-S and E-W trends

III RESULTS OF THE SURVEYS BY THE THAILAND SIDE

III RESULTS OF THE SURVEYS BY THE THAILAND SIDE

III-1 Outline of the Results of the Surveys

On the geothermal resources in the northern part of the Kingdom of Thailand, including the San Kampaeng are, another investigations and researches had been carried out by Thailand side. Part of them were executed with the cooperation of the specialists of West Germany and Japan.

General geothermal investigation was carried out in this San Kampaeng area, too (Table III.1-1).

Table III.1-1 Previous survey of the San Kampaeng area

		Contents	References
Reconnaisance Survey	Geological survey	Geological map 1:15,000	Chuaviroj et al. (1980),
	Chemical analysis	Hot spring water Main component, minor elements	Kingston Reynolds Thom & Allardice Ltd. (1976) NZ
	Isotope analysis	D, ^{18}O, Tritium	
	Gas analysis	o	
	Heat discharge	Hot spring heat discharge	
	Radioactive prospecting	o	Ramingwong et al. (1979)
	Resistivity method	Depth 500 m	
	Hydrogeology	Rainwater supply	
	1.0 m depth temperature	o	Thienprasert & Raksaskulwong (1980a,b)
	Seismic prospecting	Reflection method	Thienprasert & Raksaskulwong (1980a,b)
	Geochemical prospecting	CO_2, Hg, Rn	I. Takashima, K. Kawada (1980) GSJ.
	Short boring	19 holes (326.6 m)	
	Alteration survey	o	I. Takashima, K. Kawada (1980) GSJ.
	Structural drilling	5 holes	
	Terrestrial heat flow	Water well	Ramingwong et al. (1980b)
Regional Survey	Micro earthquake	o	Report No. 842-2301 EGAT (1980)
	Colligated study	Phase 1	Ramingwong et al. (1980b)
	Photo interpretation	Analysis from LANDSAT	M. Sasada (1982) GSJ.
	Colligated study	Phase 2	I. Takashima, K. Kawada (1982) GSJ.

The surveys carried out were; geological survey (fissure system survey, alteration survey, hydrogeological survey), geochemical survey (analysis of water and gas of hot springs, isotope analysis, gas analysis, radiometric prospecting, Co_2, Hg, Rn exploration), geophysical exploration (heat discharge, 1.0 m and 10 m depth temperature measurement, resistivity survey, seismic survey, terrestrial heat flow survey), short boring (19 holes, average depth 33 m) and geothermal exploration well (5 holes of the depth of 500 meters class).

By the results of the investigation, significant informations in this area were obtained on the geological structure, the conditions of the geothermal reservoir, the chemical ingredients of the hydrothermal solution, the hydrographical structure and so on.

Outline of the survey results by Thailand side are described in the followings.

Table III.1-2 Previous survey results of San Kampaeng area

PH of hot spring water	8.3 ~ 9.0
Temperature of hot spring water	99 (°C) (max.)
Geochemical temperature {Tsi	160 (°C)
Geochemical temperature {Tnkc	207 (°C)
Total flow out	72.0
Hot spring heat discharge	6.7 (MWt)
Terrestrial heat flow	4.4 ~ 8.1 (HFU)
Related geological structure	Fault
Assumed reservoir rock	Sandstone. Slate. Chert
Altered mineral (28 samples)	Q. Se. K. Ch. M. H. Ah. Gp. Al. Ja
Paleo ground temperature	120 ~ 150 (°C)
Resistivity method (depth 500 m)	2 area (< 100 Ωm)
Rainwater supply	150×10^4
Available ground surface water	sufficient
Topography	flatness
Localty	25 km east from Chiang Mai

Abbreviation
Q-quartz. Se-sericite. K-kaolinite. H-halloysite. Ah-anhydrite. Gp-gypsum. Ch-chlorite. M-montmorillonite. Al-alunite. Ja-jarosite
(after I. Takashima, K. Kawada (1980), Ramingwong et al. (1979))

1. Geological survey

It was clarified that the area is underlain by the Carboniferous Mae Tha Formation and the Permian Ratoburi Group. The main component rocks are sandstone, slate, chert, limestone and basalt lava. It was estimated that the faults would have played an important role as the passages of the geothermal fluid and that sandstone, slate and chert were important as geothermal reservoir.

By the hydro-geological survey, rainwater supply is estimated to be 150×10^4 kg/day/km^2.

2. Geochemical survey

Various kinds of geochemical prospecting were carried out, as the prospecting was thought to be one of the most important methods among various geothermal surveys. It is general characteristics of the chemical ingredients of the hot spring water collected in the northern part of the Kingdom of Thailand, including the San Kampaeng area that total amount of the solid contained is small (under 1,000 ppm in most cases), that they are alkaline, containing less than 10 ppm of Cl concentration, which is conspicuously low value in any of the geothermal areas ever developed in the world. It has been thought from such chemical compositions as to contain very low salts that the geothermal liquid in the northern part of the Kingdom of Thailand is originated neither from any magmatic water nor from any connate water.

By the chemical thermometer, underground temperatures (reservoir part) were estimated. The values are 160°C by SiO_2 method, 192 ~ 207°C by the Na-K-Ca method and 247°C by CH_4-CO_2 method.

Outline of the hydrogeological structure was clarified. That is, the circulation period of the geothermal fluid was suggested from the tritium content. It was suggested from the condition of no shift of ^{18}O that the ratio of water/rock was high. It was also pointed out from the seasonal

variation of the Mg-content and the Cl content that the solution was admixed with underground water.

3. Geophysical exploration

By the resistivity survey, low resistivity zones with the resistivity of less than 100 Ω-m were found in the southeastern part of the surveyed area and in the area where the geothermal indications are distributed. The heat discharge by the hot springs is 6.7 MWt and the terrestrial heat flow is 4.4 ~ 8.1 HFU.

By the distribution of the 10 m depth temperature, measured in the shallow boring, the highest value is found almost in the center of the area where the geothermal indications are distributed. The temperature drops like concentric circle toward the outer zones.

III-2 Results of the Well Logging

1. GTE-1 (PL. III.2-1)

(1) Location: in the southeastern part of the surveyed area.
East longitude 99°14'22
North latitude 18°46'20

(2) Depth: 500 m

(3) Highest temperature: 80.4°C (depth 462 m)

(4) Thermal gradient: 12.0°C/100 m

(5) Geology: composed mainly of basalts and greyish green basaltic tuff of the upper part of the Kiu Lom Formation, with the inserted layers of lava and tuff breccia. Calcite and quartz veins are developed in some parts. Chloritization is remarkable, as a whole. In the shallow part (depth of less than 150 m), many steep-angled fractures are recognized, which are scarce in the deep part.

(6) Bounded at the depth of around 200 m, gradient of the underground temperature is rather high in the deeper part, which is thought to be due to comparatively clustered fractures in the shallow part, through which underground water can penetrate into, resulting the cooling. However, as the temperature-depth curve is almost linear in this hole, it is suggested that the heat conveyance by conduction is predominant, in this area.

2. GTE-2 (PL. III.2-2)

(1) Location: in the midway between Wat Pong Hom and Ban Pong Nok, and in the area where the geothermal indications are distributed.

(2) Depth: 500 m

(3) Highest temperature:

(5) Geology: Composed of the sedimentary rocks comprising alternation of siltstone, shale and limestone of the lower part of the Kiu Lom Formation. Three limestone layers are developed at the depth of 195.1 ~ 221.0 m, 267.3 ~ 337.0 m and 430.8 ~ 483.5 m. Calcite veins, quartz veins and pyrite dissemination are recognized as a whole.
The carbonaceous shale layer at the depth of around 230 meters is observed to reveal fragility and easily fractured.

(6) By the result of the electric logging, there is a tendency that the resistivity of the limestones

is generally high, while that of the pelitic rocks is low. The spontaneous potential shows reverse correlation to the resistivity.

(7) The depth-temperature curve is linear as is the case with the well of GTE-1.

3. GTE-3 (PL. III.2-3)

(1) Location: near Wat Nong Noi, about 2.5 km east of GTE-2

(2) Depth:

(3) Highest temperature:

(4) Thermal gradient: The thermal gradient in this hole is much less than the gradient of GTE-1 and GTE-2.

(5) Geology: Composed of basaltic rocks of the upper part of the Kiu Lom Formation. They are mostly basaltic tuff but thin inserted layers of lava and tuff breccia are found partly.

4. GTE-4 (PL. III.2-4)

(1) Location: at a point about 1.4 km northwest of GTE-1.

(2) Depth: 500 m

(3) Highest temperature: 44°C at the depth of 164 m (because of the poor well condition, the logging apparatus did not descend below the depth of 166 m).

(4) Thermal gradient:

(5) Geology: Composed of the middle to lower part of the Kiu Lom Formation. Between 0 m and 302.5 m of the depth, mainly andesitic tuff and basaltic andesite (middle part of the Kiu Lom Formation) are distributed. Between 302.5 and the 500 m of the depth, fine alternation of sandstone and shale (the lower part of the Kiu Lom Formation) is distributed, Sheared and fractured as a whole, fissures are well developed, but no lost of circulation was recorded. At the depth of 415.0 meters, a fault breccia zone is recognized. Calcite and quartz veins are generally recognized, in addition to argillization and chloritization.

5. GTE-5 (PL. III.2-5)

(1) Location; at a point about 750 meters northeast of the well of GTE-2, and next to the area where the geothermal indications are distributed.

(2) Depth: 500 m

(3) Highest temperature:

(4) Thermal gradient:

(5) Geology; Composed of the sedimentary rocks of the lower part of the Kiu Lom Formation. Between 0 m and 131.0 m of the depth, the alternation of sandstone and shale is distributed. Between 131.0 m and 240.5 m of the depth, fine alternation of chert, shale, sandstone, (andesitic) tuff and tuff breccia is distributed. Between 240.5 m and about 300 m of the depth, alternation of sandstone and shale is recognized. There was no information of the geology below the depth of about 300 m.

(6) It is remarkable that all the circulation was lost at the depth of 300 m. It is thought that the lost of circulation was due to fracture zone of the fault (Ban Mae Khu Ha fault) or fractured bed (chert bed).

It can be said to be common as to every holes of GTE-1 to GTE-5 that the temperature is increasing linearly with the increase of depth. Adding the condition that little loss of circulation

was recorded while the drilling was carried out, the above fact is taken to suggest that the principal geothermal system in this area is characterized by thermal conduction, considering that open cracks capable of being passages of the geothermal fluid are poorly distributed in most of this area.

III-3 Model of the Geothermal Reservoir

By the results of the various geothermal surveys, the geothermal system in the San Kampaeng area was appraised to have high geothermal potentiality.

The reasons are as follows.

(1) The underground temperature estimated from the geochemical thermometer is more than 180°C.

(2) Faults and remarkably fractured sedimentary rocks are well developed in this area, which is thought to be qualificatory for the existence of reservoir structure.

(3) Broad surface geothermal indications and hot spring water of high temperature are recognized in this area. The natural heat discharge by the heat flow of geothermal convection is 6.7 MWt.

(4) The geothermal gradient is 54 – 96°C/km and the terrestrial heat flow is as extraordinarily high as 4.4 – 8.7 HFU.

(5) It is estimated from the results of the micro-earthquake observation that the San Kampaeng geothermal system is related to the Mae Tha fault in the eastern part. it is a active faults that controls the distribution of the hot springs.

Based upon the above data, conception model of the San Kampaeng geothermal system was brought forward by Raming wong et al. of Chiang Mai Vaniversity (Fig. III.3-1).

By the model, the source of supply of the rainwater is the Mae Tha mountaneous land in the eastern part of the surveyed area, and the rainwater is to flow down along faults to the depth in the underground. The rainwater, after penetrated deep in the underground, is heated conductively by hot rock and is converted to the geothermal fluid. The geothermal fluid ascends

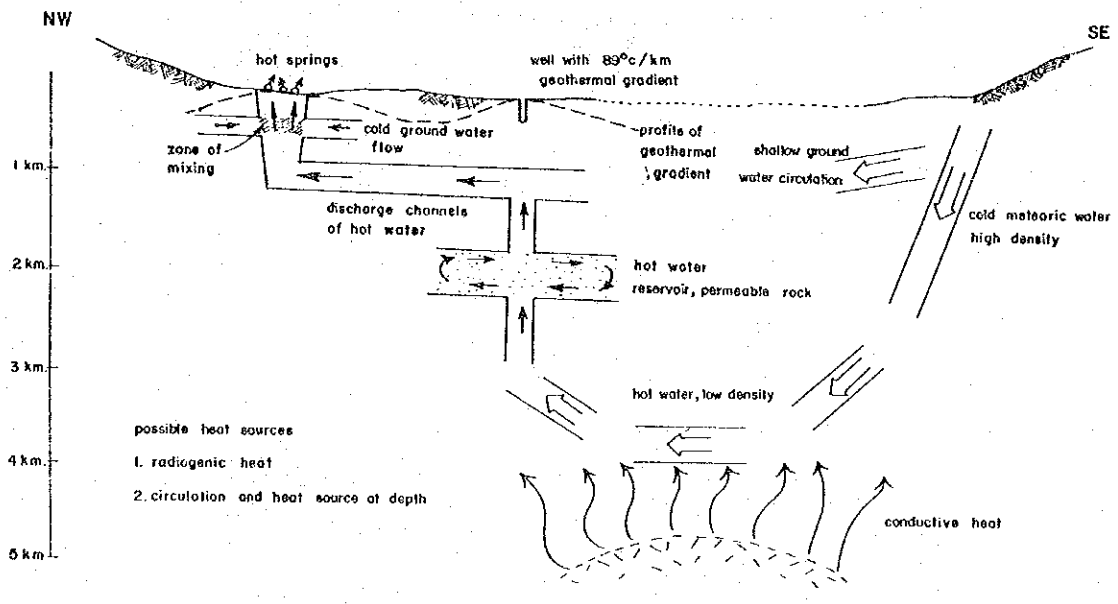

Fig. III.3-1 Interpreted model of the San Kampaeng geothermal system
Section along strike of fault controlling hot springs
(after Thai's data)

upward by buoyancy effect and is reserved in certain permeable beds seated at the depth of about 2 km. Some leaked geothermal fluid moves ascending to the side way (in NW direction), and is admixed with ground water (at the approximate depth of 500 m), which forms the surface indications in the San Kampaeng geothermal area.

By modification and correction of the model after Raming wong et al., the following geothermal model of the San Kampaeng area is brought forward by Takashima and Kawada of Geological Survey of Japan (Fig. III.3-2).

The rainwater, penetrating from the granite area, is heated conductively in the underground. It flows up through the faults, part of which forms reservoir and another part of which comes out of the surface after admixed with groundwater.

What are common to the above-stated models are that the rainwater is heated conductively to form geothermal fluid and that geothermal reservoir is assumed at the depth (2 ~ 3 km deep).

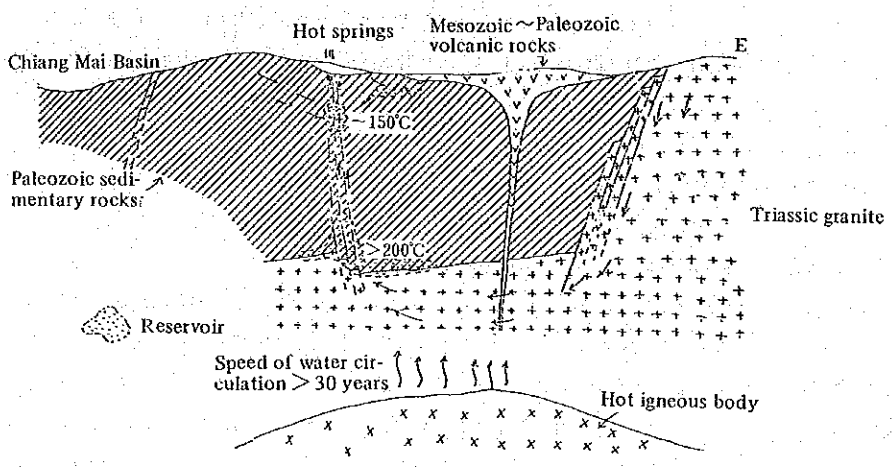

Fig. III.3-2 Geothermal model of the San Kampaeng area (after Takashima & Kawada, 1981)

IV DIGITAL MODEL

IV DIGITAL MODEL

IV-1 Introduction

By the multi-variate analysis (factor analysis) of various data obtained through the primary and the secondary investigations, qualitative permeability (fissures) of the layers and distribution of the temperature, which are determining the potential of geothermal reservoirs, have been estimated here. The process of the estimation is as follows.

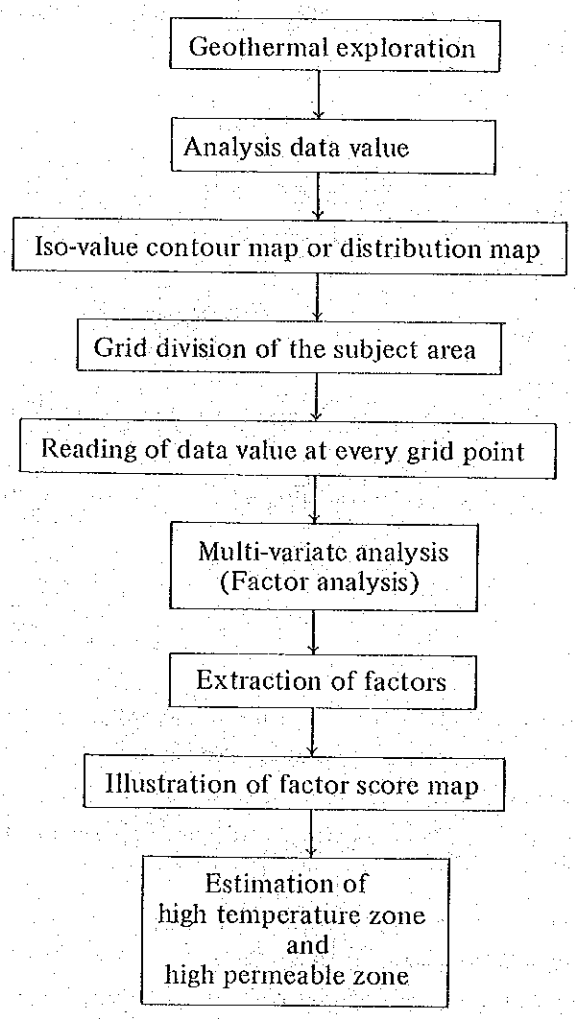

Fig. IV.1-1 Process of multi-variate analysis of data obtained in the surveys

IV-2 Method of Analysis

IV-2-1 Establishment of Grid

The object area for the multi-variate analysis has been divided into two categories; the regional area and the local area (PL. IV-1).

The regional area includes the area from Ban Huai Dua in the northern part to Doi Tham in the southern part of the surveyed area. In this regional area, the geological survey, magnetic survey and the gravity survey were carried out widely. The area of the object is 11.75 km^2 and the spacing of the grid is 500 meters with the total number of the grid points of 64.

The local area is correspoinding to the area north of Ban Pong Nok, where the geothermal indications are distributed. The 1 m depth temperature survey, the alteration survey and other various surveys were performed in this local area. The area is 0.8 km^2 and the spacing of the grid is 200 meters with the total number of the grid points of 30.

IV-2-2 Input Data

The variates given to each point for the multi-variate analysis are composed of 11 items;

1) distance from the faults
2) dip of beds
3) degree of alteration
4) anomalous value of gravity
5) value of gravity gradient
6) magnetic anomalous value
7) total conductance value
8) concentration of CO_2 gas
9) concentration of radon gas
10) ground temperature at the depth of 10 meters
11) ground temperature at the depth of 1 meter

These input values were obtained by the reading of the grid values on each of the iso-value contour maps.

IV-2-3 Method

When the number of the observation items is P in the surveys, the correlation matrix A for samples is taken to be as follows, each item is expressed in matrix, which is taken to be A. If $AX = \lambda X$, λ is called to be eigenvalue and X is called to be eigenvector. The eigenvalue λ is a common factor of A, and X indicates the position on the coordinate. Therefore, the eigenvector (factor loading) can be obtained.

After the interpretation on what is expressed by the factors thus extracted, factor scores are given to each factor for the examination of the degree how intensely each of the observation point bears the tendencies of the factor. Varimax rotation is taken effect, so that a variate might have high loading with certain factor, with the other factors having such loading as close as to zero.

By the distribution of factor score thus obtained, it can be clarified at each of the observation points whether the evaluation concerning the factor of temperature is high or low or whether the evaluation concerning the permeability is high or low.

IV-3 Results of Analysis

IV-3-1 Results of Analysis of the Regional Model

1. Correlation matrix

The correlation matrix of each of the items obtained through respective surveys is shown in Table IV.3-1. The following characteristics are pointed out.

Table IV.3-1 Correlation matrix (Regional model)

	1	2	3	4	5	6	7	8	9
1	1.0000	-0.0923	0.1951	-0.0938	0.1024	0.0797	0.0338	0.1044	-0.1074
2	-0.0923	1.0000	0.3608	0.0628	0.2518	0.2165	-0.0008	0.0600	0.0596
3	0.1951	0.3608	1.0000	0.1031	0.2829	0.5557	-0.2325	-0.1511	-0.2106
4	-0.0938	0.0628	0.1031	1.0000	0.4141	-0.2961	-0.0211	-0.2136	-0.1305
5	0.1024	0.2518	0.2829	0.4141	1.0000	-0.1054	0.0673	-0.0100	0.0578
6	0.0797	0.2165	0.5557	-0.2961	-0.1054	1.0000	-0.1003	0.0421	0.0137
7	0.0338	-0.0008	-0.2325	-0.0211	0.0673	-0.1003	1.0000	0.4147	0.5314
8	0.1044	0.0600	-0.1511	-0.2136	-0.0100	0.0421	0.4147	1.0000	0.3433
9	-0.1074	0.0596	-0.2106	-0.1305	0.0578	0.0137	0.5314	0.3433	1.0000

(1) Anomalous values of gravity have fair correlation with total conductance values of deep electric survey (correlation coefficient 0.5557). For example, the low gravity anomaly developed around Wat Pong Hom is coincident to the high total conductance area with values of more than 300 mhos. The fact that both of the above two have common character is thought to suggest that they would have been caused by alteration or brecciation of rocks.

(2) The concentration of CO_2 gas has fair correlation to the 10 m depth temperature (correlation coefficient 0.5314). It is thought that this correlation is due to the conveyance of heat and CO_2 gas by geothermal fluid.

(3) The correlation between the concentration of CO_2 gas and that of radon gas is rather high (correlation coefficient 0.4147), while the concentration of radon gas has low correlation to the 10 m depth temperature (correlation coefficient 0.3433).

(4) The values of the gravity gradient has fair correlation to the magnetic anomalous values (correlation coefficient 0.4143). It is thought by this correlation that they would reflect difference of lithofacies (density, amount of magnetic minerals) and existence of faults.

2. Factor analysis

The eigenvalues the eigenvectors the factor loading and the vector map are shown in Table IV.3-2, 3, 4 and Fig. IV.3-1. By this analysis, the following three principal factor axes have been extracted.

(1) Factor 1: Concerning this factor, dips of beds and magnetic anomalous values have same behavior. Value of gravity gradient is also related to them. This factor is regarded as the factor representing large scale geological structure, especially structural directions, shown as strikes of beddings, distribution of magnetic bodies and sudden change of lithofacies by faults.

Table IV.3-2 Eigen value · Eigen vector (Regional model)

... EIGEN VALUE ...

EFFECTIVE NUMBER : 7

2.120	1.738	1.596	1.108	0.698	0.569	0.512	0.394	0.265

... EIGEN VECTOR ...

	1	2	3	4	5	6	7	8	9
1	-0.0813	0.1730	0.0903	-0.8552	-0.0646	-0.3213	0.1998	-0.2482	0.1223
2	-0.2109	0.4213	-0.2089	0.3855	-0.5622	-0.3849	0.3172	-0.0833	0.1186
3	-0.5028	0.3997	-0.0017	-0.0540	0.2080	0.1679	0.0503	0.0463	-0.7130
4	-0.1848	-0.1879	-0.6093	-0.0176	0.1744	0.4164	0.3852	-0.4189	0.1767
5	-0.1789	0.1942	-0.6029	-0.1812	0.0286	-0.0925	-0.6100	0.3260	0.2149
6	-0.2526	0.4793	0.3789	0.1270	0.3530	0.2537	-0.0026	-0.0109	0.5981
7	0.4705	0.2869	-0.2220	-0.0831	0.2521	0.0139	0.5049	0.5668	-0.0150
8	0.3862	0.3714	0.0138	-0.1614	-0.4989	0.6105	-0.1869	-0.1555	-0.0770
9	0.4422	0.3315	-0.1429	0.1866	0.4101	-0.3182	-0.2160	-0.5495	-0.1460

Table V.3-3 Factor loading (Regional model)

	1	2	3	4	5
1	-0.2606	0.3284	0.7379	-0.1006	-0.0728
2	-0.3972	-0.0484	-0.3360	-0.3516	-0.4385
3	-0.8671	-0.0988	-0.0059	-0.1313	0.0825
4	0.0248	-0.5282	0.0759	-0.4577	0.2112
5	-0.1987	-0.2232	0.0861	-0.6176	0.0462
6	-0.7036	0.3374	-0.2491	0.2394	0.1069
7	0.2983	0.5170	-0.1281	-0.4490	0.1406
8	0.1346	0.5187	-0.0738	-0.2066	-0.0974
9	0.2392	0.4953	-0.3164	-0.3308	0.0945

Table IV.3-4 Factor loading (Varimax rotation)

	1	2	3	4	5
1	0.3751	0.1446	-0.6017	-0.6849	-0.0849
2	-0.7482	0.2220	-0.2270	0.1137	-0.5714
3	-0.4934	0.7772	-0.3021	-0.2293	0.0931
4	-0.6313	-0.2351	0.3904	-0.5578	0.2875
5	-0.7833	-0.1537	-0.1598	-0.5770	0.0667
6	-0.0985	0.7800	-0.4833	0.3645	0.1244
7	-0.1211	-0.7199	-0.6173	0.2297	0.1824
8	0.0818	-0.5009	-0.7790	0.3288	-0.1659
9	-0.1834	-0.6125	-0.5664	0.5032	0.1309

(2) Factor 2: Concerning this factor, anomalous value of gravity and conductance value are revealing high factor loading. Also, the 10 meter depth temperature and the concentration of CO_2 gas have almost same behavior (negative loading to the factor) and the concentration of radon gas has rather similar tendency. As this factor is to control temperature at the depth of 10 meters, it is thought that this factor composes factor of temperature, but viewing from the fact that certain influences are recognized on the concentration of CO_2 gas and radon gas, this factor is thought to by the factor directly reflecting existence of geothermal fluid. Although low anomalous values of gravity and high values of conductance are thought to have been brought about by brecciation and alteration of rocks, it is inferred that they also have been controled by this factor 2.

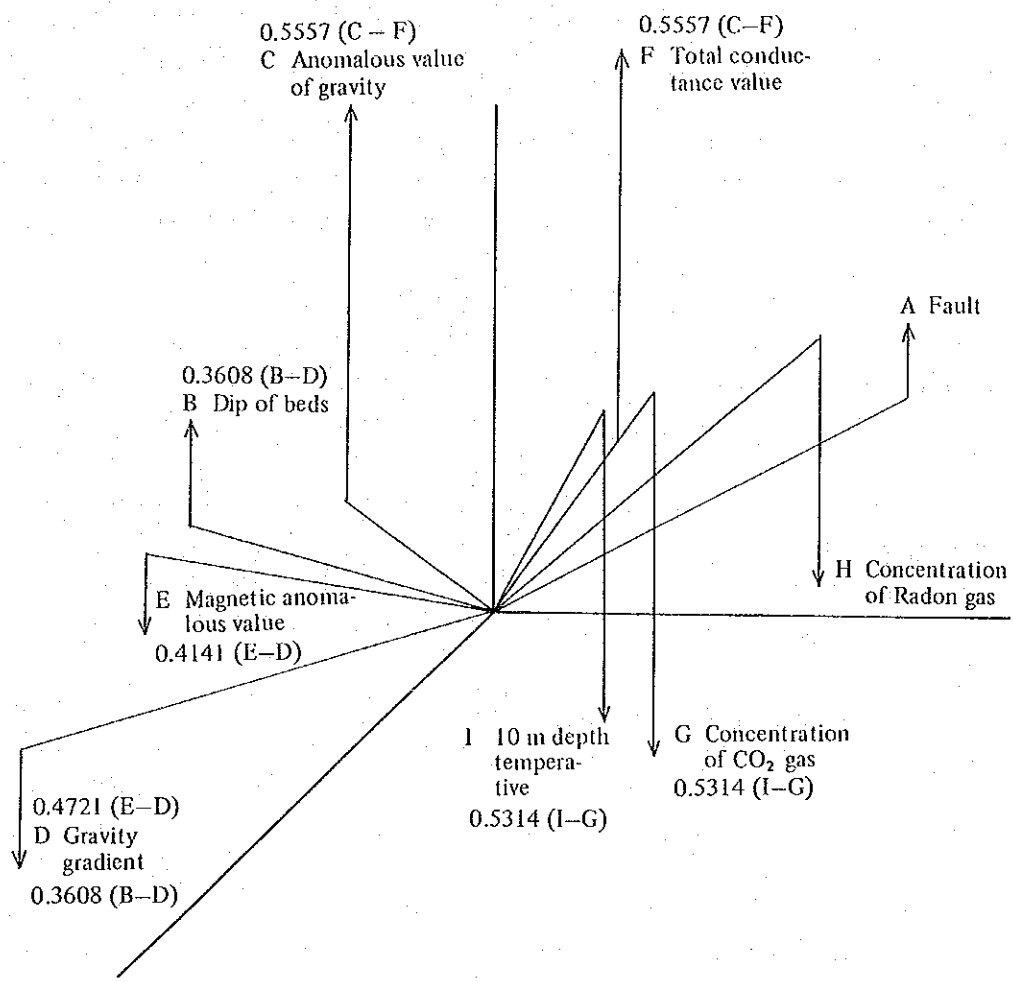

Fig. IV.3-1 Factor vector (Regional model)

(3) Factor 3: Concerning this factor, distance from the faults, density of radon gas, concentration of CO_2 gas and temperature at the depth of 10 meters have high factor loading. As this factor affects the distance from the faults clearly, it is thought that his factor is the one due to the fractures. That it, the ground temperature and the gas concentration are estimated to be controled by the existence of fractures in the layers.

Factor scores are given to the three factors extracted as above, and are displayed on the distribution map.

The Factor score map for regional model of the factor 1 (PL. IV.3-1) reveals the direction of large scaled geological structure. The contour lines in the direction of (north and south) are predominant, but partly the contour lines in the direction of NW-SE or NE-SW are recognized. This pattern is in good harmony with the directions of the geological structure in this surveyed area, which were evidenced from the results of the geological survey. High factor scores are shown around the Doi Tham mountain which is composed of limestone and is complexly folded and faulted, as well as along the middle-stream area of the Huai Ang River, where the faults of NW-SE trend are concentrated.

The Factor score map for regional model of the factor 2 (PL. IV.3-2) is thought to reveal the temperature or the existence of geothermal fluid. The direction of the contour lines is mostly north and south. The highest factor scores are revealed in the area where the present geothermal indications are distributed. In the area from Ban Pong Nok to Ban Huai Dua through Wat Pong Hom, which is surrounding this geothermal area, the next highest factor scores are shown. It is notable that, in the southeastern end of the analysed area from Wat Hua Fai to Wat Nong Hoi, are distributed the factor scores of almost same degree as those found in the area where the present geothermal indications are distributed. However, because the location of such points are in the peripheral zone of the analysed area, its extension and shape of distribution are not certain.

The Factor score map for regional model of the factor 3 (PL. IV.3-3) is revealing the degree of fractuation of the geological layers. It is thought that the more intensely fractured the layers are, the smaller the factor scores are. The remarkably fractured zones are found in the area where the geothermal indications are distributed and in the area around Ban Mai in the south-easternmost part of the analysed area. The contour lines in and around the area where the present geothermal indications are distributed are in NW-SE direction, which is same as that of the fault branched from the Huai Pong fault. Although the factor scores are small around Ban Mai, the degree of fractuation of geological layers has yet been confirmed neither by the surface geological survey nor by the drilling.

As above-stated, it has been estimated, by the distribution of the factor scores of the factors indicating the temperature and the fractures, that the area where the present geothermal indications are distributed and the other area in the southeastern periphery of the analysed area (the area from Wat Nong Hoi to Ban Mai) would be favorably bearing the condition of the high temperature and the well-developed fracturation.

IV-3-2 Results of Analysis of the Local Model

1. Correlation matrix

The correlation matrix of the variates concerning the 11 items obtained in various surveys is shown in Table IV.3-5. The following characteristics are pointed out.

Table IV.3-5 Correlation matrix (Local model)

	1	2	3	4	5	6	7	8	9	10	11
1	1.0000	-0.0662	-0.3206	-0.0562	-0.1145	0.3779	0.0067	0.3301	-0.1507	-0.1343	-0.0931
2	-0.0662	1.0000	0.3889	-0.0421	0.1516	-0.0952	-0.0258	0.1003	0.0963	0.1036	0.2012
3	-0.3206	0.3889	1.0000	0.5387	0.8140	-0.3902	0.0824	-0.2585	-0.2026	-0.2605	-0.1772
4	-0.0562	-0.0421	0.5387	1.0000	0.5775	-0.1098	0.2694	-0.3277	-0.2665	-0.3727	-0.3754
5	-0.1145	0.1516	0.8140	0.5775	1.0000	-0.3482	-0.1323	-0.4216	-0.1984	-0.2715	-0.1726
6	0.3779	-0.0952	-0.3902	-0.1098	-0.3482	1.0000	0.5056	0.5840	0.3153	0.2963	-0.3806
7	0.0067	-0.0258	0.0824	0.2694	-0.1323	0.5056	1.0000	0.3760	0.1209	0.0500	-0.4046
8	0.3301	0.1003	-0.2585	-0.3277	-0.4216	0.5840	0.3760	1.0000	0.2921	0.2694	-0.0309
9	-0.1507	0.0963	-0.2026	-0.2665	-0.1984	0.3153	0.1209	0.2921	1.0000	0.9382	0.0501
10	-0.1343	0.1036	-0.2605	-0.3727	-0.2715	0.2963	0.0500	0.2694	0.9382	1.0000	0.1424
11	-0.0931	0.2012	-0.1772	-0.3754	-0.1726	-0.3806	-0.4046	-0.0309	0.0501	0.1424	1.0000

(1) The correlation coefficients among the items are generally higher compared to those of the regional model. This is thought to represent that these measured values are controlled by comparatively small number of factors.

(2) Especially, it is natural that the 10 m depth temperature and the 1 m depth temperature have high correlation (correlation coefficient 0.9382). Also, correlation is recognized between the anomalous value of gravity and the magnetic anomalous value, between the total conductance value and the concentration of CO_2 gas, and between the total conductance value and the concentration of radon gas.

2. Factor analysis

The eigenvalues the eigenvectors, the factor loading and the vector map are shown in the Table IV.3-5, 6, 7, 8 and in the Fig. IV.3-2.

As the results, the following three principal factors have been extracted.

Table IV.3-6 Eigen value · Eigen vector (Local model)

... EIGEN VALUE ...

EFFECTIVE NUMBER : 6

3.421	2.157	1.803	1.175	0.835	0.517	0.451	0.264	0.259	0.076	0.043

... EIGEN VECTOR ...

	1	2	3	4	5	6	7	8	9	10	11
1	0.1480	0.2202	-0.3647	-0.3949	0.6206	0.1939	-0.1462	-0.2854	0.3023	0.1252	0.0901
2	-0.0583	-0.1143	0.3602	-0.6896	-0.1166	-0.2990	-0.4838	-0.0215	-0.0854	-0.1639	-0.0808
3	-0.4094	0.1175	0.3766	-0.2086	-0.0282	-0.0260	0.3309	-0.0280	0.1462	0.6160	0.3474
4	-0.3447	0.3586	0.1162	0.1328	0.0989	0.4641	-0.3572	-0.1347	-0.5862	0.0586	-0.0587
5	-0.4221	0.0969	0.2500	-0.0618	0.4166	0.0870	0.3116	0.3310	0.1965	-0.4862	-0.2887
6	0.3587	0.4144	0.0203	-0.0483	0.1133	-0.1041	-0.1164	0.7691	-0.1283	0.1844	0.1330
7	0.1188	0.5039	0.1839	0.0177	-0.4880	0.3234	-0.1321	-0.0938	0.5477	-0.1502	-0.0804
8	0.3649	0.2155	0.0411	-0.4038	-0.1360	0.1266	0.6126	-0.1985	-0.4145	-0.1216	-0.1410
9	0.3291	-0.0927	0.5115	0.1991	0.2593	0.0975	-0.0233	-0.1644	-0.0244	-0.3255	0.6091
10	0.3513	-0.1626	0.4687	0.1775	0.2505	0.0722	-0.0582	-0.0915	0.0823	0.3963	-0.5962
11	0.0495	-0.5287	-0.0474	-0.2582	-0.1334	0.7094	-0.0134	0.3384	0.0466	0.0621	0.0862

Table IV.3-7 Factor loading (Local model)

	1	2	3	4	5
1	0.2671	0.2468	-0.1850	-0.4376	-0.4120
2	-0.3211	-0.2442	0.3082	0.1597	-0.3709
3	-0.9801	-0.1073	0.1334	0.0187	-0.0044
4	-0.5871	0.1454	-0.1012	-0.3151	0.3769
5	-0.8850	-0.0405	-0.4206	-0.0996	-0.0246
6	0.4253	-0.2095	0.1380	-0.7423	-0.0834
7	-0.0159	-0.1359	0.4845	-0.5895	0.2799
8	0.3412	-0.2234	0.4254	-0.4108	-0.4085
9	0.2979	-0.9205	-0.0604	-0.0253	0.0442
10	0.3606	-0.9022	-0.0434	0.0671	-0.0144
11	0.1825	-0.0278	-0.0740	0.5821	-0.3055

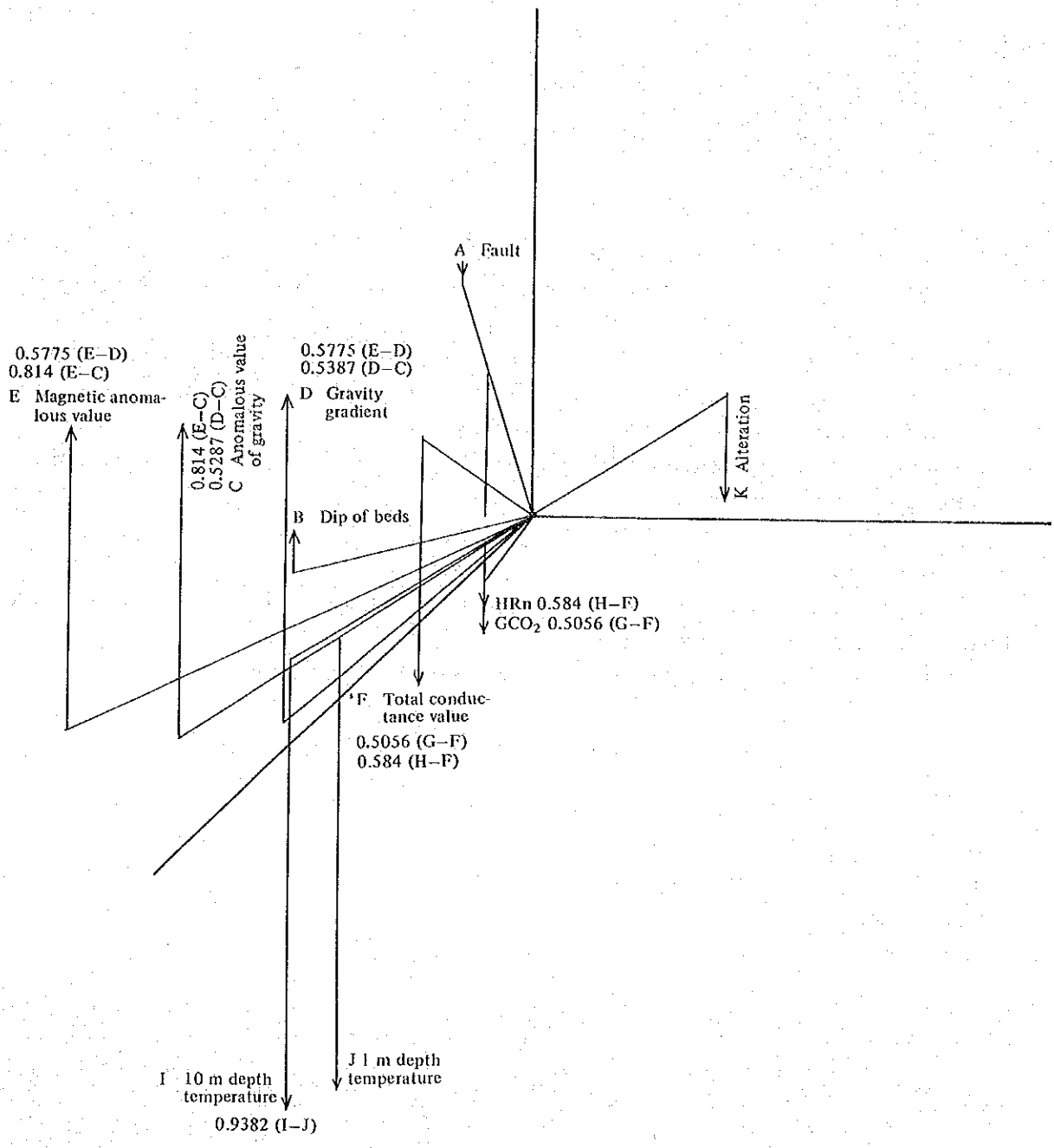

Fig. IV.3-2 Factor vector (Local model)

Table IV.3-8 Factor loading (Varimax rotation)

	1	2	3	4	5
1	-0.6154	-0.0197	-0.4732	0.2819	0.2969
2	-0.3311	0.0838	0.1706	-0.8616	-0.3345
3	-0.2196	0.6202	0.6377	-0.3919	-0.0833
4	-0.0474	0.6592	0.5980	0.1977	0.4081
5	-0.4536	0.6056	0.6165	0.1354	-0.1706
6	-0.3656	-0.5013	-0.2146	0.0172	0.7541
7	0.0443	-0.1029	0.1949	-0.3230	0.9193
8	-0.3805	-0.4831	-0.4086	-0.5058	0.4463
9	-0.1632	-0.8875	0.4190	-0.0873	-0.0501
10	-0.1307	-0.9158	0.3344	-0.1162	-0.1372
11	0.1275	-0.2164	-0.3426	-0.1332	-0.8954

(1) Factor 1: The factor loading of this factor is −0.6154 of the distance from faults and −0.4536 of the magnetic anomalous values. The meaning of this factor is uncertain.

(2) Factor 2: Concerning this factor axis, the 10 m depth temperature and the 1 m depth temperature have very similar behavior. Same tendency is exhibited by the magnetic anomalous values, the anomalous value of gravity and the gravity gradient, although they are in reverse correlation to the above two items. Furthermore, the concentration of CO_2 gas, the concentration of radon gas and the total conductance values are revealing same tendency. The factor loading of this factor is −0.8815 of the 10 m depth temperature and −0.9158 of the 1 m depth temperature. It is thought that this factor 2 is indicating temperature.

(3) Factor 3: This factor is related to the factor common to the 10 m depth temperature, the 1 m depth temperature, the concentration of radon gas, the gravity gradient, the anomalous value of gravity and the magnetic anomalous value and is thought to be the factor to represent influence of fissures.

However, the factor 2 and the factor 3 are not representing simple and independent temperature of fissure only, but it is possible that the factors are to compose such complicated factors as the influence of geothermal fluid which is controlled by fissures.

Factor scores were calculated concerning the above three factors at each of the observation points, and the distribution map of the scores was drawn up.

It is thought that the Factor score map for local model (Factor 1) (PL. IV.3-4) is expressing the degree of the influence by the distance from faults. The contour lines are mostly in the direction of NW-SE, which is in harmony with the trend of the faults located in the vicinity.

The maps of the Factor score map for local model of the factor 2 and of the factor 3 (PL. IV.3-4, 5) are taken to reveal quite same pattern. The absolute values of the factor scores are high at and around the shallow boring hole S-12 or S-13, where the contour lines are seen to form closed circles. This form is very similar to the patterns expressed by the 10 m depth temperature and by the 1 m depth temperature. From the above fact, it is thought that the factor 2 and factor 3 are reflecting temperature and fissures or existence of the geothermal fluid which is the multiplicative effect of the former two elements.

IV-4 Consideration

As there are small number of deep wells and as no measured data are available as to the permeability coefficient, it is impossible to express quantitative distribution of temperature and

permeability coefficient. However, it is thought that the distribution of the factor scores concerning such factors as to indicate temperature and fissures would represent the degree of relative level of temperature and of relative level of permeability.

Accordingly, viewing from the distribution of the factor scores, two areas could be extracted in this surveyed area, favorable for the existence of geothermal fluid, where the temperature is high and the permeability is also high. The one is the area from Ban Pong Nok to Ban Huai Dua through Wat Pong Hom, which is located around the area where the present geothermal indications are distributed. The other is the area in the southeastern peripheral zone from Wat Nong Hoi to Ban Mai through Ban Hua Fai. In the latter case, no geothermal indication has been recognized on the surface and no fracture zone has been confirmed by the present geological survey. Therefore, it is not certain as to whether the existence of geothermal fluid is possible in the area. It is estimated that geothermal reservoir would be seated in fairly deep portion, even if the reservoir would exist.

V EVALUATION OF THE PROJECT

V EVALUATION OF THE PROJECT

V-1 Structural Model of the Geothermal Reservoir

Concerning the San Kampaeng geothermal project, considerations are given on the geological structure, the geothermal structure and the hydrographical structure on the basis of the previous survey data and the informations obtained through the present surveys. A model of geothermal reservoir is brought forward by synthesizing the above considerations.

V-1-1 Geological Structure

The surveyed area is geologically underlain by the Carboniferous Mae Tha Formation, the Permian Kiu Lom Formation, the Triassic granites and the alluvial deposits. The Carboniferous and the Permian systems are composed of sedimentary rocks such as sandstone, shale, chert, limestone and basaltic rocks.

The subject area is divided into three structual units by the Huai Pong fault and the Huai Mae Koen fault. They are the Doi Luang uplifted zone, the Ban Pong Hom subsided zone and the Mae Tha uplifted zone, located in this order from the west to the east.

The Doi Luang uplifted zone is topographically corresponding to the western mou tainous land and is composed of the Mae Tha Formation which comprises mainly the massive siliceous sandstone with quartz veins well developed. Faults of the trends of NW-SE, E-W and N-S are well developed in this zone, and foldings with the axes in the directions of NW-SE are also recognized.

The Ban Pong Hom subsided zone is corresponding to the central lowland and is composed of the Permian Kiu Lom Formation, which is divided into three parts lithologically; the upper part, the middle part and the lower part. The lower part of the Kiu Lom Formation is composed of such marine sediments as limestone, chert, sandstone, shale and siltstone. The middle part of the formation is composed mainly of basaltic rocks and limestone with some inserted layers of shale in parts. Faults of the trend of NNE-SSW, NNW-SSE and NW-SE are predominantly developed. These faults are especially well developed in the western part of this subsided zone, and folds are also recognized there. In some parts of this subsided zone, folding structures of the same trend as that of the faults are recognized, but they are not so remarkable as those found in the uplifted zones, and the geological structure in this zone is, as a whole, homocline dippfing toward the east.

The Mae Tha uplifted zone is corresponding topographically to the eastern mountainous land and is composed of sandstone of the Mae Tha Formation, shale of the lower part of the Kiu Lom Formation and the Triassic granites. Faults of the trend of NNW-SSE are prevailingly distributed. Other faults of the trends of NE-SW and E-W, which are observed to have been cut by the faults of the above trend are recognized. The folding structures of the trends of N-S or NW-SE are developed.

The area where the geothermal indications are distributed is structurally located along the western marginal area of the Ban Pong Hom subsided zone. This area is the remarkable part of the surveyed area where faults and folding structures are concentrated. This geothermally active area is positioned on the east wing of the anticline, about 200 meters apart from the axis of anticline, which is extending northwestward from Ban Pong Nok. The fault branched from the Huai Pong fault, by which the Doi Luang uplifted zone and the Ban Pong Hom subsided zone are bounded, is recognized to run along the southern margin of the area where the geothermal

indications are distributed. As is above-mentioned, the geological layers have been fractured in this area by structural deformation, and the area is estimated to have favorable structure for the movement and accumulation of the geothermal fluid.

Also, as the western periphery of the Ban Pong Hom subsided zone is composed of the lower part of the Kiu Lom Formation, which has certain fragility, it can be said lithologically that this area is such area where fractures are easily developed. That is, the lower part of the Kiu Lom Formation is composed of the alternation of limestone and shale, the sandstone bed, the alternation of siltstone, sandstone and chert, the chert bed, the alternation of chert, siltstone and sandstone and the sandstone bed. Various rocks are accumulated in frequent alternation of comparatively thin layers there. It is known that such succession as the lithological difference is so remarkable in vertival direction is easily fractured during the period of structural movement. In another words, brittle rocks like chert and sandstone are easily broken to pieces, while ductile rocks like siltstone and shale are apt to be destroyed with cleavages and slides by shearing stress. This is evidenced by the result of the observation of the drill core of the holes of GTE-1 to GTE-5. For example, a shearing fracture zones, are developed in the hole of GTE-4, and the most predominantly sheared part is in the alternation of sandstone and shale. By the geological survey, it has been recognized that the layers of the lower part of the Kiu Lom Formation, especially chert and sandstone are fractured remarkably and broken into pieces. On the contrary, the sandstone in the Mae Tha Formation, composing the Doi Luang uplifted zone and the Mae Tha uplifted zone, is homogeneous and massive. This sandstone is not fractured as a whole and there is no single layer to be so remarkably fractured, although structural joints are developed in some parts. In addition, these joints have been filled with quartz veins in the process of diagenesis, and it is thought that the permeability is small in the area where the Mae Tha Formation is distributed. The basalts, which are the principal components of the middle to upper part of the Kiu Lom Formation, are composed of tuff, lapilli tuff, tuff breccia and lava. In spite of the differences of the rock species of lava and phyroclastic rocks, it can not be said so far observed at the outcrops that structural fissures are well developed. The fact that structural fissures are hardly developed in the basaltic layers of the middle to upper part of the Kiu Lom Formation is estimated to be elucidate by the points that the basaltic rocks are composed mineralogically of such minerals as to have almost uniform assemblage, and that they have rather homogeneous physical properties. Also, as the basaltic rocks contain lots of ferromagnesian minerals, and are easily weathered and altered, it is thought that the existing fissilities would be filled with weathered products and alteration minerals.

As above-stated, it is possible to conclude that the Ban Pong Hom area where the geothermal indications are distributed is located in the area with fractures well-developed, compared to the surrounding area, lithologically and structurally.

V-1-2 Geothermal Structure

1. Geothermal indications

The geothermal indications on the surface in the San Kampaeng geothermal area are recognized to be concentrated in the midway between Wat Pong Hom and Ban Pong Nok, on the right bank of the middle-stream of the Huai Ang River (PL. II.1.1-5). Further in detail, the

geothermal indications are distributed in two areas; the one is the area from the geothermal exploration well GTE-2 to Wat Pong Hom, and the other is the area at about 400 meters southeast of Ban Pong Nok. The distance between the two areas is about 500 meters. Although little indication has been recognized, in this zone between the two areas, it is anticipated that the indications in both areas would have been brought about from the same geothermal reservoir. Another geothermally indicated area in the southeast of Ban Pong Nok is swampy, and details such as its extension and distribution of hot springs are not certain. No investigations like ground temperature survey and exploration drilling have yet been carried out by Thailand side. In the area from the geothermal exploration well GTE-2 to Wat Pong Hom, geothermal indications are recognized in an approximate area of 0.5 km x 0.6 km along the branch stream on the right bank of the Huai Ang River. The indications are found in the plain along a small stream, composed of alluvium deposits. Most of the geothermal indications are hot springs and outcrops of altered rocks as well as heated ground. Fumaroles are not recognized. This is thought to be due to the chemical composition of the hot spring water, because such gas ingredients of H_2S and CO_2 are contained very little in it. There are more than 70 hot springs, so far observed, and it is inferred that the number of the hot springs would be more than 100, including those which have not been recognized being covered by grasses. The amounts of the spring water of most of the hot springs are as small as 0.1 ~ 0.5 l/min, but the temperature is as high as 70 ~ 95°C, with the highest value of 98°C, so far measured. Hot water is flowing in the stream near the hot springs, and it is dangerous to step into the stream. The hot spring water is colorless and odorless, comprising simple water spring. Most of the spring water is qushing out from the sands and gravels of the alluvium deposits and from the river bed sediments. In some boiling out or blowing out jet sound is accompanied.

2. Igneous activity

It is thought that igneous rocks and volcanic rocks would have an important role as consideration of the heat sources in any geothermal area. Consideration is given on the igneous activity in this area, for the comprehension of geothermal sources.

The igneous rocks and the volcanic rocks distributed in this area are the basaltic rocks of the Permian Kiu Lom Formation, the Triassic granites and the Tertiary basalts found in the southern part of the surveyed area.

The basaltic rocks in the Kiu Lom Formation are composed of various lithofacies as lava, tuff, lapilli tuff and tuff breccia, which were formed by the extrusion of magma. By the age determination by K-Ar method, the result shows various values between 119 ±14 m.y. and 389 ±19 m.y., but it is thought from the fossils contained in the inserted limestone layers that the period of the formation of the basaltic rocks is middle Permian. Because the volcanic activities of the basaltic rocks would have been too old as above-stated, there is no possibility that these basaltic rocks of the Kiu Lom Formation could be acting as heat sources for the San Kampaeng geothermal system.

The Triassic granites are recognized outcropping in the mountaneous land in the northeastern part of the surveyed area. The age of the granite determined by K-Ar method is 212 ±10 m.y., which is thought to indicate the period when melted magma was cooled and consolidated. As the period of the formation of the granites is pretty old, it is thought to be difficult that the remain of the heat, which these granites used to reserve when consolidated, would compose the heat source for the present geothermal reservoir, even if the granite is of huge mass.

There are many hot springs in the northern part of the Kingdom of Thailand. It has been suggested that the distribution of the hot springs is intimately related to the distribution of granites, geographically. In this suggestion, it is pointed out that the granite can be exothermic body by the heat emanation of contained radioactive elements or that the granites have some important roles as to control structurally the passage of geothermal fluid from the depth to the surface.

In the Central North Tectonic Province in the northern part of the Kingdom of Thailand, effusion of the large volume of tertiary basaltic rocks is known. As there is no volcanic activity in the Quaternary period recognized in the northern part of the Kingdom of Thailand, this offusion of basaltic rocks is the youngest volcanic activity in that area. However, the exposures of the basaltic rocks ever confirmed are distributed in the area about 60 km south of the San Kampaeng geothermal area, and no Tertiary basaltic rocks have been recognized in the surveyed area in the present survey. Accordingly, there is no positive evidence that the basaltic activity which might have occurred in this area would have supplied any heat sources. It is generally thought that basaltic magma bearing high viscosity and high fluidity is not likely to form such magmatic reservoir as to accumulate large scaled high level energy. On the contrary, acidic magma such as dacitic magma or rhyolitic magma has low viscosity and is thought to be likely to form such magmatic reservoir for large scaled high level energy to be accumulated. Therefore, even if there should be an intrusive body (sheet, dyke) of basaltic rocks at the depth in this surveyed area, it can not be expected that such intrusive body could offer any heat source because if would be aged too old and would be scaled too small.

As above-mentioned, by the results of the consideration on the igneous activity on the basis of the igneous rocks distributed on the surface in this surveyed area, it is concluded that there is very small possibility for some remaining heat, which any melted magma used to have when consolidated, to work as the heat source for the present geothermal reservoir.

3. Heat source

There are many hot springs of high temperature nearly 100°C in the San Kampaeng geothermal area. It is expected that some heat source would exist to produce geothermal fluid of high temperature. However, all what can be mentioned at present about the heat source in this area is only by estimation, because no concrete geothermal information at the depth have been avaslable. Concrete information and evidence have not been obtained in the present surveys, but by the reason described hereunder, the heat source in this San Kampaend geothermal area is estimated to be regional high heat flow and emanated heat from radioactive elements contained in the latent granite.

(1) Most of the hot springs in the northern part of the Kingdom of Thailand are distributed in inner part of or along the periphery of granite body. The intimate geographical relation like the above is thought to suggest that the granitic bodies have some influence on the genesis of these hot springs. The San Kampaeng geothermal area is located along the periphery of the large granitic batholith, exposing in the Mae Tha mountaineous land, regionally, and it is possible that the hot springs in this area are related to the granite genetically.

However, veiwing from the distance of about 6 km between the exposure of the granite and the area where the geothermal indications are distributed, and from the geological structure

of fault blockage and inclination of beddings, it is difficult to take that the geothermal fluid formed at the depth in the granite would have been conveyed laterally in a distance of more than several kilometers to spring out in the area where the geothermal indications are distributed. Therefore, existence of latent granite body is estimated here as the direct heat source, structurally at the depth of the Doi Luang uplifted zone, in the vicinity of the area where the geothermal indications are distributed. The Doi Luang uplifted zone is, as is the Mae Tha uplifted zone where the granite is exposed, composed of the Carboniferous Mae Tha Formation, and has almost same degree of the upheaval structure as the Mae Tha uplifted zone. Accordingly, the possibility of intrusion of Triassic granite in the Doi Luang uplifted zone is conceivable viewing from the geological structure. This possibility is also agreed from the viewpoints of the high gravity anomaly which has been found in the west of the Doi Luang fault as well as the assumed reflection horizons caught by the seismic survey.

As afore-mentioned, the age of the Triassic granite by K-Ar method is 212 ±10 m.y. and the remaining heat at the consolidation of magma can not be expected to exist as the heat source. There are two roles of the granite to work for heat source. The one is heat emanation by radioactive elements contained in the granite and the other is structural control, that is, the passage for the geothermal fluid.

The Masozoic granites in the southern part of the Kingdom of Thailand cotain much of radioactive ingredients such as kalium (3.5 – 5.3%), uranium (5 – 57 ppm, average 16.2 ppm) and thorium (3 – 85 ppm, average 33.0 ppm), and are known to have exothermic capability so much as three times compared to the granites distributed in the southwesten inner zone of the islands of Japan. It is said that 1.2 HFU of heat flow is expected from the granite independently, if a granite batholith is assumed to exist continuously to the depth of 10 km. Considering such high exothermic capability of granite, the Triassic granite is thought to compose parts of the heat source in this surveyed area.

Details of the structure control by the granite on the geothermal fluid are not certain in many points.

(2) Viewing the chemical composition of the hot spring water in the San Kampaeng geothermal area, the pH is 8 ~ 9, which shows it is weakly alkaline. It has little amount of soluble ingredients as seen of the density of Cl^- to be about 25 mg/l and that of SiO_2 to be about 150 mg/l. It is pointed out that this chemical composition is similar to that of the hydrothermal solution obtained by artificial circulation of it in the granite, in the process of the hot dry rock geothermal study, held at the Los Aramos Laboratory in U.S.A. From this similarity of the chemical composition, it is estimated that the hot spring water in the San Kampaeng geothermal reservoir would have been formed through the circulation in the latent granite, after the penetration of rainwater into the depth.

(3) In the northern part of the Kingdom of Thailand including this geothermal area, active structural movements are recognized and high degree of heat flow is revealed compared to the surrounding areas. It is possible that the heat which have been brought about in this process would have had certain role for the formation of the geothermal fluid.

That is, by the subduction of the Indianplate into Java Trench, the floor of the Andaman Sea has been expanded and the tension stress field has appeared in the area from Burma to the

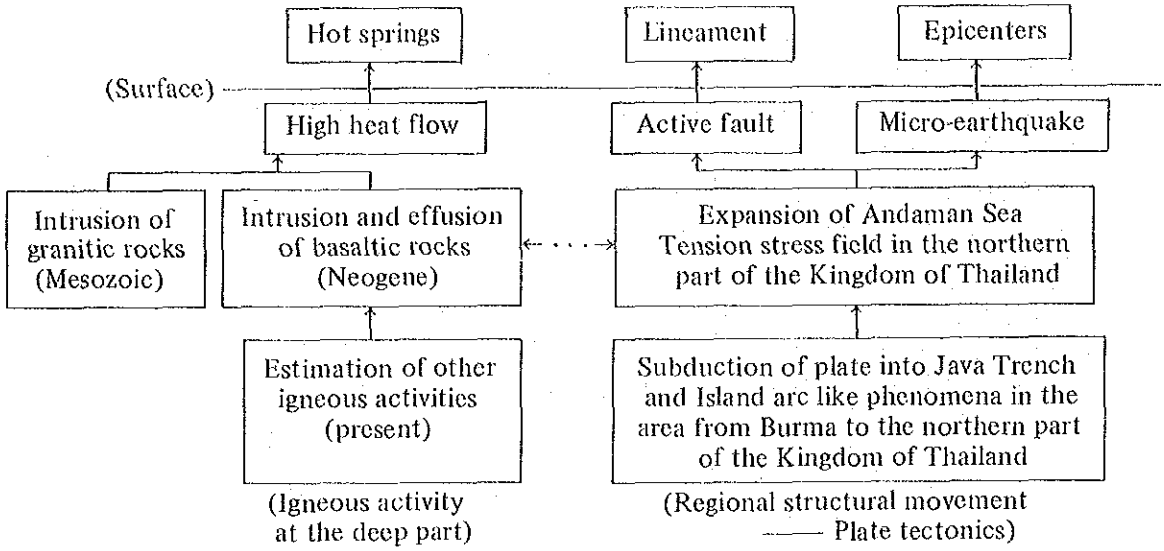

Fig. V.1-1 Regional geothermal system in the northern part of the Kingdom of Thailand

northern part of the Kingdom of Thailand. In this tension stress field, many faults were formed, and intrusion and effusion of the basaltic rocks occurred. It is thought that the high heat flow has been generated in this way in the northern part of the Kingdom of Thailand.

Also, in the Burmese side, the hypocenters of earthquake are distributed deeper toward the east, and the area has the character of island arc, geo-structurally, which is the same character of the Indnesian islands, the Philippine island and Japanese islands have. Takashima and Kawada has bought forward an idea, under the geological circumstaces as above-stated, that some igneous activity might be at the depth of the northern part of the Kingdom of Thailand, and that the high heat flow in this area would have been brought about by this igneous activity.

The Fig. V.1-2 expresses the distribution of the lineaments and the earthquake epicenters, obtained from the analysis of LANDSAT imaginary. The lineaments found in and around the San Kampaeng geothermal area are well coincident with the fault systems, which have been clarified in the present geological survey. Mentioning about the characteristics of the lineament distribution, first class lineaments are recognized running in parallel in the form of the letter of S, around Chiang Mai and along the Mae Tha fault in the eastern part of the surveyed area. Many of the earthquake epicenters are distributed along these lineaments. The distribution of the hot springs has same tendency. These lineaments are thought to represent actually active structural lines (active fault), which are accelerating upflow of geothermal fluid.

Summarizing the above-mentioned articles, it is estimated that the heat source in the San Kampaeng geothermal area, with the regional high heat flow in the northern part of the Kingdom of Thailand (average heat flow) for the background, have been formed by the emanated heat of the radioactive elements contained in the granite (Special heat source). (Fig. V.1-1)

4. Measurement of ground temperature

Ground temperatures were estimated by the geochemical thermometer. Examples of the results are given in the following table (Table V.1-1).

As geochemical thermometers, silica thermometer, Na-K thermometer and Na-K-Ca thermometer were employed.

Generally, hydrothermal solution is saturated with silica by solution of quartz in the geothermal reservoir, while amorphous silica whose solubility is higher than quartz is formed first when precipitated in the shallow part in the underground.

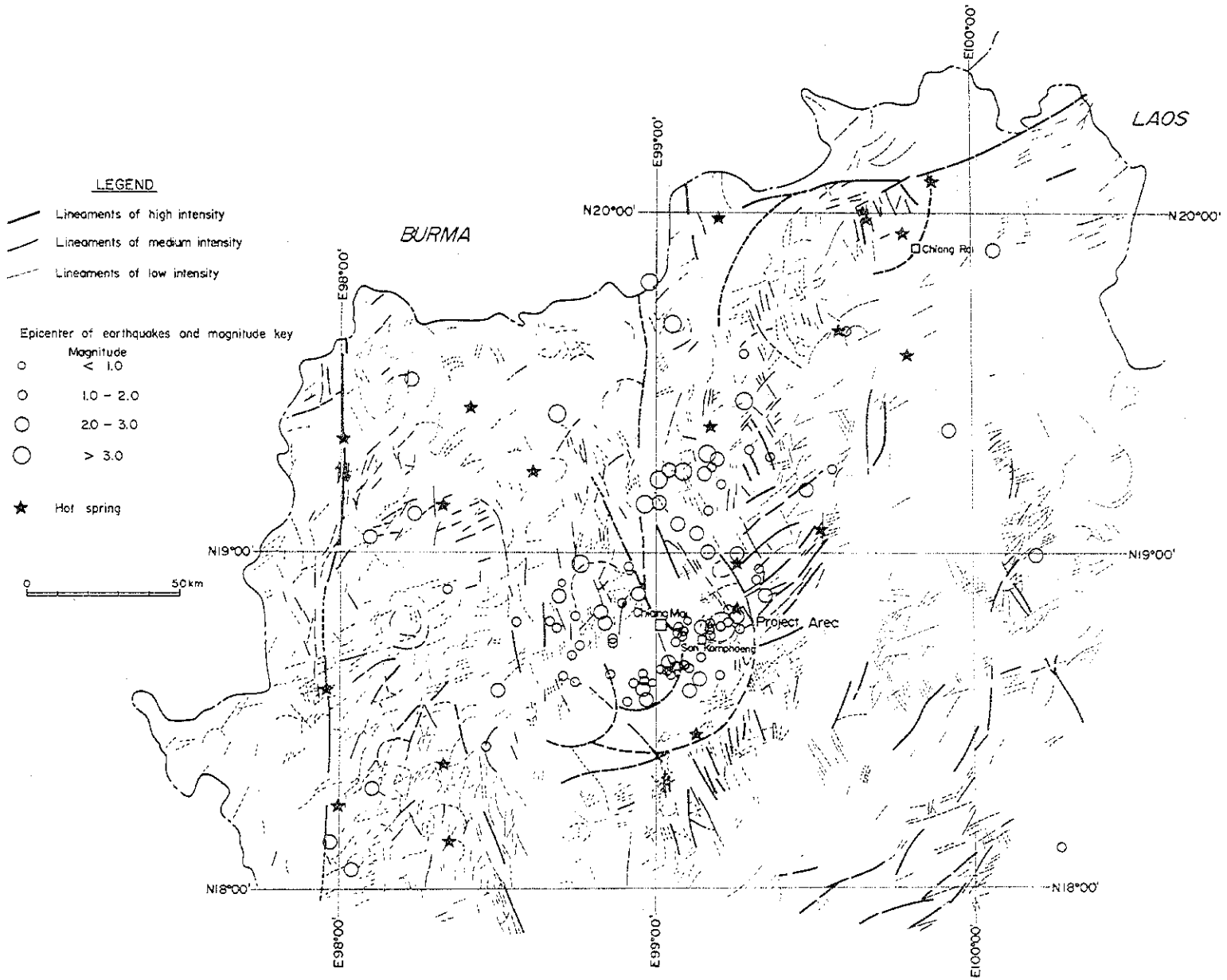

Fig. V.1-2 Earthquake distribution and Analysed structure from LANDSAT imaginary

Table V.1-1 Chemical composition of hydrothermal solution and geochemical thermometer in the San Kampaeng area

Source	T (°C)	PH	Na (mg/l)	K (mg/l)	Ca (mg/l)	SiO_2 (mg/l)	Silica thermo-meter (°C)	Alkali-ratio thermometer	
								Na-K (°C)	Na-K-Ca (°C)
1	98	8.2	151	13.5	2.42	148	159	176	192
2	100	8.9	155	14.5	0.70	150	160	180	207

(after Thai's data)

Silica thermometer is a geochemical thermometer which has been developed experimentarily on the basis of the above regularity.

In case of the San Kampaeng area, the cooling of the hydrothermal solution in the process of upflow is thought to be adiabatic, the temperature was calculated by the following formula.

$$t\,(^{\circ}C) = \frac{1{,}015.1}{4{,}655 - \log SiO_2} - 273.15$$

unit of SiO_2: ppm

The underground temperatures obtained by this formula are 159°C and 160°C. The hydrothermal solution in the San Kampaeng geothermal area is thought to have been diluted by admixture with surface water. Therefore, it is estimated that the calculated value is rather low compared to the actual temperature of the geothermal reservoir.

Generally, it is thought that the chemical equilibrium is realized with such elements as Na, K and Ca between the hydrothermal solution and the minerals as plagioclase and alkaline feldspar in geothermal reservoir. The alkaline ratio thermometer is a geochemical thermometer developed by the above principle.

For the calculation by the Na-K-Ca thermometer, the following formula is employed.

$$t\,(^{\circ}C) = \frac{1{,}647}{\log (Na/K) + \beta \log (\sqrt{Ca/Na}) + 2.24} - 273.15$$

unit of Na, K and Ca: moles/l

The underground temperatures obtained by this calculation are 192°C and 207°C (Table V.1-1). As the alkali-ratio thermometer employs density ratio of Na, K and Ca, it has tendency to indicate actual temperature of the geothermal reservoir, even if dilution of hydrothermal solution by underground water or separtion of gas from liquid occurred there. Accordingly, it is thought that the estimated temperature obtained by the Na-K-Ca thermometer is representing the temperature of the hydrothermal solution in the deeper part of that before the admixture of underground water, compared to the temperature by the silica thermometer.

For the calculation by the Na-K thermometer, the following formula is employed:

$$t\,(^{\circ}C) = \frac{855.6}{\log (Na/K) + 0.8573} - 273.15$$

unit of Na and K: ppm

The underground temperatures of the source 1 and 2 estimated by the Na-K chemical thermometer method show 176°C and 180°C, which are in the midst of the upper values obtained from Na-K-Ca method and the lower from SiO_2 method.

The fairly wide range of distribution of these estimated temperatures is thought to be due to the fact that the hydrothermal solution is diluted and cooled by the admixture of underground water and that it reacted with minerals contained in the rocks along the passages of the solution in the process of upflow from the geothermal reservoir to the surface.

By the Thailand side, concentrations, in the hot spring gas, of H_2O, CO_2, H_2S, H_2, Ar, O_2, N_2 and CH_4 were analysed, and the underground temperature was calculated on the base of the equilibrium of $CH_4 - CO_2$. The highest value of the temperature thus estimated is 247°C. The difference between this value and the result of the geochemical thermometer is more than 40°C, but the reason is uncertain. Examining the estimated values of temperature tried by $CH_4 - CO_2$ isotopic thermometer in various geothermal areas in the world, the estimated values are higher by more than 50°C than the measured values in many cases. Accordingly, it can be said to be natural that the value of the temperature of 247°C is higher than the actual temperature of the geothermal reservoir.

From the result of the estimation of temperature by the geochemical thermometer, it is inferred that the temperature of the geothermal reservoir in the San Kampaeng area is in the approximate range of 160° ~ 210°C, but predominant domain of temperature is uncertain.

5. Distribution of ground temperature

By the geothermal survey carried out by Thailand side, the distribution maps of the 1 m depth temperature and the 10 m depth temperature had been prepared. In addition to them, the 10 m depth temperature distribution map covering almost half of the surveyed area were made by the temperature measurement using the short holes for the present seismic survey (PL. II.2.2-15). By the results of these surveys, the high anomaly in the 1 m depth temperature distribution map and that in the 10 m depth temperture distribution map are quite well coincident with the area of distribution of the hot springs and the heated ground. This fact suggests that the high anomaly of the ground temperature distribution has been caused by the conveyance of the geothermal fluid.

The iso-value contour of the temperature of 40°C in the 10 m depth temperature distribution map forms an oval with major axis in the NW-SE direction. It has an approximate area of 400 m x 600 m. The highest value of the temperature is about 130°C, which was recorded in the geothermal exploration well of S-13, around which iso-value contours of the temperature are distributed in cocentric form. The high anomaly of the ground temperature distribution is separated from the other area by the steep gradient zone extending in the NW-SE direction from Wat Pong Hom. Also, the high anomaly of the ground temperature is situated in the low land where the alluvium deposits are distributed, geologically. Viewing from the cocentric distribution of iso-value contour lines of temperature around the well of S-13, it is estimated that the geothermal fluid moving up through certain narrow path has diffused outward in the subsurface alluvial deposits or in the weathered zone of the Paleozoic formations.

Other than the area where the geothermal indications are distributed, there is an anomalous zone with the 10 m depth temperature of more than 30°C from the geothermal exploration well GTE-1 to the survey line E of the seismic survey, in the southern part of the surveyed area. The

anomalous zone is corresponding to the extension of the distribution of the basaltic tuff belonging to the upper part of the Kiu Lom Formation, but no fault has been confirmed in the vicinity.

6. Alteration zone

Around the area where the present geothermal indications are distributed, alteration is recognized. Outward from the center, the alteration reveals zonal distribution in the order of alunite zone – kaolinite zone – kaolinite-montmorillonite zone – montmorillonite zone – halloysite zone. The minerals detected by the X-ray diffraction analysis include, apart from rock-forming minerals, such minerals as formed by diagenesis or metamorphism in old periods in addition to the minerals formed by the geothermal alteration. The above division of the distribution of the alteration zones are based on the assemblage of the clay minerals excluding sericite and chlorite. Generally, assemblage of the minerals formed by geothermal alteration depends upon chemical composition and temperature of the hydrothermal solution. The Fig. II.1.1-3 shows rough tendency of the stable area of temperature for the alteration minerals to be formed at. By this tendecny, it is thought that the zonal distribution of the alteration in the surveyed area would have been formed by the flow of the hydrothermal solution from the alunite zone (high temperature) to the halloysite zone (low temperature).

The temperature of the hydrothermal solution was possibly more than 200°C in the alunite zone in the center of the zonal distribution, but in most of the area it would have been less than 200°C, and in the halloysite zone, the outermost alteration zone, the temperature is thought to have been less than 100°C.

7. Outline of geothermal structure

Summarizing the above consideration, the geothermal structure in the San Kampaeng geothermal area is estimated hereunder.

It is thought that the heat source is the granitic body distributed in the deep part of the Doi Luang uplifted zone. Rainwater penetrates down to this level and circulates in the granitic body. It is heated conductively and the geothermal solution is formed here. The temperature at this point is thought to be more than 180° ~ 210°C.

The geothermal fluid thus formed is flowing up along the Huai Pong fault and its branch fault. By the conductive cooling and by the admixture with underground water in the process of the upflow, The temperature of the geothermal fluid is lowered and it is as low as 160°C partly.

The geothermal fluid flown up near to the surface has as low temperature as 140° ~ 100°C, and gush out as hot springs in the area where the geothermal indications are distributed. The heat discharge by the hot springs is approximately 7 Mwt (Table V.1-1).

By the result of the temperature measurement of the wells GTE-2 and GTE-5, drilled around the area where the present geothermal indications are distributed (PL. III.2-2, 5), the temperature gradient is almost constant and is approximately 15°C/100 m. The temperature increases up linearly and the heat conveyance by conduction is predominant. Accordingly, the geothermal system in the San Kampaeng geothermal area is comparatively narrow but high temperature convective system controled by the faults, surrounded by the conductive geothermal system bearing higher heat flow compared to the outer area.

V-1-3 Hydrographical Structure

1. Chemical composition of hydrothermal solution

In the Table V.1-2, 3, the chemical composition of the hydrothermal solution in the San Kampaeng geothermal area is shown.

Table V.1-2 Chemical composition of hydrothermal solution in the San Kampaeng geothermal area

		T (°C)	pH	TDS	Alkalinity ($CaCO_3$)	Acidity ($CaCO_3$)	S	Cl	F	K	S	Si
1	Shooting at 3–7 minutes interval, cloudy	85 100	8.5 9.0	1300	366	nd	20.56	50	85	194	25	93
2	Pool-clear	93	8.95	800	410	nd	15.25	42.4	78	164	24.5	109
3	Pool-clear	93	9.0	1500	252	nd	12.18	45.4	84	165	11.5	86
4	Bubbling-clear	100	9.4	1100	324	nd	20.96	37.4	97	140	21	93
5	Mixed by stream water	100	8.5	750	286	nd	7.97	41.0	80	135	11.5	74
6	Pool-clear	99.5	8.5	700	428	nd	11.27	78	85	182	22	87
7	Seeps in stream	99.5	8.45	700	370	nd	20.09	77	80	167	23	87
8	Pool-clear	80	8.0	450	392	nd	20.09	65	78	180	22	89
9	Mixed by stream water	97	8.3	400	366	nd	6.19	34	78	151	13.5	78
10	Pool-cloudy	95	8.3	400	432	nd	19.54	62	85	134	17	106

Table V.1-3 Chemical composition of waters of hot spring areas in the San Kampaeng (in mg/l, TNKC ; Na-K-Ca temperature)

	T(°C)	pH	Li	Na	K	Rb	Cs	Mg	Ca	SiO_2	Cl	SO_4	HCO_3	TNKC	T_{sio_2}
1	92	7.4	.32	142	12.2	.17	.22	9.83	0.19	123	25	21	292	213	149
2	98	8.2	.35	151	13.5	.21	.28	0.18	2.42	148	26	35	312	192	159
3	100	8.9	.36	155	14.5	.22	.30	0.12	0.70	150	20	40	278	207	160
4	42	8.0	.28	140	13.0	.16	.20	3.35	11.52	123	15	71	280	178	149

By the results of this chemical analysis, the pH of this hydrothermal solution is about 8 ~ 9, to be weak alkaline, and its alkaline degree is about 300 ~ 430 (mg/l $CaCO_3$). The analysed values have certain variation, as every water has different condition as to the circumstances of the degree of admixture of underground water and river water.

It is most characteristic as to chemical composition of the hydrothermal solution in this area that the total amount of soluble solid is as small as less than 1,500 mg/l, and that the concentrations of Cl and SiO_2 are so small as less than 80 mg/l and about 120 ~ 150 mg/l respectively. These values are smaller than the values of the hydrothermal solution in any of the geothermal areas ever developed.

The hydrothermal solutions in the northern part of the Kingdom of Thailand are similar on another compositionally. The principal cation is Na, while the main anions are HCO_3 and SO_4. It belongs to the chemical phase of Na-HCO_3-SO_4 type (Fig. V.1-3). It is suggested from such low values of salt density in the hydrothermal solutions that magma is not responsible for the formation of these hydrothermal solution.

The fact that the solutions contain such small amount of soluble solid is thought to be due to

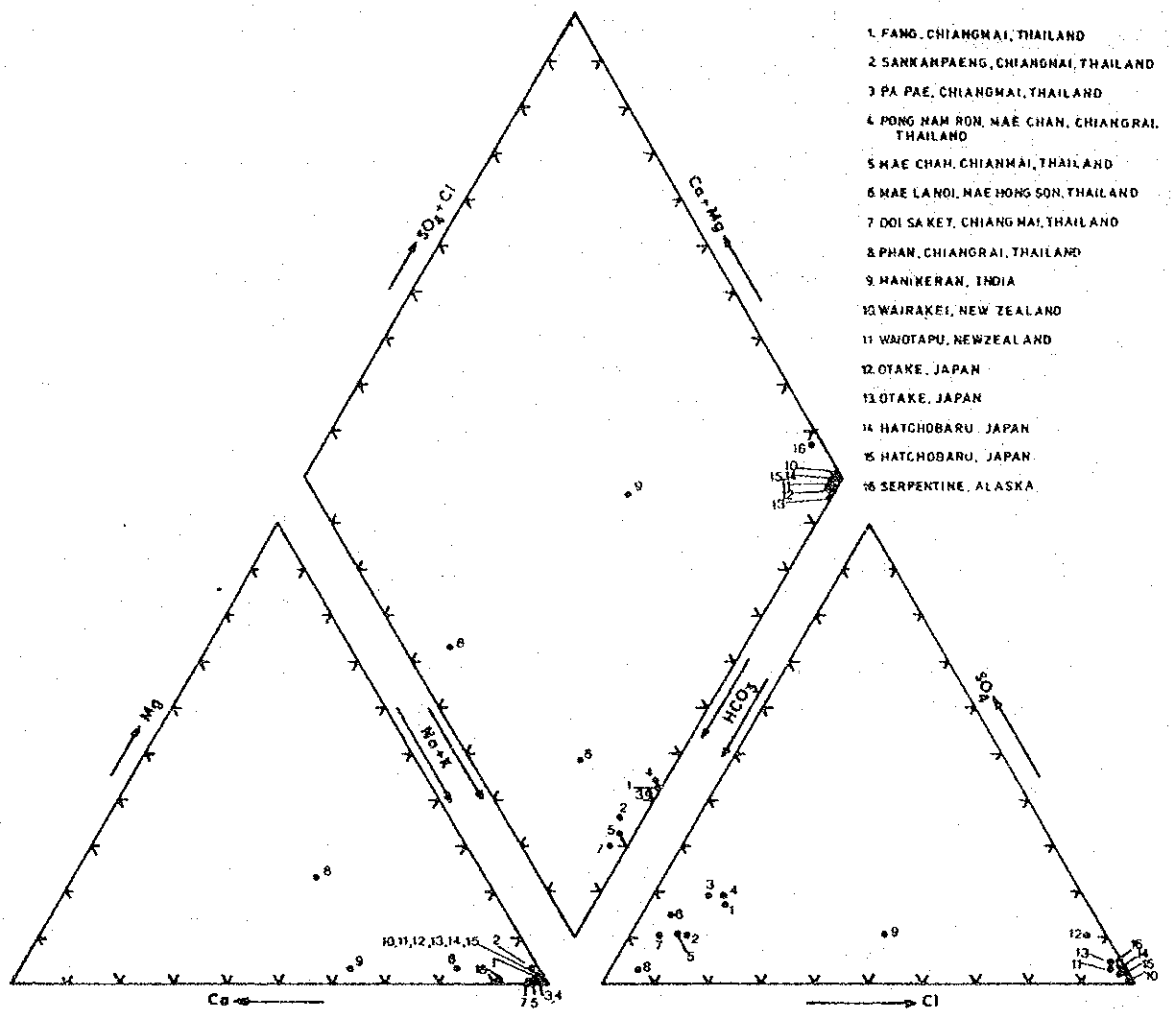

Fig. V.1-3 Hydrochemical characteristics of thermal waters from Northern Thailand and other parts of the world (after Thai's data)

the reason that the chemical reaction between meteoric water and rocks was not sufficient as the circulation of the meteoric water in the heat source rock was very short in time, or because the temperature of the heat source rock was not so high as to accelerate the chemical reaction between the rocks and the meteoric water. Generally, the more easily the ingredients contained in rocks are dissolved, the higher the temperature is, although reverse is true in some cases. Especially SiO_2 is quite sensitive to the temperature and equilibrium can be reached in short time. Also, it is anticipated that the chemical reaction would be accelaerated between the rock and the water when the heat source rock is fractured or is porous remarkably because broad area is expected for the chemical reaction. Accordingly, it is thought about the geothermal fluid in the San Kampaeng geothermal area that chemical exchange of the ingredients between the fluid and the rocks would not have been sufficient in the points of time, temperature and area for reaction.

In any case, there is very small possibility that the geothermal solution has been formed directly depending upon the heat source of volcanic gas or high temperature vapor originated from magma.

The next characteristics of the chemical composition is that the hydrothermal solution is comparatively similar to that of the hydrothermal solution obtained by artificial circulation of it

in the granite, in the process of hot dry rock geothermal study, held at the Los Aramos Laboratory in U.S.A. It is estimated from this similarity that the geothermal fluid in this area would have been formed through the circulation of underground water originated from the rainwater in the granite seated deep in the underground.

The geothermal fluid thus formed is thought to have been diluted by admixture of the surface water in various degrees in the process of the upflow to spring out onto the surface. The reason is as follows.

(1) The underground temperature obtained by the SiO_2 thermometer is about 160°C and the temperature obtained by the Na-K-Ca method is about 200°C. There is difference of about 40°C between the two methods. It is thought that the underground temperature by the Na-K-Ca method is indicating the temperature in the deep part while that by the SiO_2 method is representing the temperature in the shallow part after the admixture of subsurface water.

(2) The hydrothermal solution in this area is comparatively rich in magnesium. It has been evidenced by the comparison of the hot springs that Mg content is apt to be in reverse correlation to the temperature of the spring water. It is general that underground water in the shallow part is rich in Mg. Therefore there is high possibility for the hydrothermal solution in this area to be admixed by shallow underground water.

(3) The *Cl* concentration of the hydrothermal soltuion varies according to the seasons, as is displayed in the Fig. V.1-4. The *Cl* concentration has a tendency to become high rapidly in August and September, at the end of the rainy season. The fact that the *Cl* concentration is lowered is thought to be by the admixture of the rainwater, which is abundant in the rainy season, after the penetration in the underground. It is also thought that hydrothermal solution with high *Cl* concentration flows up from the depth in the dry season, by the pressure of the rainwater after the abundant rainwater goes down to the geothermal reservoir after the rainy season in three or four months. There are many hot springs whose temperature and outflow amount are influenced by rainfall and of river water.

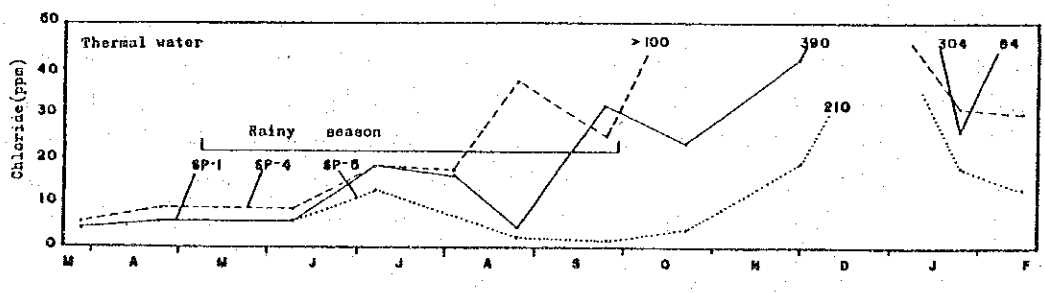

Fig. V.1-4 Variation of chloride concentration with time in the San Kampaeng area (after Thai's data)

2. Alteration zone

As afore-mentioned, the mineral assemblage formed by geothermal alteration depends upon the chemical composition of rocks, but is also controled principally by the temperature and chemical composition of hydrothermal solution. Accordingly, it is possible to estimate chemical compositions of the hydrothermal solution to a certain degree by examining alteration minerals and their assemblages.

The zonal distribution from alunite zone to halloysite zone is recognized outward from the center, concerning the alteration in this area.

It is inferred that the temperature of the hydrothermal solution has variation from high to low from the center outward, and that the property of the solution is found to have variation from acidic character including sulphuric acid to intermediate or weak alkaline character at the same time.

The present alteration survey was carried out around the area where the geothermal indications are distributed, and it has been clarified that the alteration zone is corresponding to the present geothermal indication area. However, viewing it more in detail, there are several different points in the distribution of the above two. The center of the 10 m depth temperature distribution (the center of the area where the geothermal indications are distributed) is at the well whose record of temperature is over 130°C, while the alunite zone, which is thought to be the center, is located about 30 meters south of the geothermal exploration well GTE-2. As there is an approximate distance of 200 meters between the S-13 well and the GTE-2 well, the distance from the center of the alteration zone to the center of the 10 m depth temperature distribution is thought to be at least more than 200 meters. There is a little difference of the direction of the distribution. The extension of the alteration zones is in WNW-ESE direction, while the 10 m depth temperature distribution has a shape with the major axis extending roughly in the NW-SE direction.

It is thought from the difference of the location of the above two factors that the center of the hydrothermal activities has been shifted toward north in the course of time. This shift could be elucidated principally by the sealing of pre-existing spaces and fissilities (self sealing) through the alteration mainly of argilllization.

It is significant that the center of the alteration zone is at the south of the GTE-2 well, because this fact indicates that the supply of the geothermal fluid from the depth would have been from the south. By the above estimation, the upflow of the geothermal fluid has been influenced by the fault of NW-SE trend which is a branched fault from the Huai Pong fault, passing Ban Pong Nok.

By the alteration survey by Takashima and Kawada, it is reported that the alteration zone is continuously distributed for about 1 km in the south of the area where the present hot springs are found. The alteration minerals are quartz, sericite, kaolinite, chlorite, montmorillonite, halloysite, anhydrite, gypsum, alunite and halotrichite, which are almost similar to those found in the area where the geothermal indications are distributed. Therefore, the distribution of the alteration is thought to be a part othe larger alteration zone in the direction of NNW-SSE, shown by Takashima and Kawada, viewing from the distribution and the species of the alteration minerals.

Also, by the present alteration survey, a kaolinite alteration zone has been recognized around Ban Pong Hom in the north of the area where the geothermal indications are distributed. It was

not possible to clarify whether this alteration zone is continuous to, or chronologically same as, the alteration zone extending from the geothermally indicated area to the south.

The alteration zone is distributed structurally in the area between the Huai Pong fault and the Ban Mae Khu Ha fault, and it is thought that this alteration zone is structurally controled by faults in NW-SE direction.

3. Hydrographical survey

The hydrographical survey in this area had been carried out by the Thailand side. By the results of the survey, the latent supply to the underground water from rainwater is 408×10^3 gallons/day/km^2 and there is sufficient surface water which can be utilized for the geothermal development.

It is important to estimate the supply from rainwater to the underground water, for the estimation of scale of the geothermal reservoir and possible amount of geothermal fluid for use. This sort of hydrographical survey was carried out in the Fan geothermal area, which can be refered to, because of its similarity of the circumstances to the San Kampaeng geothermal area.

In the Fan geothermal area, it was inferred by the results of the isotopic analysis of the hydrothermal solution (D/H, $^{18}O/^{16}O$) that the hydrothermal solution is originated from rainwater and that the altitude of the supplying area of the rainwater is 250 to 350 meters above the level of the geothermal area. The recharge area is underlain by granite in the Fan geothermal area. The porosity and permeability of the granite are small as a whole, and the amount of the outflow is estimated to reach about 90% of the total effective rainwater. By the meteorological data based on the observation by the Chiang Mai meteorological station, the average annual rainfall is 1,776 mm/year. The amount of evaporation is 1,173 mm/year, according to the Penman's experiential formula. The possible effective supply of rainwater into the geothermal area is obtained by the following formula.

$$Q = 0.10 \times (P - E) \times A \times 5.59 \times 10^6$$

Here Q: supply (gallons/day)
A: area (km^2)
P: rainfall (inches/day)
E: evaporation (inch/day)

The recharge of the effective rainwater to the Fan geothermal area obtained by the above formula is 365×10^3 gallons/day/km^2.

Meanwhile, the rainwater supply in the San Kampaeng geothermal area, although detailed survey data are uncertain, is estimated to be 408×10^3 gallons/day/km^2. It is known in a geothermal area actually developed in Japan that the rainwater supply is 1.44×10^4 tons/day/km^2 (380×10^5 gallons/day/km^2). Accordingly, it can be said that the rainwater supply in the San Kampaeng area is sufficient.

The hydrographical structure in this area is here considered geologically. The area is geologically underlain, from the lowest, by the Carboniferous Mae Tha Formation, the Permian Kiu Lom Formation (the lower part, the middle part and the upper part) and Triassic granites. Generally, the porosity of the Paleozoic strata and the granites is less than several percent, and their transmissibility is in the order of 10^{-5} m^3. Therefore, it can be said that, in the area where fissilities are not well developed, the rocks composing this area have small capability to keep geothermal fluid (reservability) and poor permeability. In many cases, the main beds from which productive vapors are obtained are composed of Paleozoic and Mesozoic rocks in the

already-developed geothermal areas such as Larderello in Italy, Geyser in U.S.A. and Nigorikawa In Japan. All these beds are fractured well, and faults are known to be important as the passage of the fluid or as the reservoir.

The outline of the hydrographical charcter of the beds composing this area is given below.

The Mae Tha Formation is composed of quartzose massive sandstone, in which fissilities like joints are poorly developed. Structural fractures developed in parts are recognized to have been filled with quartz veins in many cases, and therefore the permeability as a whole is expected to be small. The lower part of the Kiu Lom Formation is composed of alternations of various sedimentary rocks such as sandstone, shale, siltstone, limestone and chert. Fractures like joints and cleavages are well developed in them comared to the Mae Tha Formation and to the middle to upper part of the Kiu Lom Formation. It is recognized in the field geological survey that chert bed and muddy bed (shale, siltstone) are especially broken into pieces. Accordingly, if these existing fissures are open, it is thought that the lower part of the Kiu Lom Formation has fairly high permeability. The middle to upper part of the Kiu Lom Formation is composed mainly of basaltic rocks (lava, pyroclastic rocks), though limestone and shale are inserted in parts. As the fissures in these beds are adhered by weathering and alteration products in many cases, permeability is thought to be low as a whole.

Accordingly, the following hydrographical division is possible from the rough stratigraphical viewpoint (Table V.1-4).

Table V.1-4 Hydrographical stratigraphy in the San Kampaeng area

Middle to upper part of the Kiu Lom Formation	basaltic rock	hardly permeable
	conformity	
Lower part of the Kiu Lom Formation	chert, siltstone, sandstone, and limestone, etc.	permeable (if fractures are open)
	uncomformity	
Mae Tha Formation	sandstone	hardly permeable

The result of this stratigraphical division seems to be correspondent to such system as Cap rock (hardly permeable confining layer) – Reservoir (permeable aquifer) – Impermeable basement, which is generally seen in the ordinary geothermal area. However, viewing from the geological and structural characteristics in the San Kampaeng geothermal area, lateral widely-extending cap rock and reservoir are not conceivable. As the fault planes (almost 80° ~ 90°) and bedding planes (60° ~ 80° in many cases) have fairly steep inclination in this area, it is inferred that fracture zones associated with faults and cracked zones in certain beds are also dipping steeply. In such case as this, the movement and the reservation of geothermal fluid is expected to be in vertical direction, viewing from the points that the fractured zones as the passages are dipping in high angle (60° ~ 90°) and that the buoyance of the geothermal fluid acts vertically upward, unless geothermal fluid moves horizontally by the lateral influence of the underground water. Accordingly, it is thought that would be little possibility that the basaltic rocks of the middle to upper part of the Kiu Lom Formation are playing the role of cap rock, under which geothermal fluids are reserved extensively.

4. Period of circulation of the hydrothermal solution

There is a method to estimate the period from the penetration of surface water into underground to the spring out of the hydrothermal solution on the surface after heated in the deep. This method is by the measurement of tritium density.

The analysis result of tritium in the hydrothermal solution in the San Kampaeng geothermal area is 4.5 and 9.0 TU (T/U x 10^{18}). The age of the hydrothermal solution containing tritium is thought to be as follows unless admixture of recent underground water is recognized.

(1) The water with tritium content of less than 3 TU is older than 30 years roughtly.

(2) The water with tritium content of 3 ~ 20 TU contains high tritium concentration by the experiments of hydrogen bomb in 1952 ~ 1962.

(3) The water with tritium content of more than 20 TU contains recent high tritium concenttration.

Therefore, the hydrotermal solution in the San Kampaeng geotermal area can be said to be as old as nearly 30 years. However, it is inferred that the hydrothermal solution flowing out on the surface has been admixed with recent underground water. Considering the influence of this admixture, the age of the hydrothermal solution gushed out after the circulation in the depth is estimated to be more than 30 years.

5. Underground water flow system

Geothermal system (including geothermal reservoir) is surrounded by the ordinary underground water flow system. The two systems are thought to be influence each other by the exchange of heat and water or by the interaction of pressure. The underground water flow system is important in the points that it supplies rainwater to the geothermal reservoir, that it affects pressure to the geothermal reservoir and that it deprive heat of the reservoir after the penetration of rainwater into the reservoir.

The motion of underground water is thought as complicated threedimensional flow-system, not only as lateral flow in aquifer.

Toth's model of the underground water flow system is a model in which pattern of flow system is illustrated as steady flow, considering regional features of topography and its local variation on a profile on which geology is assumed to be isotropic and homogeneous (Fig. V.1-5).

On this profile, in spite of isotropic, homogeneous and simple geological profile, the motion of the underground water is complicated and is divided into several local flow systems. According to the potential of position reflecting topographical variation, the following three flow systems are taken from regional system to the local one, depending upon the scale.

(1) Regional flow system: the large scaled flow toward the high recharge area of the basin, following large scaled topography of the whole of the underground water basin.

(2) Intermediate flow system: moderate scaled flow of underground water caused by the difference of elevation of topography, which is rather small in scale compared to the

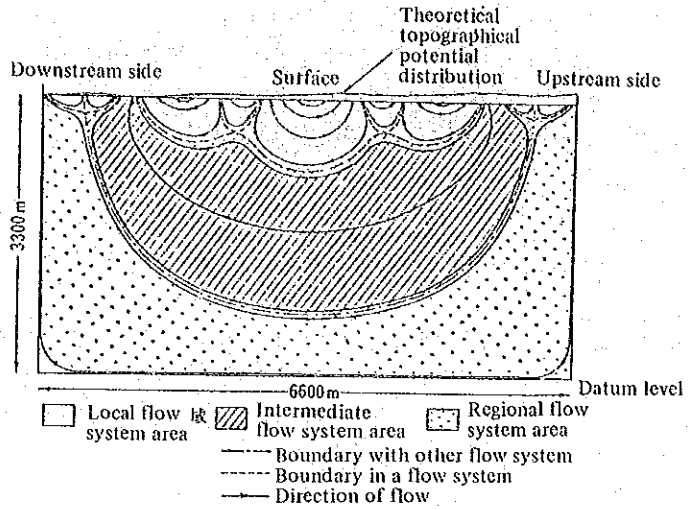

Fig. V.1-5 Pattern of theoretical flow system on the profile of simple underground water basin (After Toth)

topographical variation controling the regional flow system.

(3) Local flow system: small scaled flow of underground water caused by the difference of elevation of local topography.

Viewing topographically, the regional flow system is thought to be large scaled flows from the Doi Luang uplifted zone to the Chiang Mai basin and from the Doi Luang uplifted zone and the Mae The uplifted zone to the Ban Pong Hom subsided zone. Against this system, it is the intermediate flow system that is controled by the topographical division by the Huai Pong River flowing northward and the Huai Wai River flowing southward in the Ban Pong Hom subsided zone. Also, the local flow system is corresponding to the drainage basin of the branch stream on the right bank of the Huai Pong River which is flowing in the area where the geothermal

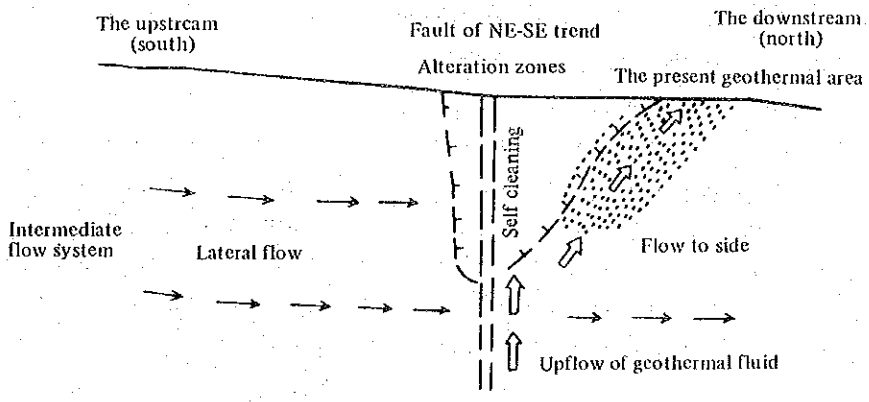

Fig. V.1-6 Geothermal system and underground water flow system